



Section of Environmental Fluid Mechanics,
Department of Hydraulic Engineering,
Faculty of Civil Engineering & Geosciences,
Delft University of Technology

In association with:

Deltares, Zee- en Kust Systemen
The Port of Rotterdam Authority, Projectorganisatie Maasvlakte 2

Modelling the wind-driven motions in the Rhine ROFI

by

Joost VAN WIECHEN

March 2011

Committee members:
Prof. Dr. Ir. Guus S. STELLING
Dr. Julie D. PIETRZAK
Dr. Ir. Gerben J. DE BOER
Prof. Ir. Tiedo VELLINGA
Dr. Meinte BLAAS
Dr. Onno VAN TONGEREN
Ir. Wil G. BORST

Thesis submitted to obtain the academical degree of
MASTER OF SCIENCE IN HYDRAULIC ENGINEERING

Abstract

This Master Thesis presents a numerical model analysis of the response of the Rhine ROFI to wind direction and speed. The aim of this study is to gain a further insight into the physical processes of the Rhine ROFI. Previous work on the Rhine ROFI focused mostly on tidal effects (straining and mixing) and inertial motions (earth rotation). Other studies have focussed on the response of freshwater plumes to wind forcing alone. Recently, the combined forcing has been studied in an idealised model of the Rhine ROFI. The current study extends this research, however with the incorporation of the actual bathymetry and coastline of the Netherlands in a new, state-of-the-art three-dimensional hydrodynamic model.

A sensitivity analysis of the number and distribution of vertical layers in the model found that 48 vertical layers is recommended under strongly stratified conditions

The numerical results show that the effect of the Earth's rotation on the wind-driven flow plays an important role in the stratification of the Rhine ROFI. Under neap tide conditions the Rhine ROFI exhibits periods of stratification. Due to a reduced eddy viscosity at the pycnocline, the surface layer responds more independently and is less affected by bottom friction. It implies that Coriolis force becomes relatively more important in the dynamics of the surface layer. Differential advection and depth mean advection make the size and shape of the freshwater plume highly variable. If the system is forced by an upwelling-favourable wind the freshwater plume is transported offshore, resulting in an increase of stratification. Downwelling-favourable winds transport the freshwater landwards, which results in a vertically well-mixed water column.

An increased magnitude of the wind causes a more stratified water column for the upwelling-favourable winds and a more mixed state for the downwelling-favourable winds. Direct wind-induced vertical mixing of the plume is observed for an increased magnitude of the wind.

The integrated potential energy anomaly is presented. It is found to be a powerful tool in analysing the interaction and competition of the wind and the ebb-flood tidal cycle in mixing and straining of the Rhine ROFI. The mixing and straining by the ebb-flood tidal cycle is found to be dominant over the mixing and straining by the wind. The influence of the wind on the Rhine ROFI is however clearly observed.

The spatial changes in the potential energy anomaly show that for upwelling-favourable winds an increase of stratification occurs in the far-field. In the near-field a decrease is observed. For downwelling-favourable winds the opposite happens. The influence of the Ekman dynamics is observed in the results. For increased downwelling-favourable winds a reduction of the potential energy anomaly is found in both the near- and farfield of the Rhine ROFI.

Acknowledgements

This Master Thesis has been carried out as the finalising part of the Master of Science program Hydraulic Engineering at the Faculty of Civil Engineering and Geosciences, Delft University of Technology, The Netherlands. The project has been funded by the Port of Rotterdam Authority within the framework of the Maasvlakte 2 project. The research has been conducted at the offices of Deltares (former WL|Delft) and the Port of Rotterdam Authority. This unique cooperation between Delft University of Technology, Deltares and the Port of Rotterdam Authority has resulted in an improved knowledge of the hydrodynamics in the Rhine ROFI.

I would like to thank my graduation committee for their supervision during the project. My expressions of gratitude go especially to dr. J.D. Pietrzak, dr. M. Blaas, dr. ir. G.J. de Boer, dr. O. van Tongeren and ir. W.G. Borst, who provided input and also guided me through the whole project. Furthermore I would like to thank Prof. dr. ir. G.S. Stelling and Prof. ir. T. Vellinga for their interest and advises in my work. Additionally I want to show my expression of thanks to T.S. Tutert for creating some of the nice cartoons as used in this report.

Furthermore I would like to thank Deltares and the Port of Rotterdam Authority for facilitating a place of work.

Delft, March 2011

J.J.J. van Wiechen

Contents

Abstract	iii
Acknowledgements	v
1 Framework	1
2 Introduction	3
3 Theoretical Background	7
3.1 Introduction	7
3.2 Rhine ROFI	7
3.3 Stratification	9
3.4 Potential Energy Anomaly	9
3.5 Tide	9
3.6 Wind	12
3.7 Other processes	16
4 Methods	19
4.1 Introduction	19
4.2 Model set-up	19
4.3 Sensitivity analysis of the model	22
4.4 Physical analysis of the model results	24
5 Sensitivity analysis of the model	29
5.1 Introduction	29
5.2 Vertical grid analysis	29
5.3 Horizontal grid analysis	33
5.4 Conclusions and Recommendations	34
6 Physical analysis of the model results	35
6.1 Introduction	35
6.2 Freshwater plume	36
6.3 Temperature	43
6.4 Potential Energy Anomaly analysis	46
6.5 Upwelling and downwelling	53
6.6 Presentation of the results	55
7 Discussion	59
8 Conclusions & recommendations	65
A Supporting figures	67

B Mathematical support	85
References	92
List of Figures	94

Chapter 1

Framework

Maasvlakte 2 is the second large-scale harbour extension of the Port of Rotterdam, adding 2000 ha of new port facilities. During the construction (2009-2013) 240 million m³ of sand will be extracted from the North Sea, 15 km out of the Rotterdam coast, beyond the -20 m depth contour line. Maasvlakte 2 will be situated west of the existing port, between the mouths of the Rotterdam Waterway and the Haringvliet. Here the freshwater of the Rhine-Meuse system is discharged into the Southern North Sea, which gives rise to the so-called Rhine ROFI (Region of Freshwater Influence), see Souza & Simpson (1996). The Maasvlakte 2 project has been approved by the Dutch government, but required the Port of Rotterdam Authority to monitor the possible affected areas in the Southern North Sea.

Possible effects of the project have been written down in an extensive environmental impact assessment, see Berkenbosch (2007). The large scale sand extraction will result in a temporary increase of SPM (Suspended Particle Matter) and turbidity in the Rhine ROFI. To monitor the SPM and turbidity, the Port of Rotterdam Authority set up her own monitoring campaign including data gathering through field measurements and satellite imagery. Analysis of a first set of field measurements by Smolders (2010) is encouraging for further research to SPM.

Key to understanding the distribution and behaviour of SPM is stratification, see De Nijs *et al.* (2009); de Nijs *et al.* (2010a,b); de Nijs & Pietrzak (2011). Besides the monitoring campaign, a proper numerical model is therefore indispensable in the project. In the MoS² project The Port of Rotterdam Authority contracted Deltares for the development of the MoS² ZUNO-DD model. The model calculates the hydrodynamics in the Rhine ROFI, including the development and breakdown of stratification. With the DELWAQ model of Deltares it is hereafter possible to calculate the SPM distributions. The field measurements are used for validation of the model.

With the MoS² project finished a more comprehensive, physically consistent picture can be drawn of the situation concerning SPM in front of the Dutch coast, both before, during and after the construction of Maasvlakte 2. An indispensable first step, before being able to investigate other phenomena such as SPM, is to gain a better understanding of the physics in the Rhine ROFI. In this study the interaction and competition between the wind and tide in stratifying and mixing of the Rhine ROFI is investigated.

Chapter 2

Introduction

Regions of freshwater influence (ROFI), a term adopted by Simpson *et al.* (1993) are those areas of shelf seas where freshwater runoff from rivers contributes strongly to the buoyancy input. In ROFI's freshwater plumes are formed varying in size and lifetime depending upon the competition between processes that stratify and mix the water column (Simpson, 1996). It should be noted that ROFI's are also referred to as river plumes.

Studies of North American river plumes such as at the Columbia River on the west coast and the Hudson River on the east coast have laid the foundation for our understanding of river plumes. Under the influence of Coriolis force riverine water that exits the river mouth is deflected to the right (on the northern hemisphere), typically forming a bulge region near the river mouth and a narrow downstream coastal current, whose offshore width is governed by the internal Rossby Radius of Deformation. Both observations and numerical studies have shown the importance of wind forcing on river plumes (Fong & Geyer, 2001; Berdeal *et al.*, 2002). Typically, these rivers connect with a deep offshore region. A series of numerical experiments by Chao & Boicourt (1986) showed the importance of Ekman dynamics. Upwelling-favourable winds cause a seaward excursion of river plumes, downwelling-favourable winds narrow the plume. The same consistency with Ekman drift was observed in observations of the western Gulf of Maine plume by citetfong1996. Model results by Kourafalou *et al.* (1996a) showed an offshore removal of the freshwater plume for upwelling-favourable wind stresses. Field observations by Hickey *et al.* (2005) indicated that the Columbia River plume is bi-directional. Typically, the plume is found on the right of the river mouth, however under certain wind events it turns to the left. Modelling studies by Berdeal *et al.* (2002) confirmed this tendency. Downwelling wind events result in a narrowing of the plume extending to the north of the river mouth, upwelling wind events result in a southward river plume that is advected offshore.

In contrast to the North American situation, many European ROFI's are situated in shallow frictional systems dominated by the tides. Typically, ROFI's are forced by tides, wind, river discharge, wave mixing and atmospheric heating and cooling. They are complex systems where different physical factors compete and interact on different timescales to determine the state of the water column. The Rhine ROFI is located in the Southern North Sea, a shallow coastal sea dominated by the tides and winds. Here the freshwater of the Rivers Rhine and Meuse contributes strongly to the buoyancy input. The Rhine-Meuse system discharges on average $2200 \text{ m}^3\text{s}^{-1}$ of freshwater through the Rotterdam Waterway and the Haringvliet in the Southern North Sea. It gives rise to the approximately 30 km wide and 100 km long Rhine ROFI (Souza & Simpson, 1996). Here the competition between the different processes leads to a ROFI which tends to switch between a well-mixed and a stratified state.

Over the fortnightly spring-neap tidal cycle the Rhine ROFI switches between mixed and stratified conditions. High input of mixing energy under spring tide conditions mixes the

strong cross-shore horizontal density gradient away, resulting in a well-mixed Rhine ROFI. Under typical neap tide conditions with low input of mixing energy it results in periods of stratification (Simpson *et al.*, 1993). During those periods, the effect of the semi-diurnal ebb-flood tidal cycle comes into play. Under stratified conditions the water column is partially decoupled due to the presence of a pycnocline. Strong cross-shore exchange currents interact with the dominant density gradient through differential advection. Due to the switching of the tide, the exchange currents change direction on semi-diurnal timescale. The resulting alternately switching between stratified and well-mixed conditions over the ebb-flood tidal cycle is clearly described by Simpson *et al.* (1990) and denoted as tidal straining.

In the Rhine ROFI the tide propagates as a weakly damped Kelvin wave in the alongshore direction and interacts with the main density gradients in the cross-shore direction. Under typical neap tide conditions Visser *et al.* (1994) observed counter-rotating tidal current ellipses of up to 40 % of the alongshore velocities in the surface and bottom layer of the Rhine ROFI. The presence of cross-shore velocity shears made it possible for Simpson & Souza (1995) to apply the theorem of tidal straining to the Rhine ROFI. Due to the propagating nature of the Kelvin wave in the Southern North Sea, the Rhine ROFI is maximally stratified at high water and closest to a well-mixed state at low water (see Figure 2.1). In contrast, Van Alphen *et al.* (1988) suggested from their cruise data that the Rhine ROFI was dominated by alongshore advection.

Both the discharge and temperature of the freshwater have an effect on the state of the Rhine ROFI. Variations in discharge take place on seasonal time scales; the largest discharges can be expected in the months December to April, see Pietrzak *et al.* (2011). With more freshwater in the system, more energy is required to mix the water column and stratification is more likely to occur. In summertime, the difference in temperature between the river and sea water

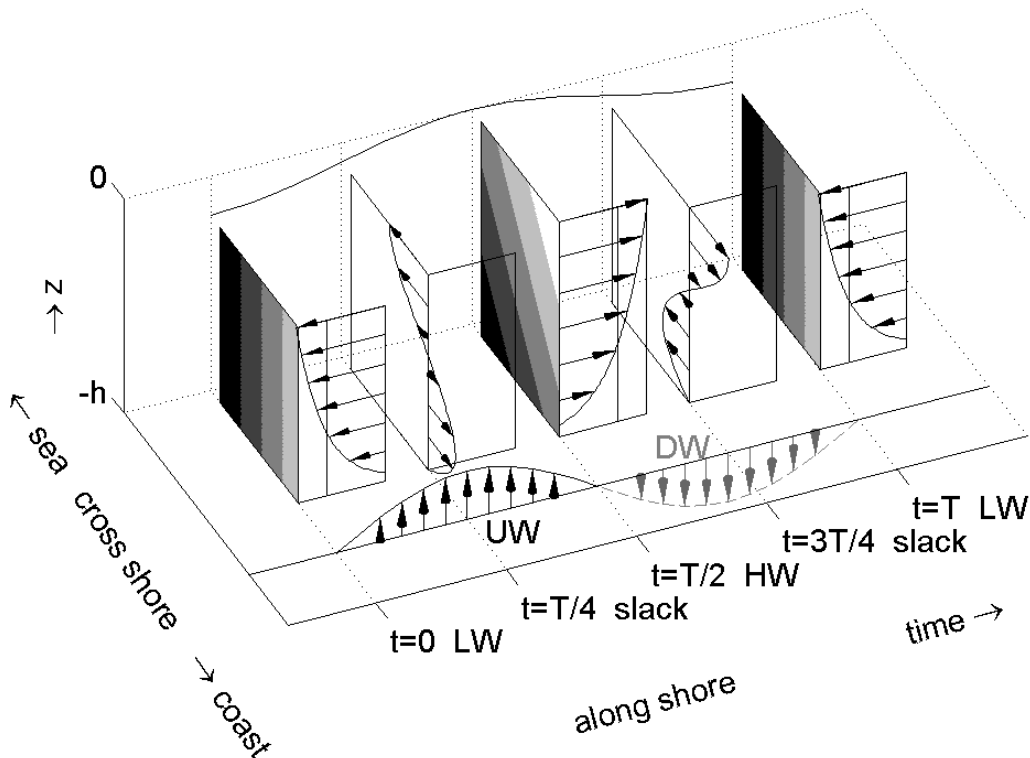


Figure 2.1: A sketch of cross-shore tidal straining in the Rhine ROFI (Simpson & Souza, 1995). Figure by de Boer (2009).

can increase up to over 10 °C. Water in the shallow River Rhine is quickly heated, while the seawater still remains relatively cold (De Kok *et al.*, 2000; Arentz, 2005; Pietrzak *et al.*, 2011). In wintertime, no additional thermal stratification occurs as the temperature of the River Rhine is comparable to the temperature of the North Sea. Heat exchange between the sea and atmosphere and solar radiation change the sea surface temperature. In a well-mixed Rhine ROFI the surface temperatures do not differ from the ambient seawater (de Boer *et al.*, 2009). Under stratified conditions temperature differences between the plume and surrounding waters can exceed over 3 °C (De Kok *et al.*, 2000). The reduced mixing between the surface and bottom layer under stratified conditions also prevents the exchange of heat. Hence, in summer increased stratification due to temperature differences will occur amplified by haline stratification.

To study the competing factors in mixing and stratification, Simpson & Bowers (1981) considered changes in potential energy relative to the well-mixed condition and defined those in a scalar parameter, ϕ [Jm^{-3}], the potential energy anomaly. It is the depth averaged amount of energy required to obtain a fully mixed water column:

$$\phi = \frac{1}{H} \int_{-h}^{\eta} (\hat{\rho} - \rho)gzdz, \quad \text{where} \quad \hat{\rho} = \frac{1}{H} \int_{-h}^{\eta} \rho dz. \quad (2.1)$$

H is the depth of the total water column [m], given by $H = \eta + h$, η the free surface, h the location of the bed with reference to the mean water level. ρ is the water density [kgm^{-3}], g the acceleration due to gravity (9.81 ms^{-2}) and z the depth interval [m].

De Boer *et al.* (2007) had a closer look at the different datasets used by Simpson & Souza (1995) and Van Alphen *et al.* (1988). They concluded that both sets displayed alongshore and cross-shore effects at the same moment. In order to investigate other tidal straining configurations and tidal advection, de Boer *et al.* (2007) derived the potential energy anomaly equation suitable for three-dimensional flows. The full equation incorporates sixteen terms of which, besides the sources and sinks, the cross-shore and alongshore straining and the (depth mean) advection were found to play an important role. A similar set of equations was derived independently by Burchard & Hofmeister (2008).

Furthermore De Boer & Pietrzak (in prep.) made a first attempt at extending this analysis by integrating over depth and area, the results of which for idealized simulations are described in Pietrzak & De Boer (in prep.). This study uses the same method, but will address it more extensively and includes more realistic simulations. From the original potential energy anomaly as given by Simpson & Bowers (1981), the value of ϕ is integrated over depth and over an area enclosing the Rhine ROFI:

$$E = \iiint \phi dAdz. \quad (2.2)$$

The method provides an effective means to analyse mixing and straining of the Rhine ROFI over time. Here the method will be used to meet the aim of this study.

This study investigates the interaction and competition of the wind (varying in direction and magnitude) and the ebb-flood tidal cycle in mixing and straining of the Rhine ROFI under stratified conditions. To that end a three-dimensional numerical model, the so-called MoS² ZUNO-DD model system (Cronin *et al.*, 2010), was employed. A condition of neap tide combined with a typical mean river discharge of $1900 \text{ m}^3\text{s}^{-1}$ was selected as the background reference case. The tidal reference scenario allows to investigate the role of tidal straining and depth mean advection by the tides in the absence of winds. This reference case extends the

work in de Boer *et al.* (2007) as it incorporates both realistic bathymetry and the coastline of The Netherlands. A series of idealised numerical simulations were then performed to understand how the Rhine ROFI responds to onshore and offshore directed wind forcing, and upwelling and downwelling favourable wind forcing, with magnitudes of 5 and 10 ms^{-1} . The interactions and competition between the wind and the tide in mixing and straining of the water column is then studied. In order to analyse the competition and interaction between the wind and the tide as sources of straining and mixing in the Rhine ROFI, the method of the integrated potential energy anomaly analysis is used.

This study extends the numerical investigation of Pietrzak & De Boer (in prep.) which used a straight coastline and flat bed of 20 m depth. Here the impact of realistic bathymetry and coastline on the evolution of the plume is also investigated. In addition, the impact of the number of layers in the vertical on the reproduction of stratification in the Rhine ROFI is investigated.

The model setup is described in Chapter 4. The model has been validated as part of the MoS² project. However, in order to investigate the influence of the number of vertical layers and their distribution on the reproduction of stratification in the Rhine ROFI a further sensitivity analysis is performed in Chapter 5. In Chapter 6 the results of the physical analysis of the model results are presented. The response of the Rhine ROFI to forcing by the wind is analysed. Chapter 7 discusses the results and highlights the role of the competition between the processes that mix the Rhine ROFI and those that act to stratify it. Conclusions, recommendations for future research and notions on the numerical model are given in Chapter 8.

Chapter 3

Theoretical Background

3.1 Introduction

This chapter discusses the theoretical background of the research towards the influence of wind on the Rhine ROFI. First an introduction and overview of the Rhine ROFI are presented in Section 3.2. It is followed by a small general description of stratification, Section 3.3. Hereafter the Potential Energy Anomaly equation for three-dimensional flows by de Boer *et al.* (2007) is presented in Section 3.4. In Section 3.5 the influence of the tide on the system is described. Previous research and general knowledge of the influence of the wind on the Rhine ROFI is presented in Section 3.6. This section can also be regarded as an introduction into the subject of the research as conducted in this Master Thesis. Finally a brief overview of the other processes acting in the Rhine ROFI is presented in Section 3.7.

3.2 Rhine ROFI

The Rhine ROFI is an approximately 30 km wide and 100 km long body of low salinity coastal water situated in the Southern North Sea, in front of the Dutch coast (Souza & Simpson, 1996). Freshwater is brought into the system through the combined discharge of the Rivers Rhine and Meuse. The Rotterdam Waterway handles the largest part of the freshwater: on average $1400 \text{ m}^3 \text{ s}^{-1}$. The averaged discharge through the Haringvliet is $800 \text{ m}^3 \text{ s}^{-1}$. Variations in discharge occur on seasonal scale. The highest discharges are expected in the months December till April. Once the freshwater enters the Southern North Sea, it is deflected to the right under the influence of Coriolis and forms a northwards extending freshwater plume.

De Kok *et al.* (2000) showed that the density differences in the Rhine ROFI are controlled by salinity rather than by temperature. The freshwater discharge by the rivers Rhine and Meuse influences the density field close to the coast significantly. Suijlen & Duin (2002) concluded from observations that the density gradients in the Rhine ROFI are predominantly found in cross-shore direction. In alongshore direction the time averaged density field is approximately uniform. The cross-shore density (salinity) gradient in combination with the Coriolis force causes the presence of the alongshore currents in front of the Dutch coast. The density structure in the Rhine ROFI is a result of these alongshore currents. Residuals of up to 10 cms^{-1} have been measured in the surface layers (De Ruijter *et al.*, 1993).

Heaps (1972) added a description of the vertical velocity structure of a stationary density-driven flow to the system, which makes the overall picture three dimensional. Under consideration of a straight infinitely long coast with cross-shore sections of the same geometry, the dependency in alongshore direction is eliminated. The density difference between the

saline offshore water and the fresher water near the coast causes a depth-dependent baroclinic pressure gradient. The sloping sea-surface results in a barotropic pressure gradient, which is depth independent. The sum of both leads near the surface to an offshore directed gradient, while near the bottom the gradient is directed shorewards.

In the frictionless limit case, only the generated Coriolis force can balance the cross-shore pressure gradient. It will result in an alongshore geostrophic flow towards the north; the so-called ‘thermal wind balance’. Conversely, if friction is important, the pressure gradient is balanced by the non-uniform velocity shear, generated by the cross-shore exchange current. This limit case is called ‘estuarine circulation’. Heaps formulas combine the alongshore thermal wind balance and the cross-shore estuarine circulation in a joint residual current structure. The formulas are found in Appendix B.

In the Rhine ROFI a horizontal density gradient is present in both the alongshore and cross-shore direction. The cross-shore gradient dominates over the alongshore gradient. In offshore direction both gradients diminish rapidly. Without a gradient the alongshore and cross-shore currents also decay to zero. A sketch of the theory of Heaps applied to the Rhine ROFI is given in Figure 3.1. Presented is the governing three-dimensional residual current field in front of the Dutch coast. Important to notice is that the profile as described by Heaps assumes a vertically well-mixed water column. Once stratification occurs (Section 3.3), the profile no longer holds. Also the presence of the River Rhine mouth within the system results in a more difficult overall picture (de Boer, 2009).

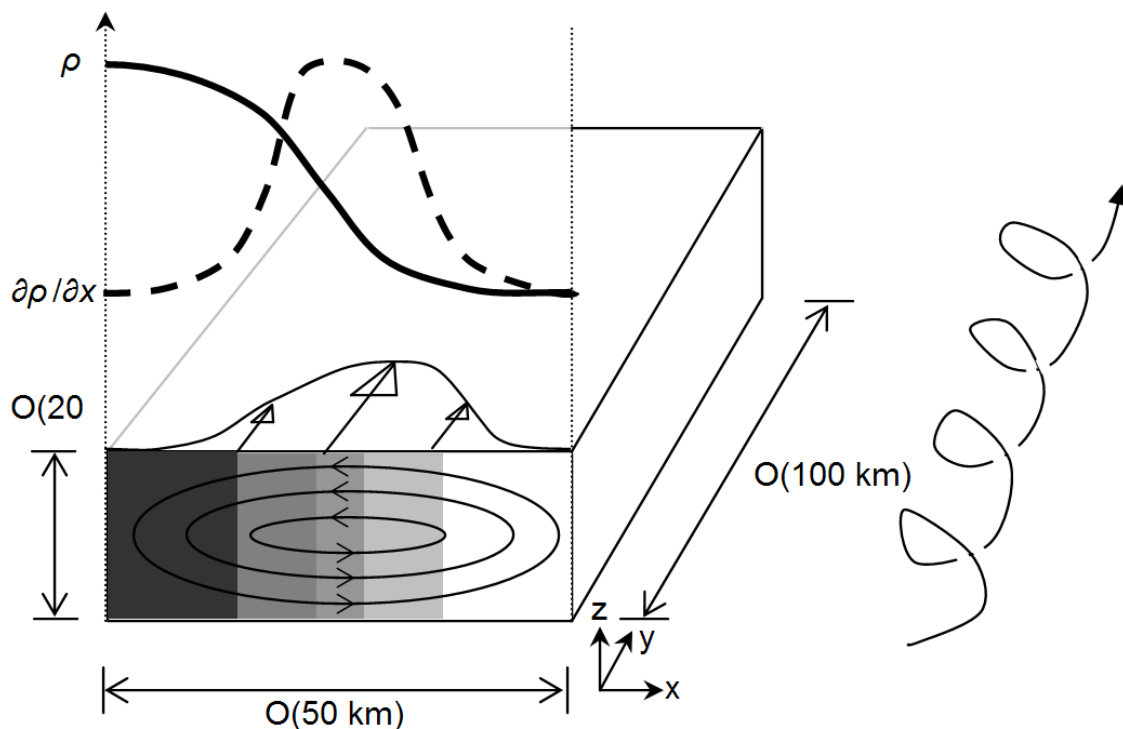


Figure 3.1: Sketch of the 3D residual current structure in the Rhine ROFI. The density structure in cross-shore direction (s-shaped) results in the bell-shaped cross-shore density gradient. The density gradient in its turn results in the bell-shaped distribution of both the alongshore velocity and the cross-shore exchange current. The right-hand side presents the path a non-buoyant particle would follow in this current field (Visser & te Utrecht, 1993). Figure by de Boer (2009) after Visser & te Utrecht (1993).

3.3 Stratification

During periods of stratification less dense freshwater is found on top of denser (saline) seawater. In the case of stable stratification the water column consists of two layers with a sharp interface in between, the so-called pycnocline. It results in a partial decoupling of the velocity profile and a redistribution of turbulence over the water column. The transfer of momentum through the pycnocline is suppressed. Different physical factors tend to mix or stratify the water column.

The Rhine ROFI is a complex system where different physical factors (tides, wind, river discharge, waves and atmospheric radiation) compete and interact in mixing and straining of the water column. Simpson & Bowers (1981) considered changes in potential energy relative to the well-mixed condition as the mode for studying the competing factors in a ROFI. They defined those changes in a scalar parameter, ϕ [Jm^{-3}], the potential energy anomaly. It is the depth averaged amount of energy required to obtain a fully mixed water column, see Equation 2.1.

3.4 Potential Energy Anomaly

Following the potential energy anomaly equation by Simpson & Bowers (1981), de Boer *et al.* (2007) derived the potential energy anomaly equation for three-dimensional flows. The equation is based on the Reynolds averaged advection-diffusion equations for density with sources and sinks added:

$$\begin{aligned} \frac{\partial \varphi}{\partial t} = \frac{g}{H} \int_{-h}^{\eta} & \left(\underbrace{\tilde{u} \frac{\partial \tilde{\rho}}{\partial x}}_{S_x} + \underbrace{\tilde{v} \frac{\partial \tilde{\rho}}{\partial y}}_{S_y} + \underbrace{\tilde{u} \frac{\partial \tilde{\rho}}{\partial x}}_{A_x} + \underbrace{\tilde{v} \frac{\partial \tilde{\rho}}{\partial y}}_{A_y} + \underbrace{\tilde{u} \frac{\partial \tilde{\rho}}{\partial x}}_{N_x} + \underbrace{\tilde{v} \frac{\partial \tilde{\rho}}{\partial y}}_{N_y} - \underbrace{\frac{1}{H} \frac{\partial \tilde{u} \tilde{\rho} H}{\partial x}}_{C_x} - \underbrace{\frac{1}{H} \frac{\partial \tilde{v} \tilde{\rho} H}{\partial y}}_{C_y} + \underbrace{w \frac{\partial \rho}{\partial z}}_{W_z} + \underbrace{\frac{\partial \langle \rho' w' \rangle}{\partial z}}_{M_z} + \dots \right) z dz + \dots \\ & \int_{-h}^{\eta} \left(\underbrace{\frac{\partial \langle \rho' u' \rangle}{\partial x}}_{D_x} + \underbrace{\frac{\partial \langle \rho' v' \rangle}{\partial y}}_{D_y} - \frac{1}{H} \left(\underbrace{\langle \rho' w' \rangle|_s}_{D_s} - \underbrace{\langle \rho' w' \rangle|_b}_{D_b} \right) \right) z dz - \underbrace{\frac{\varphi}{H} \frac{\partial H}{\partial t}}_{B_H} - \underbrace{\left(\frac{g}{H} \right) \left(\tilde{\rho}(\eta) \eta \frac{\partial \eta}{\partial t} \right)}_{B_\eta} \end{aligned} \quad (3.1)$$

The terms S_x and S_y denote the straining in cross-shore (Simpson *et al.*, 1990) and alongshore direction respectively. A_x and A_y are the advective terms in the two directions. N_x, N_y, C_x and C_y describe the non-linear interactions between the deviation of both the density and the velocity over the vertical. W_z is the term related to upwelling and downwelling and M_z describes the effect of vertical mixing of the density profile. D_x and D_y are the horizontal depth averaged dispersion terms and D_s and D_b the surface density and bed density fluxes respectively. The terms B_H and B_η represent changes in the water depth and the surface elevation (de Boer *et al.*, 2007). It has to be noted that a similar set of equations was also derived independently by Burchard & Hofmeister (2008).

3.5 Tide

The influence of the tide on the terms S_x, S_y, A_x and A_y within the Rhine ROFI has been investigated by de Boer *et al.* (2007). Note that S_x is the well-known tidal straining term

of Simpson *et al.* (1990). The influence of the tide can be separated into two timescales. The largest timescale is the fortnightly spring-neap tidal cycle, followed by the semi-diurnal ebb-flood tidal cycle. Hereunder both timescales are discussed, followed by the explanation for the existence and the influence of tidal ellipses in the (Rhine) ROFI. The theorem of tidal straining applied in general as well as to the Rhine ROFI is explained in the last section.

Spring-neap tidal cycle

Over the spring-neap tidal cycle the Rhine ROFI switches between well-mixed and stratified conditions in vertical direction. During spring tide the Rhine ROFI is well-mixed in vertical sense. In horizontal direction it is stratified, with the more saline water found offshore, see Simpson *et al.* (1990). Van Alphen *et al.* (1988) and de Ruijter *et al.* (1997) have shown that there is no systematic interaction between the alongshore tidal currents and the average cross-shore density gradients for a well-mixed Rhine ROFI. The fresh water entering the Southern North Sea is transferred by the tide, due to alongshore advection.

Stratification in the Rhine ROFI occurs during neap tide. It is maximum at slack tide between low and high water. During periods of stratification Visser *et al.* (1994), by radar, observed tidal current ellipses with cross-shore velocity components of up to 40% of the alongshore velocities. Those tidal ellipses were only small during periods of a well-mixed water column. With an in-situ placed device they observed that during the presence of the surface current ellipses, also current ellipses were present in the bottom layer, however in the opposite direction. The existence of tidal ellipses is explained hereafter.

Ebb flood tidal cycle

The second time scale is the semi-diurnal ebb-flood tidal cycle. In the Southern North Sea the tide propagates as a Kelvin wave with maximum flood and ebb velocities around high and low water. The Rhine ROFI, in tidally averaged sense, can be regarded as stratified during neap tide. Simpson *et al.* (1993) showed that a semi-diurnal variation in the cross-shore velocity field can be combined with a semi-diurnal variation in stratification in the Rhine ROFI, a process identified as tidal straining. The existence of the tidal current ellipses results in non-zero tidal currents at slack tide.

During periods of a well-mixed Rhine ROFI (spring tide) there is no combination between a semi-diurnal variation in the cross-shore velocity field and a semi-diurnal variation in stratification. The tidal currents are zero around slack tide; the tidal ellipses do hardly exist. The Rhine ROFI is always well-mixed under spring tide conditions (de Boer, 2009).

Tidal ellipses

The existence of tidal current ellipses can be clarified with the use of Ekman dynamics. In general tidal current vectors cover an elliptic path over a tidal cycle. Prandle (1982a) was able to clarify the vertical structure of these tidal ellipses. First he decomposed the tidal current in an alongshore and a cross-shore vector. As they vary in time, the two vectors together make it possible to describe an elliptic path. This ellipse is then rewritten in an anti-clockwise and a clockwise motion with constant amplitudes (R^+ and R^- respectively). This decoupling into phasors creates the possibility to solve the momentum equations separately. On a Cartesian grid this is impossible since the u and v momentum equations are coupled together through the Coriolis parameter. The mathematics behind Prandle's solution are presented in Appendix B.

The decomposition into phasors by Prandle can also be given a geophysical interpretation by using the terms cyclonic and anti-cyclonic, instead of anti-clockwise and clockwise (for

the Northern Hemisphere). The component rotating in the same direction as the planetary rotation (cyclonic) will be less affected by the bottom friction than the component that rotates anti-cyclonic. With equal amplitudes of the rotating components, the near-bottom velocity will have the tendency to rotate in the same direction as the planetary rotation (cyclonic). Vice versa the anti-cyclonic component is less affected by the Ekman dynamics. It will result in the tendency of the near-surface component to rotate anti-cyclonic.

The presence of the coast implies a special application of Prandle's model for the Rhine ROFI. Since continuity is required, the depth-averaged velocity has to be zero at all times. With cross-shore currents present, the fluxes in the surface layer have to be compensated by fluxes in the bottom layer. Under well-mixed conditions the large eddy viscosity will result in a strong vertical mixing, suppressing possible cross-shore exchange currents.

During periods of stratification a partial decoupling of the velocity profile and a redistribution of turbulence occurs. It results in an independent response of the bottom and surface layer. Also the transfer of momentum through the pycnocline is suppressed. The bottom layer will have a stronger response to the bottom friction (compared to well-mixed periods), which will result in a larger cyclonic rotation. In the surface layer the response will be stronger to the Coriolis force and result in a larger anti-cyclonic rotation. Due to the presence of the coast and continuity, any cross-shore current in the bottom layer has to be compensated immediately by an opposite cross-shore current in the surface layer and vice versa (de Boer, 2009).

Tidal straining

The classic tidal straining theorem is described by Simpson *et al.* (1990), who performed their research in the Liverpool Bay. There the tidal wave can be seen as a standing wave. Under neap tide conditions the semi-diurnal tidal cycle results in a switching between stratified and well-mixed conditions of the ROFI. During the ebb-flow the fresher surface water is transported faster offshore than the deeper saline water. At the end of ebb a stratified water column is created, see Figure 3.2. Maximum stratification occurs at low water. Once flood starts, the process is reversed and the water column will be back to well-mixed conditions at high water.

Applying this theorem to the Rhine ROFI is more difficult. In the Rhine ROFI the direction of the propagating Kelvin wave is alongshore, while the main density gradients are found in cross-shore direction. The maximum flood and ebb velocities happen around high and low water. During well-mixed periods (spring tides) the tidal currents are zero at slack water, as a result tidal straining does not occur during spring tide.

During stratified conditions the tidal current ellipses are present. From low to high water the anti-cyclonic surface currents are directed offshore, moving the fresher surface water away from the coast. The bottom layer currents are in opposite direction and bring the more saline water shorewards; at high water the Rhine ROFI is maximally stratified. Going from high to low water, the currents in the surface layer are directed onshore and offshore in the bottom layer. Fresh water at the surface is kept close to the shore, while the more saline water near the bottom is transported in offshore direction. The Rhine ROFI is closest to being well-mixed at low water. A sketch of tidal straining in the Rhine ROFI is presented in Figure 2.1.

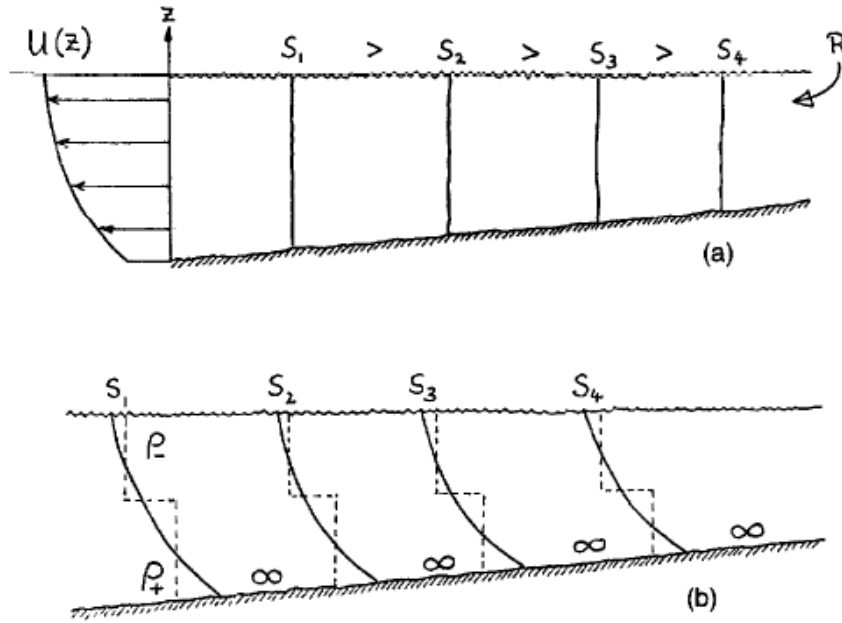


Figure 3.2: The principle of tidal straining by Simpson (1996). (a) The water column is well-mixed at the start of the ebb flow, with the more saline water found in offshore direction. (b) The water column at the end of ebb. Fresher water has been transported on top of the more saline water, resulting in a stratified water column. Figure by Simpson (1996).

3.6 Wind

In this Master Thesis the influence of the wind is investigated, it can work as a mixing or stratifying process. Both the direction and the force of the wind influence the behaviour of the system. The response of the Rhine ROFI to the wind can be separated into an ageostrophic (frictional) and a geostrophic (Ekman) component.

Frictional and Ekman response to the wind

Once the wind blows over the water surface, the drag will take the water with the winds' direction. This is the ageostrophical (frictional) response of the water column to the wind. Once the watermass is moving the effect of a balance between the wind stress and the Coriolis force causes a flow of the watermass deflected to the right with respect to the wind stress vector (for the Northern Hemisphere). This is the geostrophical (Ekman) response of the water column to the wind.

If a deep water column is assumed and bottom friction is ignored, the linearised equations of motion for a rotating fluid are, (Csanady, 1982):

$$N \frac{\partial^2 u}{\partial z^2} = -fv + \frac{1}{\rho} \frac{\partial p}{\partial x}, \quad (3.2)$$

$$N \frac{\partial^2 v}{\partial z^2} = fu + \frac{1}{\rho} \frac{\partial p}{\partial y}. \quad (3.3)$$

N is a coefficient of eddy viscosity. u and v are the alongshore and cross-shore velocities. f is the Coriolis parameter, $2\omega \sin \phi$, where ω is the angular speed of the Earth's rotation and ϕ the latitude. ρ is the density of the water and p the pressure at any position in the sea.

The velocities can be expressed as the sum of a pressure induced and a wind induced term. Each part can be solved separately and then added back together:

$$u = u_{ag} + u_E \quad \text{and} \quad v = v_{ag} + v_E \quad (3.4)$$

$$f u_{ag} = -\frac{1}{\rho} \frac{\partial p}{\partial y} \quad \text{and} \quad f v_{ag} = \frac{1}{\rho} \frac{\partial p}{\partial x} \quad (3.5)$$

$$f u_E = N \frac{\partial^2 v_E}{\partial z^2} \quad \text{and} \quad f v_E = -N \frac{\partial^2 u_E}{\partial z^2} \quad (3.6)$$

For the components that describe the geostrophic part, a homogeneous water column with a zero slope is assumed:

$$-f u_E + N \frac{\partial^2 v_E}{\partial z^2} = 0 \quad (3.7)$$

$$f v_E + N \frac{\partial^2 u_E}{\partial z^2} = 0 \quad (3.8)$$

With a wind in y-direction the solutions of the geostrophic parts of the equations are:

$$u_E = \pm V_0 \cos \left(\frac{\pi}{4} + \frac{\pi}{D_E} z \right) \exp \left(\frac{\pi}{D_E} z \right), \quad (3.9)$$

$$v_E = V_0 \sin \left(\frac{\pi}{4} + \frac{\pi}{D_E} z \right) \exp \left(\frac{\pi}{D_E} z \right). \quad (3.10)$$

Here $V_0 = (\sqrt{2\pi\tau_{yn}}) / (D_E\rho|f|)$ is the total geostrophic surface current and D_E is the so-called Ekman depth. With the process continuing over depth an Ekman spiral is formed. At the surface the water will be pushed under an angle of 45 degrees to the right of the wind direction.

Upwelling & downwelling

Besides the ageostrophic and geostrophic response of the water column to the wind, the presence of the coast in the Rhine ROFI causes a third movement of the water mass. Assume a stratified water column forced by either an alongshore northerly or an alongshore southerly wind. Due to the Coriolis force the surface water will be pushed to the right of the wind direction. Northerly alongshore winds enhance an off-shore movement of the water surface. By continuity, the water that is pushed away has to be replaced. In front of the coast this water can only come from the bottom layer, a process called upwelling. With southerly alongshore winds the opposite happens. The water at the surface is pushed coastwards, logically this has to result in an offshore movement of the water in the bottom layer. This process is called downwelling. For offshore and onshore directed winds, it is the ageostrophic response of the system that will cause upwelling (offshore directed winds) or downwelling (onshore directed winds). In the Rhine ROFI the prevailing winds come from the southwest and do therefore not simply act upwelling or downwelling favourable (Souza & Simpson, 1996).

Wind direction: straining and mixing

Concerning wind direction, four limit cases for mixing and straining of the water column in the Rhine ROFI can be identified. Alongshore southerly winds, alongshore northerly winds, onshore directed winds and offshore directed winds. In combination with the presence of the coast, the winds can result in either straining or mixing of the water column. In Figure 3.3 a conceptual overview of the different responses of the water column to the different directed winds is presented. In the sketch a start from a water column that is stratified (during a typical neap tide) and one that is well-mixed are considered. For this research the stratified scenarios are of concern.

Northerly winds push the water initially southwards (A1). The Coriolis force then takes the water mass towards the west in offshore direction (A2). The water column will be stratified. As the water at the surface is being transported away from the coast, upwelling in front of the coast has to occur. Southerly alongshore winds push the water in an initial response to the north (B1). Coriolis pushes the water at the surface landwards (B2). The water column will become vertically well-mixed. Due to the presence of the coast additional downwelling will occur. The landward pushed water at the surface has to be compensated by an offshore directed return flow in the bottom layer. An offshore directed wind transports the water in offshore direction (C1). The Coriolis force then transports it northwards (C2). The water column will remain stratified. An onshore directed wind pushes the water initially coastwards (D1), the Coriolis force will then transport the water mass southwards (D2).

The influence of the wind on freshwater plumes have been widely studied in North America. Here the offshore regions are typically deep, which results in a wind-dominated behaviour of the freshwater plume. Hickey *et al.* (2005) showed for instance by field observations the bi-directional behaviour of the Columbia River. During winter the winds are in northerly direction, the plume is also found in northward direction. The wind changes direction in summertime towards the south, which also pushes the freshwater plume southwards. The influence of the Coriolis force transports the plume additionally in offshore direction. The importance of the Ekman drift dynamics (the geostrophic response of the system) is further described by various authors such as Chao & Boicourt (1986); Kourafalou *et al.* (1996a); Fong *et al.* (1997); Fong & Geyer (2001) and Berdeal *et al.* (2002).

Extending these studies, Fong & Geyer (2002) present a simple conceptual model to estimate both the offshore excursion length and the thickness of the freshwater plume under upwelling-favourable alongshore wind conditions. If the alongshore momentum is assumed to be in Ekman balance, the mean cross-shore plume velocity can be estimated as:

$$\bar{u} = \frac{\tau^w}{\rho h f}, \quad \text{where} \quad \tau^w = C_D \rho_a U_a |U_a| \quad (3.11)$$

ρ is the density of the plume, h the thickness of the plume and f the Coriolis parameter. The alongshore wind stress τ^w is calculated by C_D the drag coefficient, ρ_a the density of the air and U_a the velocity of the wind at a height of 10 m above the surface. With an upwelling wind event lasting, the freshwater plume will grow wider in offshore direction over time.

In the Rhine ROFI the tide and wind are competing factors in stratifying and mixing the water column. Souza & Simpson (1996) show with their measurements that wind as a mixing process influences stratification. In experiments carried out in 1992 stratified conditions were measured during spring tide. A well-mixed water column was only observed during periods of strong stirring by the wind. From calculations and experiments they also found that for the Rhine ROFI stirring by the tide and wind are, annually averaged, comparable. However,

since wind stirring occurs over a wider dynamic range than the stirring by the tide, they claim that the wind appears to be the controlling factor over stratification in the Rhine ROFI.

Wind magnitude: advection and mixing

Wind, depending on its magnitude, can work in an advective and mixing manner. For moderate winds (e.g. 5 ms^{-1}) the wind will act as described in the section above; the mixing or straining of the water column is due to the advective transport of the surface layer by the wind. With an increased magnitude of the wind (e.g. 10 ms^{-1}) the water column can also be mixed by what Chao (1988) calls direct wind-induced vertical mixing. This direct mixing by the wind becomes especially interesting once the advective transport of the wind acts straining-favourable. Offshore directed and northerly alongshore winds tend to stratify the water column, the fresh water is pushed over the saline water in offshore direction. As the plume is pushed in offshore direction it becomes thinner. At a certain moment it is thin enough to be mixed directly by the wind. With an increasing magnitude of the wind, the rate of mixing by the wind will also increase.

The conceptual model of Fong & Geyer (2002) can be used for different magnitudes of the wind. Continuing from Equation 3.11, the cross-shore velocity and the density anomaly within the plume can be approximated by linear profiles that vanish beneath the plume. The stability of a stratified flow can then be characterised by a bulk Richardson number:

$$Ri_b \approx \frac{g'h^3}{4\left(\frac{\tau^w}{\rho f}\right)^2} \quad (3.12)$$

Here g' is the mean reduced gravity ($g\overline{\Delta\rho}/\rho_0$; $\overline{\Delta\rho}$ is the mean plume density anomaly). It is now hypothesised that the thickness of the plume at the seaward front is set by the stability of the front to shear-induced turbulence. If therefore the Richardson number is set to some critical value Ri_c , the matching thickness of the plume at the front, h_c , can be estimated by:

$$h_c \approx \left[\frac{4Ri_c \left(\frac{\tau^w}{\rho f}\right)^2}{g\frac{\Delta\rho}{\rho_0}} \right]^{1/3} \quad (3.13)$$

If Equation 3.13 is substituted into 3.11 it is also possible to calculate the cross-shore velocity at the seaward front of the plume:

$$\bar{u}_{front} = \frac{\tau^w}{\rho f h_c}. \quad (3.14)$$

Although the conceptual model of Fong and Geyer is lacking in mixing dynamics, it does suggest something about mixing in the plume. From Equation 3.12 it can be derived that for those parts of the plume thicker than h_c , the plume is stable and not altered by shear-induced turbulence. However if the thickness of the plume approaches the value of h_c , the Richardson number will also approach its critical value, which assumes the likelihood of turbulent mixing. If no gradients in the cross-shore buoyancy exist, the mixing process will lead to a reduction of the salinity anomaly and thereby to an increase in the thickness of the plume, whereby the total buoyancy remains constant (Fong & Geyer, 2002).

3.7 Other processes

Atmospheric radiation and waves also have influence on the behaviour of the Rhine ROFI. Results of heating of the water column will be discussed in short in Chapter 6, waves fall outside the scope of this research. Hereunder both their influence is discussed in short.

Atmospheric radiation

De Kok *et al.* (2000) describe how the salinity front in the Rhine ROFI coincides very often with a temperature front. Near the mouth of the New Waterway and Haringvliet the temperature of the freshwater entering the Rhine ROFI is different from the temperature of the ambient seawater. In the months May and June this difference can be over 10 °C, the seawater is still cold from the winter, while the riverine water has already warmed up due to the shallowness of the river. Depending on the state of the Rhine ROFI the temperature contrast remains visible once the freshwater enters the sea area.

In the near-field freshwater plume, heat exchange between the sea and atmosphere and solar radiation change the the sea surface temperature. The initial difference in temperature between sea- and riverine water is no longer of importance. De Boer *et al.* (2009) state that in a well-mixed Rhine ROFI the surface temperatures do not differ from the adjacent seawater. In contrast once the Rhine ROFI is stratified temperature differences between the plume and surrounding waters can exceed 3 °C (De Kok *et al.*, 2000). The reduced mixing between the surface and bottom layer under stratified conditions also prevents the exchange of heat. Under warm and sunny conditions the heat is confined in the surface layer, which causes higher temperatures in the upper layer. De Kok *et al.* (2000) add that in the case of a moderate wind, bottom-induced turbulent mixing is only found in the bottom layer which thereby does not distribute the solar heat input evenly within the surface layer. It creates the possibility that a strong temperature gradient can arise in the upper layer.

Waves

Two types of waves exist in the southern North Sea. Local wind-generated waves depend on the wind forcing as described previously in this section. Swell waves are created by far away storms and enter the system through its boundaries. Both types of waves mix the water column and larger waves act more de-stratifying. Waves are also very important when determining SPM (Suspended Particulate Matter) concentrations in the Rhine ROFI. Waves mix SPM over the water column, especially during storm- and large swell waves.

Swell waves propagate into the Rhine ROFI as long waves, created in far away storms. As these long waves travel through the shallow Rhine ROFI they create large orbital velocities near the bed. These large orbital velocities induce stirring of the water column through turbulence produced by the boundary stresses (Simpson, 1996). For Souza & Simpson (1996) it was not possible to separate the mixing by locally generated wind-waves from the stirring by swell waves.

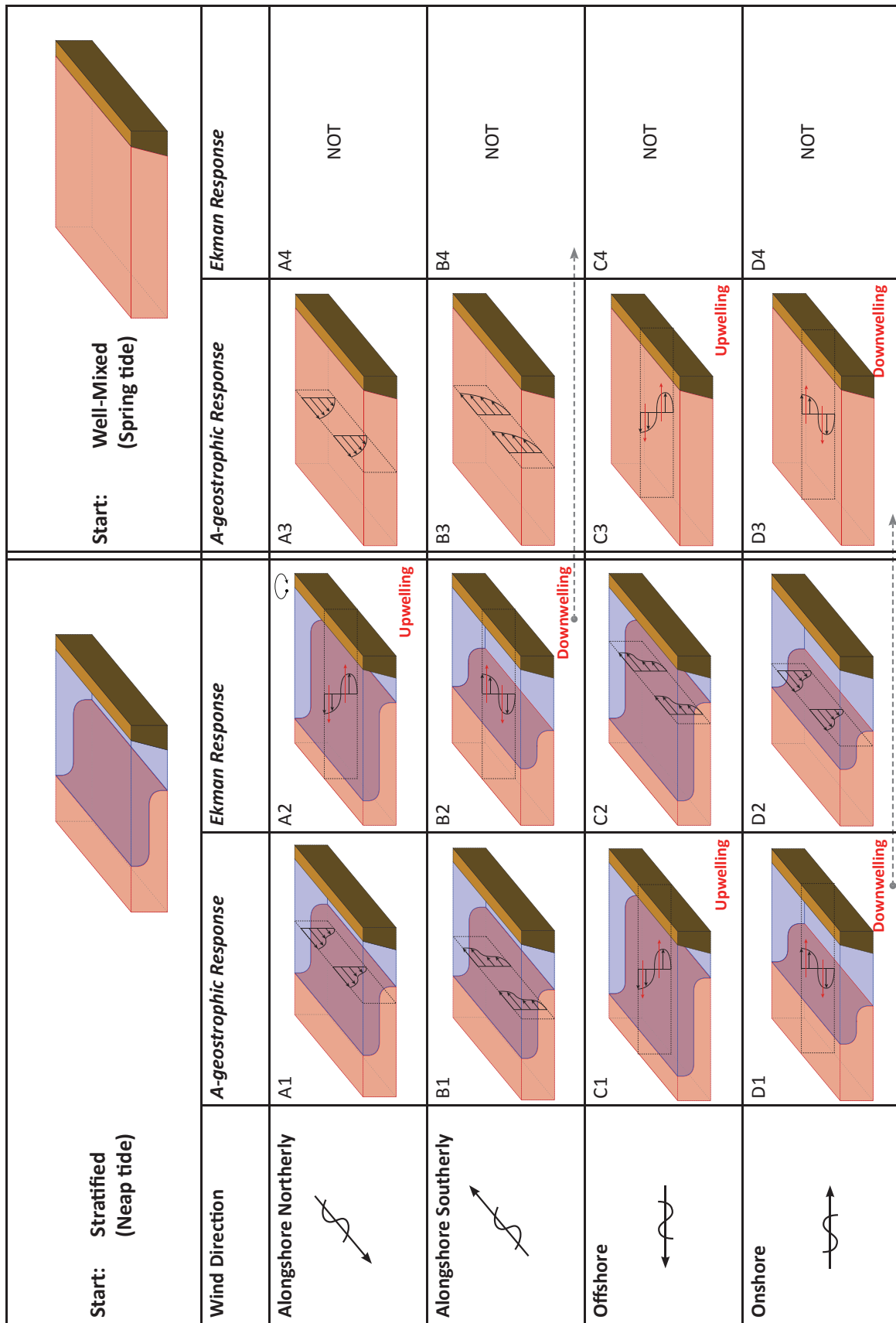


Figure 3.3: Four limit cases of wind in the Rhine ROFI. The conceptual overview presents the ageostrophic and geostrophic responses of the water column to the different types of forcing by the wind.

Chapter 4

Methods

4.1 Introduction

In this Master Thesis the numerical results of the wind-driven motions in the Rhine ROFI are investigated. In this chapter is started with a description of the model setup. The model used is the MoS² ZUNO-DD model, which from here on will be referred to as the model. Prior to the analysis of the numerical results, a sensitivity analysis to the distribution of vertical layers in the model is performed. Six cases were set up that were explored for five different configurations of layers. The main body of this study consists of the physical analysis of the numerical results. Based on one case of the sensitivity analysis, nine wind scenarios were set up and investigated. The approach of the analysis is presented. It is here that the integrated potential energy anomaly, based on the potential energy anomaly method by Simpson & Bowers (1981), is introduced as a new application for the analysis of mixing and straining in the Rhine ROFI.

4.2 Model set-up

The numerical model application used in this study is based on the hydrodynamic modelling package of DELFT3D-FLOW. The model is developed by Deltares and describes the Southern North Sea (ZUNO) with a refinement of the grid towards the Dutch coast through a domain decomposition (DD) technique. In vertical direction the σ (sigma) co-ordinate system is used.

In the σ -coordinate system the vertical layers in the model are bounded by two sigma planes, which are not strictly horizontal but follow the bottom topography and the free surface. DELFT3D-FLOW solves the Reynolds averaged Navier Stokes equations for shallow water under Boussinesq assumptions. The depth averaged equation of state is solved, as well as the equations of transport in both horizontal directions. For the σ -grid the vertical equation of transport is solved under the assumption of hydrostatic pressure. Vertical accelerations due to buoyancy effects and due to sudden changes in bathymetry are not taken into account. The k- ϵ model (Rodi, 1984) is used as turbulence closure scheme to solve the averaged Reynolds equations (Deltares, 2009; Stelling, 1984).

The DELFT3D-FLOW model is forced by the tide at the open boundaries. A space varying windstress is imposed over the full grid. Freshwater discharges of all major rivers into the Southern North Sea are implemented. Heating and cooling occurs at the free surface. Waves are not incorporated in the model. An extended description of DELFT3D-FLOW and its numerical aspects are given in the user manual (Deltares, 2009) and by Stelling (1984). Further description of the MoS² ZUNO-DD model can be found in internal reports by Deltares, such

as Cronin *et al.* (2010).

In the original model a non-equidistant distribution of 12 σ -layers over the vertical has been implemented. In horizontal direction the domain decomposition of the hydrodynamic grid results in three computational grids: a coarse, an intermediate and a fine grid, see Figures 4.1, 4.2 and 4.3. All grids have the same distribution of σ -layers over the vertical. The grid is refined in both horizontal directions by a factor three between the coarse and intermediate grid and another factor two towards the fine grid. Table 4.1 gives the resolution ranges.

Table 4.1: The ranges of horizontal resolution in the three domains of the MoS² ZUNO-DD model. The sizes are global, harbour and river mouth areas can have different shapes and sizes.

Grid:	min (Dx, Dy): [m]	max (Dx, Dy): [m]
Coarse	(6.000, 5.000)	(20.000, 30.000)
Intermediate	(1.000, 2.000)	(2.500, 3.000)
Fine	(500, 1.000)	(1.000, 1.500)

In the model a space-varying bathymetry (depth schematisation) is applied. The bathymetric data for the fine grid originates from a compilation of surveys by the Dutch Hydrographic Service and Rijkswaterstaat, with 2005 as most recent year of surveying. The intermediate and coarse grid bathymetry follow from an international compilation by the North West European Shelf Operational Oceanographic System (NOOS). The data has been interpolated on the multi-domain grid. Calibration of the model by Deltares gave that a correction of 2.5 m extra depth on the NOOS bathymetry was necessary for an accurate representation of the tidal propagation along the Dutch coast. The correction is only applied to the coarse grid, the fine and intermediate grid bathymetric data have not been corrected (Cronin *et al.*, 2010). Influence of the correction on the results in our area of interest is therefore not likely to be expected. Figure 4.4 presents the bathymetry of our area of interest.

Vertical mixing of salt and momentum are solved with the k- ϵ model (Rodi, 1984). The vertical Forester filter for buoyancy destruction (Stelling, 1984) is switched off. Background vertical viscosity and diffusivity are set for all three grids at $5 \cdot 10^{-5}$ and $1 \cdot 10^{-5}$ m²s⁻¹ respectively. The background horizontal viscosity and diffusivity are set at 5, 2.5 and 1.25 m²s⁻¹ for the coarse, intermediate and fine grid respectively. To prevent the development of numerical wiggles over the boundaries of the fine to the intermediate and the intermediate to the coarse grid, the background viscosity and diffusivity is set to 250 m²s⁻¹ at the boundaries. The model is run with a time step of 300 s. It has been spun up over the year 1996 to get the salinity distribution approximately right. It was then followed by a spin up over 2006 to reach equilibrated initial conditions at the start of 2007, the year of interest.

In the current ZUNO-DD version the temperature of the rivers discharging in the Southern North Sea is taken constant at 10 °C. For spring and autumn this comes close to reality, for summer and winter temperatures are warmer and colder respectively. Waves are not incorporated in the model and are therefore left out of consideration in this Master Thesis. It has to be noted that the accompanying MoS² DELFT3D-WAQ model for the calculation of SPM includes waves.

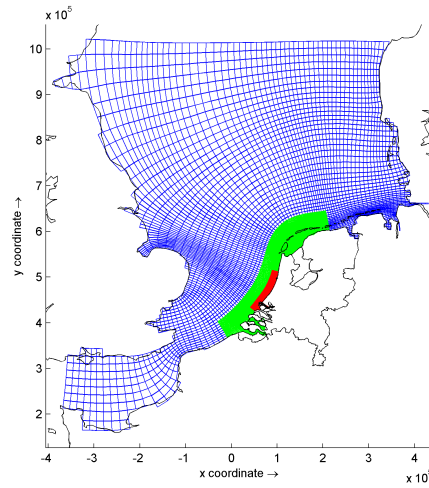


Figure 4.1: Overview of the coarse, intermediate and fine hydrodynamical grids in blue, green and red respectively. The x and y coordinates are in meters (Paris coordinates).

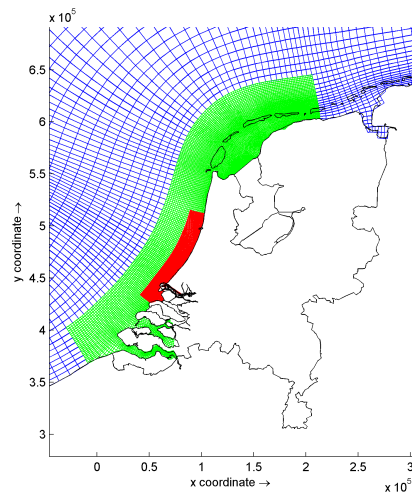


Figure 4.2: As Figure 4.1, zoom into the intermediate and fine hydrodynamical grid.

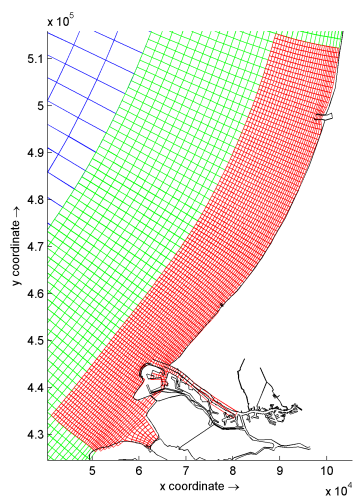


Figure 4.3: As Figure 4.1, zoom into the fine hydrodynamical grid.

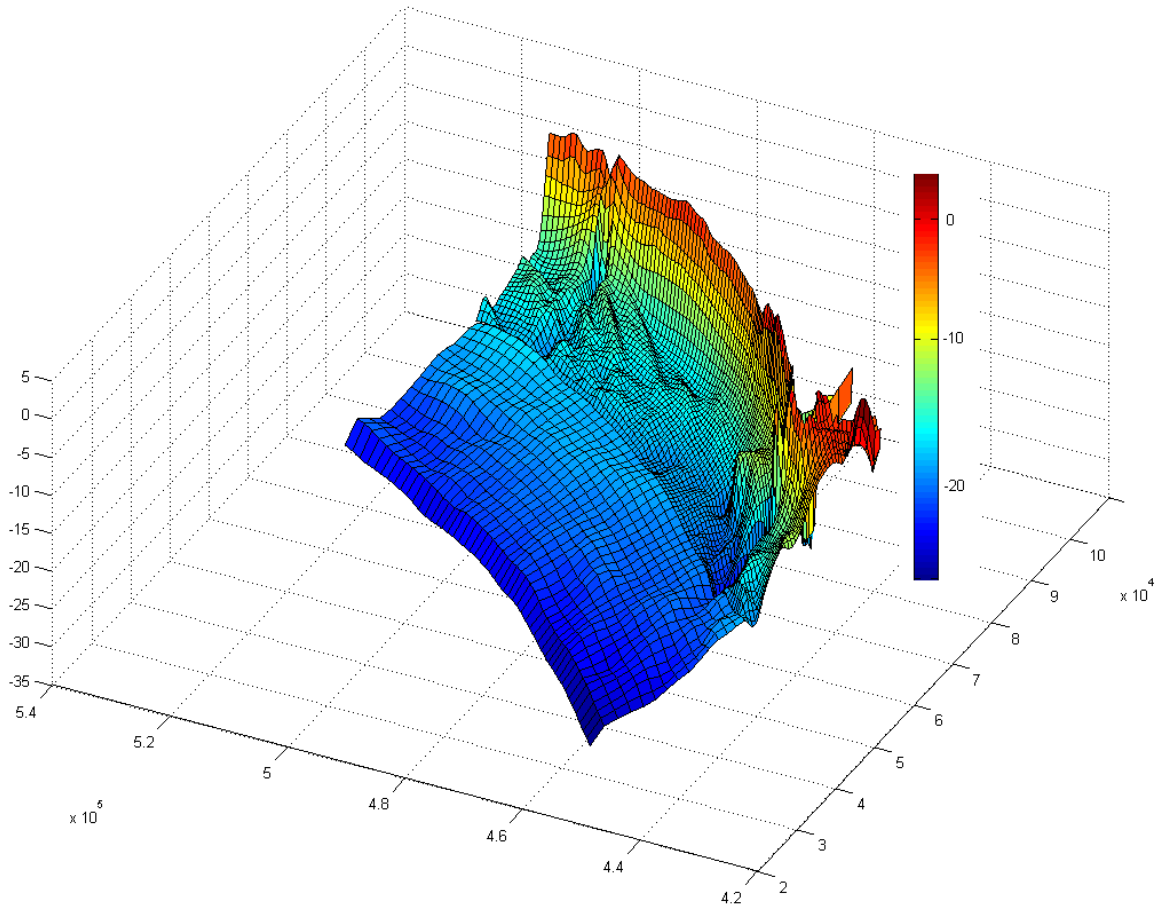


Figure 4.4: Bathymetry of the coast of The Netherlands. The plotted bathymetry stretches from Rockanje in the south to Wijk aan Zee in the north.

4.3 Sensitivity analysis of the model

4.3.1 Vertical grid analysis

In the original ZUNO-DD model a non-equidistant distribution of 12 σ -layers over the vertical was implemented. This choice was made after series of calibration experiments and has been a trade off between maximum accuracy and computational costs. Here is investigated if an extension of the number of layers in the current model would better reproduce stratification in the Southern North Sea. Hence it was decided to study different distributions of layers over the vertical. Table 4.2 gives the five configurations that were tested.

The non-equidistant configurations (B and D) have a higher resolution near the surface and the bottom, in the middle of the water column less layers are present. For the configuration with 48 layers, a high resolution is guaranteed over the whole water column. Since differences in results for the two 48 layers distributions were not expected, it was decided to only run the equidistant 48 layer configuration.

For the numerical analysis of the vertical grid the model was run over the full year of 2007. The first two weeks of January were used as spin-up time for the Configurations B, C, D and E, which are based on the original Configuration A. Six different periods were selected from the input data for the numerical analysis. The six cases have different states concerning tide, wind and river discharge. The state of the water column is largely determined by those three variables. Table 4.3 gives an overview of the cases.

Table 4.2: The five σ -layer configurations tested in the ZUNO-DD model. Configuration E was chosen for the analysis of the numerical results in Chapter 6.

Configuration:	No. of layers:	Vertical distribution:
A	12	equidistant
B	12	non-equidistant
C	24	equidistant
D	24	non-equidistant
E	48	equidistant

Table 4.3: The six cases used for the numerical analysis. Discharge is the combined three day averaged discharge of the Rotterdam Waterway and the Haringvliet.

Case:	Date:	Tide:	Discharge: [m ³ s ⁻¹]	Wind force: [ms ⁻¹]	Direction:	State:
01	15/01/07	Neap	3600	12	southwesterly	stratified
02	28/03/07	Neap	2800	7	southeasterly	stratified
03	13/04/07	Neap	1900	6	northeasterly	stratified
04	05/05/07	Spring	900	7	northwesterly	well-mixed
05	08/12/07	Spring	4700	13	westerly	stratified
06	16/12/07	Neap	5100	6	southeasterly	stratified
mean			2200	5	southwesterly	

Case 04 gives a well-mixed water column. For the numerical analysis of the amount and distribution of layers over the vertical the stratified periods of the Southern North Sea are most valuable due to the presence of a pycnocline. The well-mixed periods are less interesting since no pycnocline has to be captured by the model. It was therefore decided to only use the stratified cases for the numerical analysis.

For the numerical phenomena to be measured, the smaller timescales and the instantaneous model results have to be investigated. In the fine and intermediate grid of the model four stations of interest were chosen: Ter Heijde 10, Noordwijk 01, Noordwijk 10 and Noordwijk 30, see Figure 4.5. For those stations the Salinity, Eddy Viscosity, Richardson Number profiles, the position of the pycnocline and whether the different configurations showed convergence have been investigated for increasing vertical resolution.

4.3.2 Horizontal grid analysis

As already stated the vertical grid analysis is based on the six cases as given in Table 4.3. While performing the physical analysis of the numerical results nine scenarios were constructed. From that analysis it followed that some study on the horizontal grid was required. Under strongly stratified conditions the freshwater plume can extend over a wide region, as far up as in the intermediate grid. Steep gradients over the grid cells are likely to be expected. Cronin *et al.* (2010) in their report of the model also give remarks and conclusions on the hydrodynamical grid of the model. The analysis carried out is limited and mainly consists of observations and recommendations.

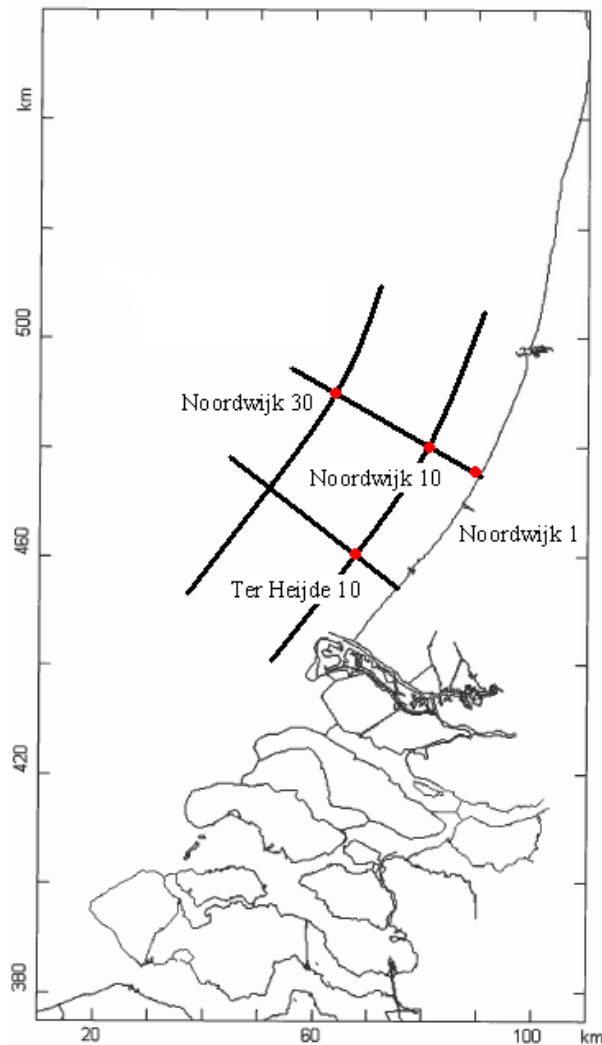


Figure 4.5: The four observations stations used for the numerical analysis: Ter Heijde 10, Noordwijk 01, Noordwijk 10 and Noordwijk 30. Also indicated are the cross-shore and alongshore transects used in the physical analysis of the model results.

4.4 Physical analysis of the model results

The focus in this study is on the straining and mixing by the tides and wind. In the physical analysis of the model results the interest is with the response of the Rhine ROFI to the wind. To that end the salinity and temperature profiles of the Rhine ROFI due to different forcings by the wind are investigated. It is of interest whether a certain response to the forcing can be observed. Based on Simpson & Bowers (1981), who developed the potential energy anomaly (ϕ) concept, this study will use a new application of this method; the integrated potential energy anomaly. The combination of this new application with the spatial change of ϕ provides the possibility to analyse combined mixing and straining by the wind and the tide. The tide and the wind can work in either an upwelling- or downwelling-favourable direction. It is investigated whether upwelling or downwelling occurs off the coast of The Netherlands.

For the physical analysis of the model results, Case 03 as used in the sensitivity analysis is used as a start situation. Case 03 is run April 13 2007, under neap tide and with an averaged value for river discharge and wind. Simpson (1996) found that for such a typical neap tide the water column is stratified. Based on Case 03 nine scenarios were defined with winds

varying in direction and magnitude. Table 4.4 gives the set-up of the different scenarios. The different directions of the wind are in alongshore and cross-shore direction. In Scenario 01 a zero wind is implemented as tidal reference scenario, Scenarios 02 to 05 are forced by moderate winds, Scenarios 06 to 09 by strong winds. All scenarios cover a 60 hour period.

Table 4.4: The nine scenarios used for the physical analysis of the wind-driven motions in the Rhine ROFI. All scenarios are based on Case 03 of the sensitivity analysis, 13/04/2007, where the Rotterdam Waterway and Haringvliet have a combined discharge of 1900 ms^{-1} under neap tide conditions.

		Direction			
		Northerly	Offshore	Southerly	Onshore
Magnitude	0 [ms^{-1}]	01			
	5 [ms^{-1}]	02	03	04	05
	10 [ms^{-1}]	06	07	08	09

4.4.1 Salinity profiles

The physical analysis of the Rhine ROFI is started by creating salinity profiles. All scenarios were ran for 60 hours, of which the first twelve as spin-up time. The remaining 48 hours were used for the analysis.

To capture the processes in the Rhine ROFI, 48-hour averaged salinity profiles in cross-shore and alongshore direction were made and combined with snapshots of the salinity profiles over the entire Rhine ROFI in the surface layer of the model. The cross-shore sections are taken off the coast at Ter Heijde and Noordwijk over a length of 35 km in offshore direction. The alongshore transects are taken 10 and 30 km offshore between Rockanje and Wijk aan Zee. The combination of the four transects presents the state of the Rhine ROFI over the vertical in x - and y -direction. Snapshots of the salinity profile in the top layer of the Rhine ROFI were also created. The snapshots show the size of the stratification. The snapshots are taken every two hours during the last ebb-flood tidal cycle. It creates the possibility to observe the interaction of the plume with the tide, both in alongshore and cross-shore direction. Since the final state of the system is of concern in this study, it was decided to create the profiles over the last ebb-flood tidal cycle of the 60 hours of computations.

4.4.2 Temperature

The same snapshots that are created for the analysis of the salinity field in the Rhine ROFI are made for the temperature of the water in the surface layer of the Rhine ROFI. The snapshots show whether the freshwater plume heats up during the day and whether the ambient seawater remains constant in temperature. It will also provide the possibility to observe whether the largest gradients in salinity and temperature coincide with each other.

4.4.3 Potential Energy Anomaly

This part of the study focusses on the competition and interaction between the wind and the tide as sources of straining and mixing in the Rhine ROFI. Expressions of potential energy have been found to be valuable in studying the competing processes in ROFI's. Simpson & Bowers (1981) introduced the potential energy anomaly (ϕ) concept. It is based on the fact that a certain amount of potential energy is required to bring a stratified water column into a well-mixed state. Changes in potential energy relative to the well-mixed condition are

considered and defined in a scalar parameter ϕ [Jm^{-3}]. It is the depth averaged amount of energy required to obtain a fully mixed water column:

$$\phi = \frac{1}{H} \int_{-h}^{\eta} (\hat{\rho} - \rho)gzdz, \quad \text{where} \quad \hat{\rho} = \frac{1}{H} \int_{-h}^{\eta} \rho dz. \quad (4.1)$$

H is the depth of the total water column [m], given by $H = \eta + h$, η the free surface, h the location of the bed with reference to the mean water level. ρ is the water density [kgm^{-3}], g the acceleration due to gravity (9.81 ms^{-2}) and z the depth interval [m]. For a larger ϕ , the water column is more stratified.

The same spatial plots of ϕ as of the salinity and temperature in the Rhine ROFI are created. The plots do not only present the total stratification in the Rhine ROFI (if present), but also the spatial distribution of ϕ and thereby the positioning of the (strongest) stratification within the Southern North Sea.

To be able to investigate the interaction and competition between the tide and the wind in mixing and straining of the Rhine ROFI a new application of the ϕ concept is applied. Based on Simpson & Bowers (1981), ϕ is integrated over depth and over the total surface area of the Southern North Sea as given in Figure 4.5, which captures the whole area of the Rhine ROFI. It results in the total amount of energy required to bring the whole Rhine ROFI into a well-mixed state:

$$E = \iiint \phi \, dAdz. \quad (4.2)$$

With this new method it is possible to present the evolution of the total amount of ϕ over time. By plotting the results of all nine scenarios into one figure a comparison is easily made.

Besides the temporal evolution of ϕ for the different directions and magnitudes of the wind, it is also of interest to investigate the spatial changes of ϕ . During the last high water of the investigated time interval the results of the tidal reference scenario are subtracted from the results of the different wind scenarios. The results provide the possibility to present, for the different directions and magnitudes, the spatial distribution of straining and mixing by the wind. It will be shown that the results of the integrated potential energy anomaly and the results of the spatial change of the potential energy anomaly can be linked together.

4.4.4 Upwelling & downwelling

As described in Chapter 3 both the tide and the wind can cause cross-shore currents that lead to upwelling and downwelling near the coast. From de Boer (2009) it is known that upwelling by the tide is maximal at slack before flood. Slack before ebb results in downwelling. Concerning the influence of the wind, it is hypothesised that winds with an onshore component (southerlies and onshore directed) work in favour of downwelling, while winds with an offshore component (northerlies and offshore directed) work upwelling-favourable.

From the numerical results the vertical velocity ω , defined at the σ -surfaces, is extracted. ω is the vertical velocity relative to the moving σ -plane. Vertical velocities caused by variations in water level during high- and low water are thereby filtered out and ω may be interpreted as the velocity associated with up- or downwelling motions (Deltares, 2009).

For all scenarios plots (snapshots) of ω over the entire Rhine ROFI are created, in order to observe the spatial distribution of up- and downwelling. The plots are based on the results in

the middle layer of the model. Analysis of the results showed that the same velocity profile was also observed in the other layers of the model. For each scenario two plots are presented, one at slack before ebb, a second at slack before flood.

Chapter 5

Sensitivity analysis of the model

5.1 Introduction

In the sensitivity analysis of the model the five different layer configurations as given in Table 4.2 are compared to investigate whether a better reproduction of stratification in the Rhine ROFI can be achieved. The six cases from the 2007 input data of the ZUNO-DD model (Table 4.3) are the basis of this analysis.

In Section 5.2 the systematic similarities and differences between the 5 layer configurations are discussed. In this study the sensitivity and the convergence of the model are relevant for the reproduction of cross-shore straining and mixing. It is important to notice that the original implementation of 12 non-equidistant distributed σ -layers seems to reproduce the state of the Rhine ROFI well. It is only under certain stratified conditions that an increased amount of layers could be desirable. In a summarised form those periods are discussed. The sensitivity analysis as performed is lacking field data for proper validation. Within the context of this study a relative comparison of the five layer configurations is carried out. The point of departure in the analysis is that the 48 layer configuration gives the most accurate results.

A thorough analysis of the horizontal grid has already been performed by Deltares, see e.g. Cronin *et al.* (2010) and other internal Deltares reports. Results of the physical analysis of the model (Chapter 6) showed however that also some remarks on the horizontal grid of the model are required. The results are presented in Section 5.3.

5.2 Vertical grid analysis

According to the theory of tidal straining in the Rhine ROFI by Simpson & Souza (1995) and further studied by de Boer *et al.* (2007), the water column is maximally stratified at high water. The aim of this sensitivity analysis is to investigate whether the pycnocline is properly captured by the model. For the four stations (Ter Heijde 10, Noordwijk 01, 10 and 30, see Figure 4.5) is therefore focussed on periods of high water under stratified conditions.

5.2.1 Salinity Profiles

Station Ter Heijde 10 is situated close to the mouth of the New Waterway. For this station the salinity profiles of Configurations C, D and E are for all cases largely consistent. Near the bottom Configurations A and B also show convergence for most of the cases. At the surface and around the pycnocline Configurations A and B are divergent. From Figure 5.1(a) is observed that for Case 01 the salinity profiles for the twelve layer distributions show a

statically unstable solution: The water column at -4.0 m is more saline than at -6.0 m depth. The plots of the Eddy Viscosity (Figure 5.1(b)) and Richardson Number confirm these results.

For modelling with the 24 and 48 layer configurations (C, D and E) a new numerical phenomenon shows up, so-called ‘staircases’. The stations Noordwijk 10 and Noorwijk 30 also exhibit the phenomenon. A good example is shown in the results of Case 06 for Station Noordwijk 10, see Figure 5.1(c). Between -9.0 m and -2.0 m depth the salinity profiles have a step-wise profile. It also results in the peaked profiles of Eddy Viscosity between -9.0 m and -2.0 m depth, see Figure 5.1(d). The phenomenon is treated in Section 5.2.2.

Station Noordwijk 01 is situated close to the shore. Except for Case 02 the water column is, for all configurations, always well-mixed and results in straight vertical salinity profiles. The eddy viscosity profiles for those cases are also consistent for all five configurations. However some differences exist between the salinity values for the five configurations. Maximum differences range from 0.2 PSU (Case 01) to 0.6 PSU (Case 03). In most cases the value of salinity for the 48 layer configuration lies between the 12 and 24 layer configurations, but not necessarily (e.g. Case 03). Most probably the differences have come already to existence close to the Rotterdam Waterway and while moving northwards they have not disappeared.

Results for Station Noordwijk 10 are most of the time not consistent, only cases 01 and 02 show reasonable convergence for Configurations C, D and E. In case 06 the differences between Configurations D and E are noticeable. Both configurations have the same distribution of layers near the surface and bottom of the water column. However results for salinity differ from each other. Certain phenomena occur in the middle of the water column which influence the results in other parts of the water column. This idea is confirmed if the results for Configurations C and E are observed. They are the configurations with the highest resolution in the middle of the water column. Towards the bottom and surface C and E also give the same results, however Configuration C has a factor two less resolution in those regions.

Cases 02, 03 and 06 give for the 24 and 48 layer configurations again staircases. Plots of the eddy viscosity also show the presence of the staircases by their peaky profiles. However in most cases the eddy viscosity profiles do make it possible to give the height where the actual pycnocline is situated in the water column.

Station Noordwijk 30 gives variable successes concerning convergence. In Cases 01 and 05, for all configurations, the salinity profiles give a well-mixed water column. This is also confirmed by plots of the eddy viscosity. Cases 02 and 06 have both a pycnocline around -2.0 m depth. For Case 06 the 24 and 48 layer configurations (C, D and E) are convergent, staircases are also present. Case 02 is convergent in the bottom and middle layers for all 5 configurations, at the surface no convergence is observed. From the eddy viscosity plot a clear pycnocline is visible at -2.5 m depth for all five configurations.

Case 03 shows convergence in the bottom layer for Configurations B, C, D and E. Near the surface large differences in values of salinity are observed, over 2 PSU of difference between Configurations A and B. The results for the other configurations do also not converge, see Figure 5.2(a). A possible explanation can be found in the time field of salinity for Station Noordwijk 30. The water column is only for short periods after high water stratified. Figure 5.2(b) gives the 48 hour time field of Configuration E. The configurations with less layers, especially those with 12, have difficulties reproducing this salinity field.

5.2.2 Staircases

A problem that arises when modelling with a higher vertical resolution is the formation of so-called ‘staircases’. Staircases are step-wise temperature and density profiles. A certain

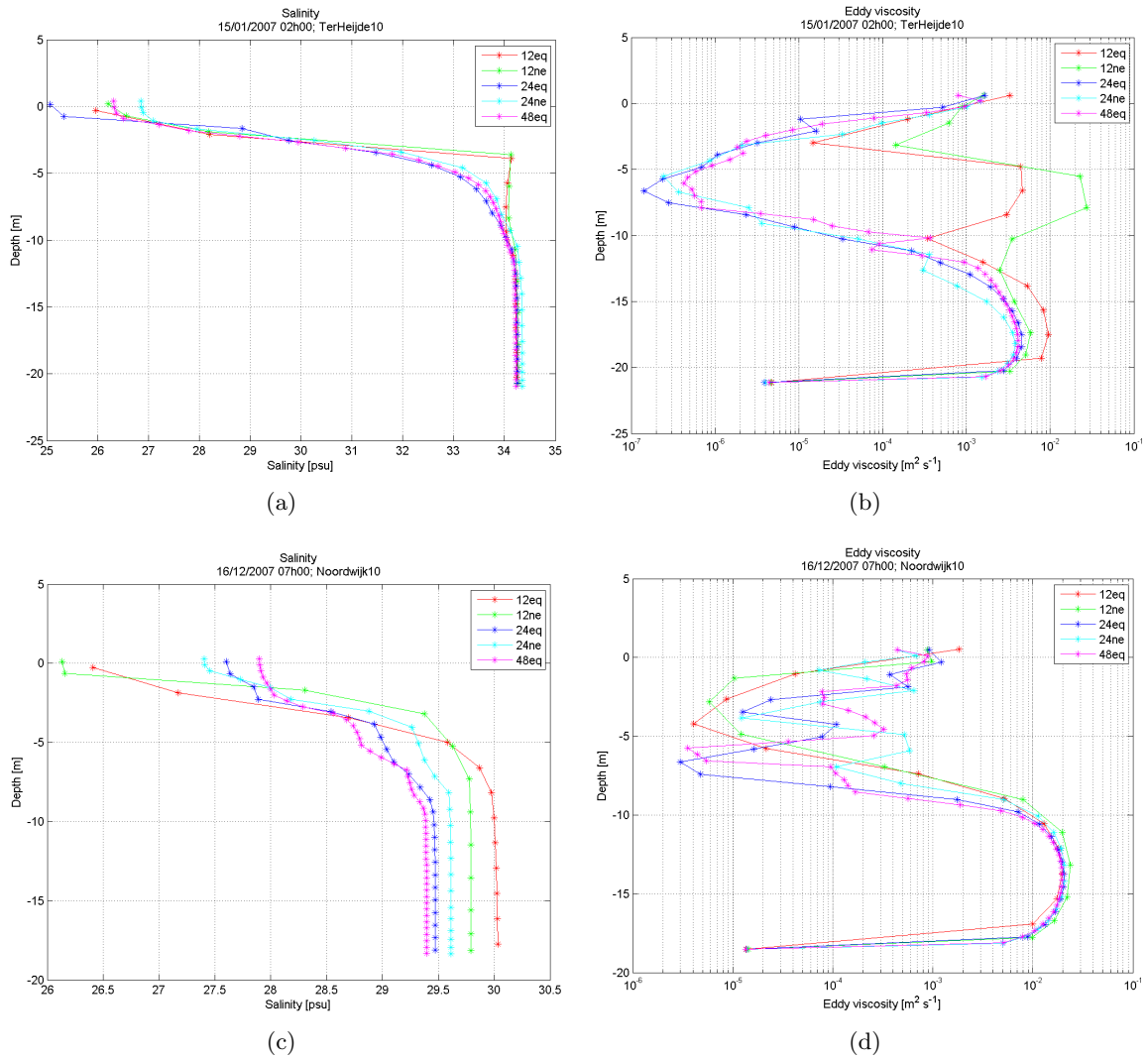


Figure 5.1: (a) Salinity profile of Case 01 for station Ter Heijde 10 at 15/01/07 02:00. Configurations A and B show statically unstable solutions at -4.0 m depth. (b) As in (a), but now for the eddy viscosity. Configurations C, D and E show a pycnocline around -6 m depth. The twelve layer configurations confirm the behaviour of the salinity profiles. (c) Salinity profiles of Case 06 for Station Noordwijk 10 at 16/12/07 07:00. Configurations C, D and E show a staircase salinity profile between -9.0 and -2.0 m depth. (d) As in (c), but for the eddy viscosity. The staircases for Configurations C, D and E in the salinity profiles result in the peaky eddy viscosity profiles in the upper part of the water column.

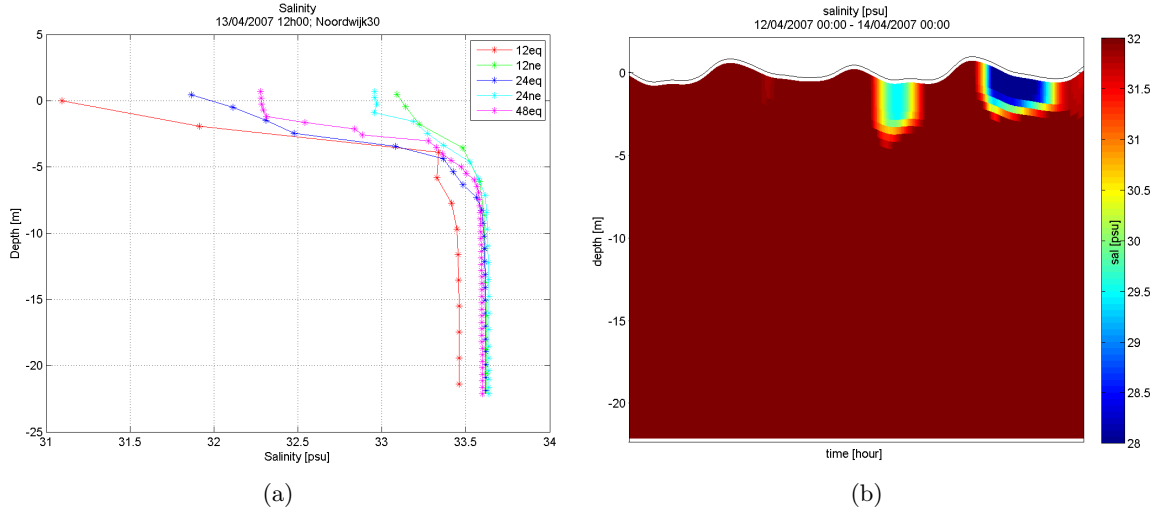


Figure 5.2: (a) Salinity profile of Case 03 for station Noordwijk 30 at 13/04/07 12:00. Near the bottom Configurations B, C, D and E are convergent, at the surface no convergence is seen. (b) 48 hour time field of salinity distribution in Station Noordwijk 30 for Configuration E. The second ‘blob’ of freshwater corresponds with the salinity profiles of (a).

type of staircases does exist in nature. Their main presence is however in isolated water masses in the ocean, induced by stratification and different rates of diffusion of heat and salt, see e.g. Phillips (1972). In the Southern North Sea such double-diffusive phenomena are not expected to occur. The presence of the staircases in the ZUNO-DD model is of numerical nature. The mathematical background for the staircases to exist both in the nature as in the numerics is though the same and is described by Barenblatt *et al.* (1993).

Under the assumption that no horizontal differences in the local field of concentration (or salinity) exist, the evolution equation for concentration over the vertical is given by:

$$\frac{\partial c}{\partial t} - \frac{\partial}{\partial z} D_v \left(\frac{\partial c}{\partial z} \right) \frac{\partial c}{\partial z} = 0 \quad (5.1)$$

$$\frac{\partial c}{\partial t} - \left(D_v \frac{\partial c}{\partial z} \frac{\partial^2 c}{\partial z^2} + D_v \frac{\partial c}{\partial z} \frac{\partial^2 c}{\partial z^2} \right) = 0 \quad (5.2)$$

$$\frac{\partial c}{\partial t} - \left(D_v \frac{\partial c}{\partial z} \frac{\partial c}{\partial z} + D_v \frac{\partial c}{\partial z} \right) \frac{\partial^2 c}{\partial z^2} = 0 \quad (5.3)$$

Where c is the local concentration and D_v the vertical diffusivity.

Now Φ is taken as the magnitude of the diffusive vertical concentration flux: $\Phi = D_v \left(\frac{\partial c}{\partial z} \right)$, typical choices of D_v are suggested experimentally according to Figure 5.3. For stable stratification the turbulence is suppressed and the concentration exchange efficiency is reduced. Φ has to go to zero. It results in two possible solutions:

$$D_v \left(\frac{\partial c}{\partial z} \right) = 0 \quad \text{for} \quad \frac{\partial c}{\partial z} = 0 \quad (5.4)$$

$$D_v \left(\frac{\partial c}{\partial z} \right) = 0 \quad \text{for} \quad \frac{\partial c}{\partial z} \rightarrow \infty \quad (5.5)$$

With these solutions the formation of staircases is explained, see Figure 5.4. Attempts were made to suppress the formation of staircases by the application of a vertical Forrester filter

for buoyancy destruction (Stelling, 1984). Some tests gave however no satisfying results, the step-wise salinity profiles were still observed.

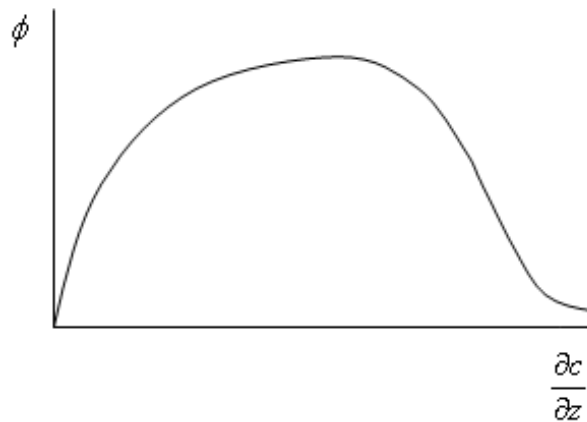


Figure 5.3: Experimentally found distribution of the absolute value of concentration flux, Φ . Figure by Barenblatt *et al.* (1993).

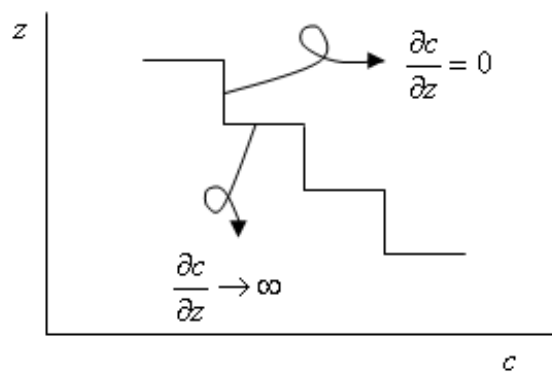


Figure 5.4: Schematic overview of a staircase, the limit values follow from Equations 5.4 and 5.5.

5.3 Horizontal grid analysis

From the numerical analysis of the physical results in Scenario 06 (see Table 4.4), it was concluded that it is most desirable to capture the stratification within the fine grid of the model. Processes of mixing and straining affecting the stratification that are calculated on the finest numerical grid should in principal give the most accurate solutions.

In the results of Scenario 06 the freshwater plume reaches up into the intermediate grid (see Figures 5.5(a) and 5.5(b)). This is undesirable for the analysis of the stratification since less resolution of the gradients in plots of salinity, temperature and potential energy is available. It has to be noticed that for Scenario 06, although large gradients exist, no wiggles in the velocity distribution arise.

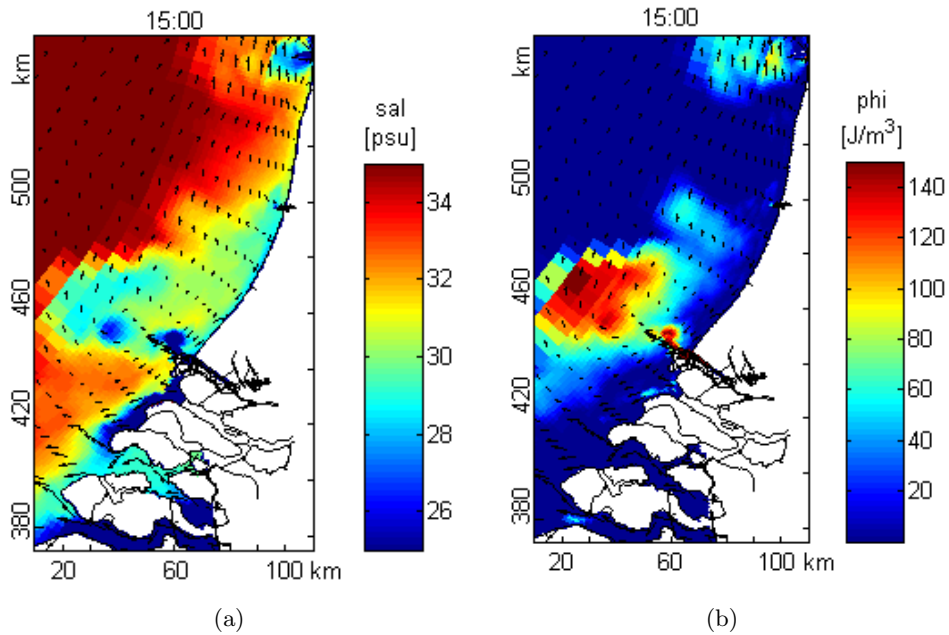


Figure 5.5: (a) Topview of the salinity distribution over the Southern North Sea for Scenario 06. The plume is pushed into the intermediate grid, where large gradients come to existence. (b) The same as in (a) only for the potential energy distribution.

5.4 Conclusions and Recommendations

The original implementation of 12 non-equidistant distributed σ -layers reproduces the state of the Rhine ROFI well. However, under certain stratified conditions at least 24 layers are required. From the combined results of both 24 layer configurations it can be concluded that a high resolution is desirable both in the middle and near the edges of the water column. Therefore best is worked with an equidistant 48 layer distribution.

Working with 24 and 48 layers introduces a new phenomenon: staircases. Some tests trying to suppress the phenomenon with a vertical Forrester filter gave unsatisfying results. Since time-averaged values of the scenarios will be used for the physical analysis in Chapter 6, the staircases will be flattened out and no longer form a critical problem.

Under certain conditions the freshwater plume reaches up into the intermediate grid. It is undesirable for the analysis of the stratification since less resolution of the gradients in plots of salinity, temperature and potential energy is available. It is recommended to enlarge the fine grid seawards, roughly between the Haringvliet and Noordwijk in order to capture the whole freshwater plume within the fine grid.

Chapter 6

Physical analysis of the model results

6.1 Introduction

The physical analysis of the model results is the main topic of this Master Thesis. The aim is to gain a further understanding of the interaction and competition between the wind and the tide in mixing and straining of the water column. In Table 6.1 the nine scenarios that are used in this numerical experiment of the wind-driven motions in the Rhine ROFI are presented. All scenarios are based on Case 03 as used in the sensitivity analysis of Chapter 5. The scenarios are run under neap tide conditions with a combined discharge of the Rotterdam Waterway and Haringvliet of $1900 \text{ m}^3\text{s}^{-1}$, which can be considered as an average discharge. First the results of the no-wind tidal reference scenario will be presented. They provide a good reference for analysing the influence of wind-mixing and wind-straining in the Rhine ROFI.

Table 6.1: The nine scenarios used for the physical analysis of the wind-driven motions in the Rhine ROFI. All scenarios are based on Case 03 of the sensitivity analysis, 13/04/2007, where the Rotterdam Waterway and Haringvliet have a combined discharge of $1900 \text{ m}^3\text{s}^{-1}$ under neap tide conditions.

		Direction			
		Northerly	Offshore	Southerly	Onshore
Magnitude	0 [ms^{-1}]	01			
	5 [ms^{-1}]	02	03	04	05
	10 [ms^{-1}]	06	07	08	09

The temporal evolution of the freshwater plume is investigated in Section 6.2. Both the ageostrophic (frictional) and geostrophic (Ekman) response of the system will be presented. The salinity profiles of the different scenarios will also be analysed. First the results of the tidal reference scenario (no wind) are presented. Then the impact of the magnitude and direction of the wind is investigated. Use is made of 5 and 10 ms^{-1} wind scenarios, such that the influence of direction and magnitude of the wind can be analysed. The thermal heating of the freshwater plume by solar radiation is presented in Section 6.3. The results of the the newly developed integrated potential energy anomaly method are presented in Section 6.4. In Section 6.5 the results of wind-driven upwelling and downwelling are presented. Results of the reference tidal scenario make it possible to also show upwelling and downwelling by the tide.

In the literature of wind-driven motions in river plumes it is commonly used to refer to upwelling- and downwelling-favourable winds if one discusses alongshore winds. Due to the presence of the Dutch coast at the east side, alongshore northerly winds are regarded to as upwelling-favourable winds, alongshore southerly as downwelling-favourable winds.

6.2 Freshwater plume

Tidal reference scenario

In Figure 6.1 the 48-hour averaged salinity profiles of the cross-shore sections Ter Heijde and Noordwijk and the alongshore sections 10 and 30 km offshore are presented, see Figure 4.5. In the cross-shore section of Ter Heijde the first 20 km of coastline are stratified. In the upper layer salinity values of 25 PSU are found, whereas near the bottom the values go up to 33 PSU. The part of the freshwater plume off the coast at Ter Heijde can be regarded as the bulge of the plume. In the cross-shore section of Noordwijk the width of the freshwater plume is brought back to 10 km, this part of the plume is regarded to as the coastal current. Since the cross-shore section of Ter Heijde is situated close to the mouth of the Rotterdam Waterway it is there that the strongest stratification is observed. Neap tide is in favour of straining, see Figure 2.1, variation over the ebb-flood tidal cycle results in mixing of the water column while going from high to low water. The water column in the cross-shore section of Noordwijk is less stratified. The alongshore section 10 km offshore confirms this analysis. Near the mouth of the Rotterdam Waterway the freshwater plume is thickest. Both towards the north and to the south the plume becomes thinner. Moving in offshore direction, the results of the 30 km offshore transect show that the water column is well-mixed with a salinity of 35 PSU.

The top panels in Figure 6.2 present the two-hourly snapshots of salinity in the top layer of the Rhine ROFI during the last ebb-flood tidal cycle. In the absence of wind both the cross-shore and the alongshore tidal currents can be observed. In the alongshore direction the freshwater plume moves with the ebb-flood tidal cycle. The plume has made its maximum northwards excursion at slack when ebb begins (17:00), at slack when flood begins (23:00) the plume has reached the farthest south. The freshwater plume makes roughly a 20 km north-south excursion over the ebb-flood tidal cycle. In the cross-shore direction the effect of the straining-favourable flood and the mixing-favourable ebb is observed (Simpson & Souza, 1995). The averaged width of the plume is 40 km. It is with 45 km at its widest at high water (13:00) and with 35 km at its smallest at low water (19:00). The results are consistent with the theory of tidal straining in the Rhine ROFI as derived by Visser *et al.* (1994); Simpson & Souza (1995) and de Boer *et al.* (2007), see Figure 2.1.

6.2.1 Direction of the wind

Alongshore winds

Figure 6.2 shows the response of the Rhine ROFI to alongshore winds, both northerly (middle panel) and southerly (bottom panel). For both directions of the wind the Ekman response of the system to the wind is directly observed. The frictional (ageostrophical) response to the alongshore northerly wind (middle panel) pushes the freshwater southwards. The Ekman dynamics transport the freshwater in offshore direction. The freshwater plume swings with the tide, the north-south excursion over the ebb-flood tidal cycle is roughly 15 km. The plume has a maximum width of 60 km in front of the mouth of the Rotterdam Waterway at high water (13:00). At low water the plume is most narrow (19:00). The southerly alongshore wind pushes the freshwater northwards, Ekman dynamics force it in onshore direction. The freshwater plume is between 10 and 20 km wide. Around the mouth of the Rotterdam Waterway the influence of the ebb-flood tidal current is best observed. The plume has moved

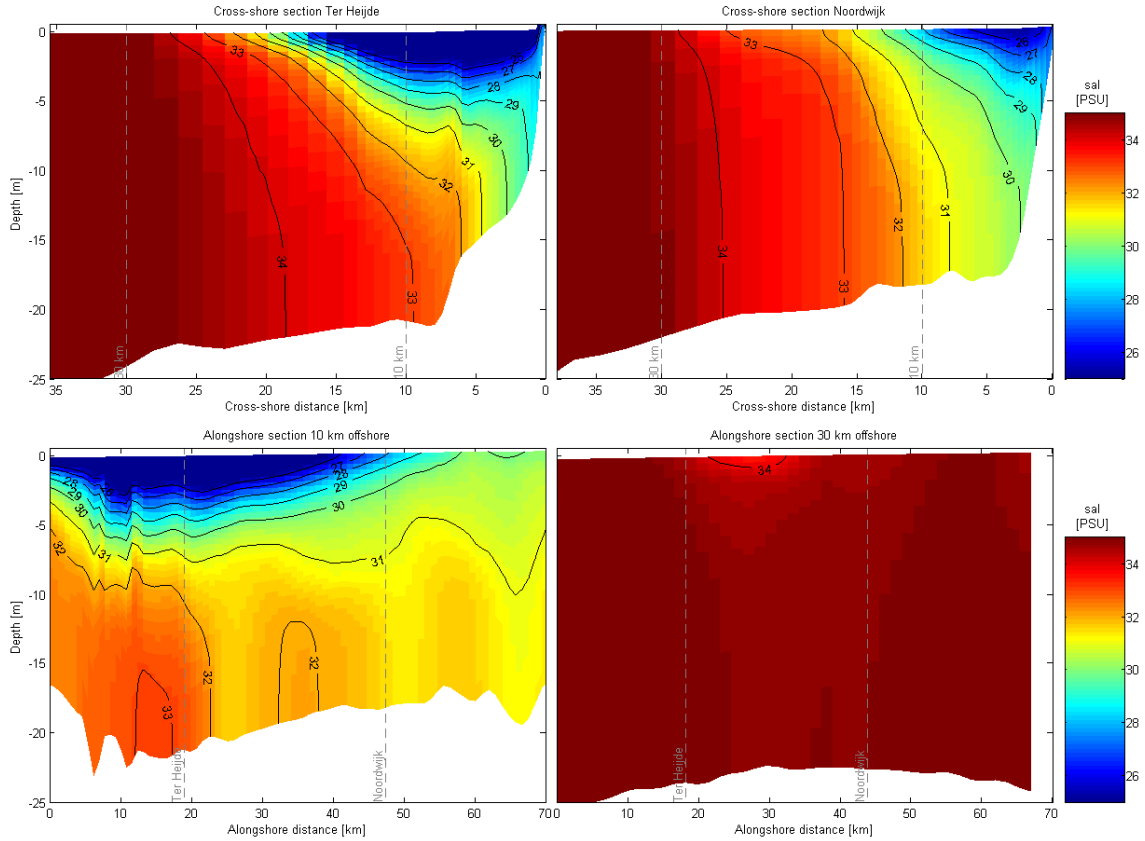


Figure 6.1: 48-hour averaged salinity profiles of the no wind scenario. The top left panel presents the results of the cross-shore section in Ter Heijde, the top right is the cross-shore section in Noordwijk. The bottom left panel is the alongshore sections 10 km offshore, the bottom right is the alongshore section 30 km offshore.

maximally northwards at slack before ebb (17:00) and maximally southward at slack before flood (23:00). It has stretched maximally in offshore direction at high water (13:00) and has come closest to the coast at low water (19:00). From the 48-hour averaged salinity profiles, Figure 6.4 (discussed in more detail hereafter), it is observed that mixing by the wind is happening and that it results in a vertically well-mixed water column.

Although the Ekman dynamics dominate the system, there is also an ageostrophic (or frictional) response of the freshwater to the wind visible in the results (Figure 6.2). The alongshore southerly wind pushes the water northwards: water with a salinity of 26 PSU is found as far north as IJmuiden. For the forcing by the northerly wind the Ekman dynamics dominate the system. Therefore the freshwater plume is not transported as far southwards as the southerly wind brought the freshwater plume northwards. The 26 PSU boundary in the north has however, compared to the results of the no wind scenario (top panel), clearly been pushed south of Scheveningen.

Figure 6.3 presents the 48-hour averaged salinity profiles for the northerly wind forcing. The ageostrophic response of the water column to the wind is to be pushed southwards. The Ekman response is to push the freshwater in offshore direction. The freshwater is accumulated near the mouth of the Rotterdam Waterway (Ter Heijde) and stretches over a width of 35 km. The plume becomes thinner as the plume stretches farther offshore. In Noordwijk the minimum salinity of the water column has gone up to 29 PSU. The Ekman response in offshore direction can be noticed in the salinity profile of the alongshore section 30 km offshore. Over

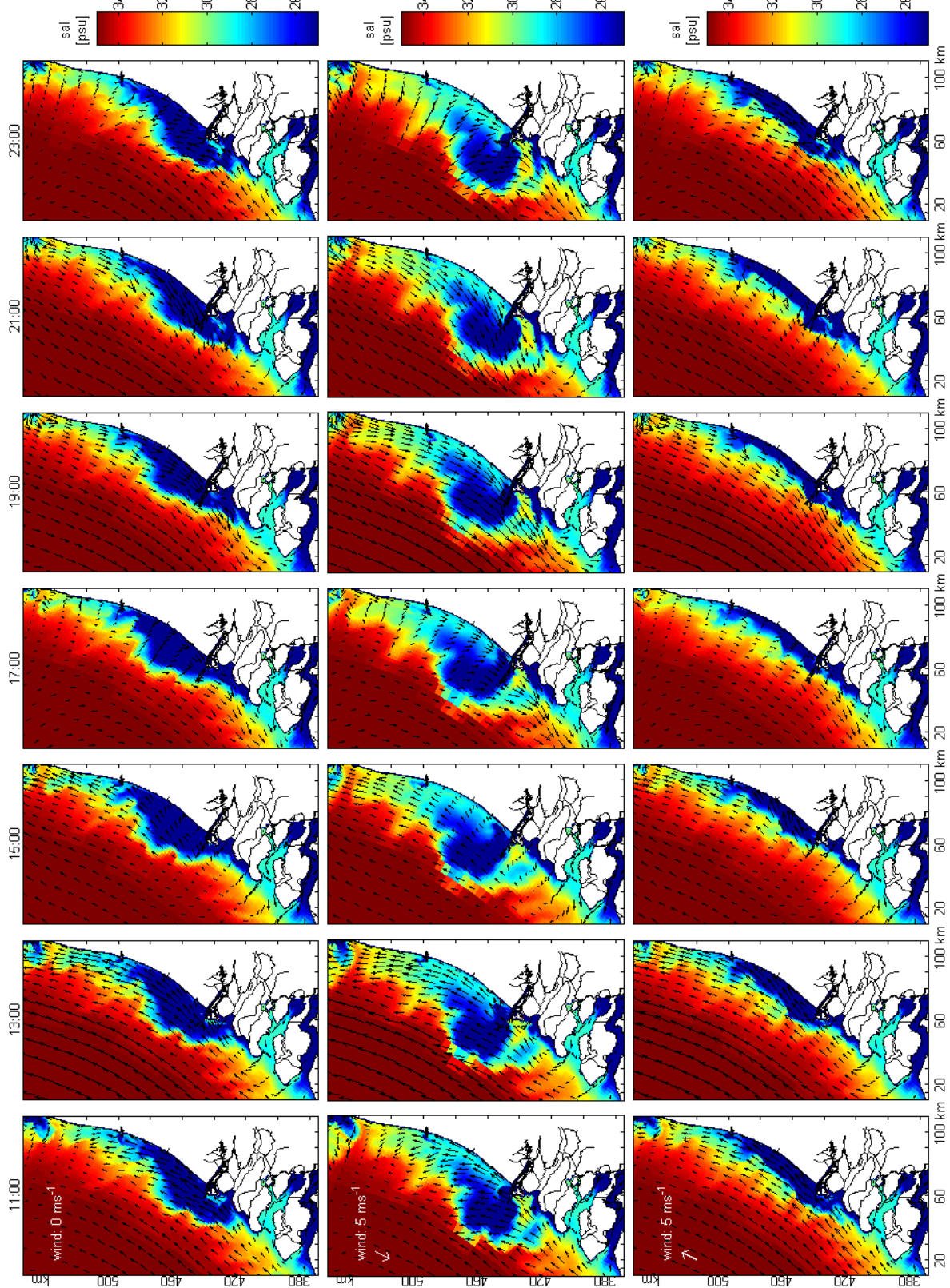


Figure 6.2: Three panels with the snapshots of the salinity profile over the last tidal cycle taken every two hours. The top panel gives the results of the no wind scenario, in the middle the results of the 5 ms^{-1} northerly wind are presented and the bottom panel gives the results for the 5 ms^{-1} southerly wind forcing.

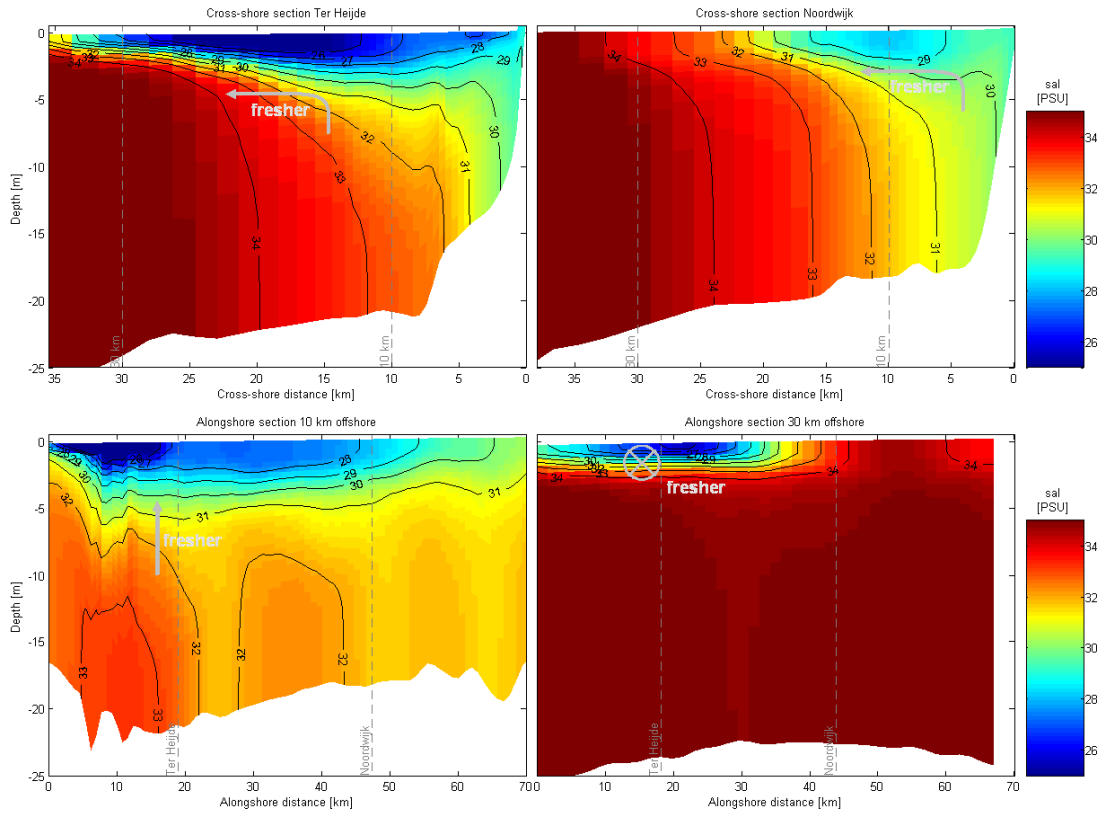


Figure 6.3: 48-hour averaged salinity profiles for the 5 ms^{-1} northerly wind forcing. The annotations show the differences with respect to the reference scenario.

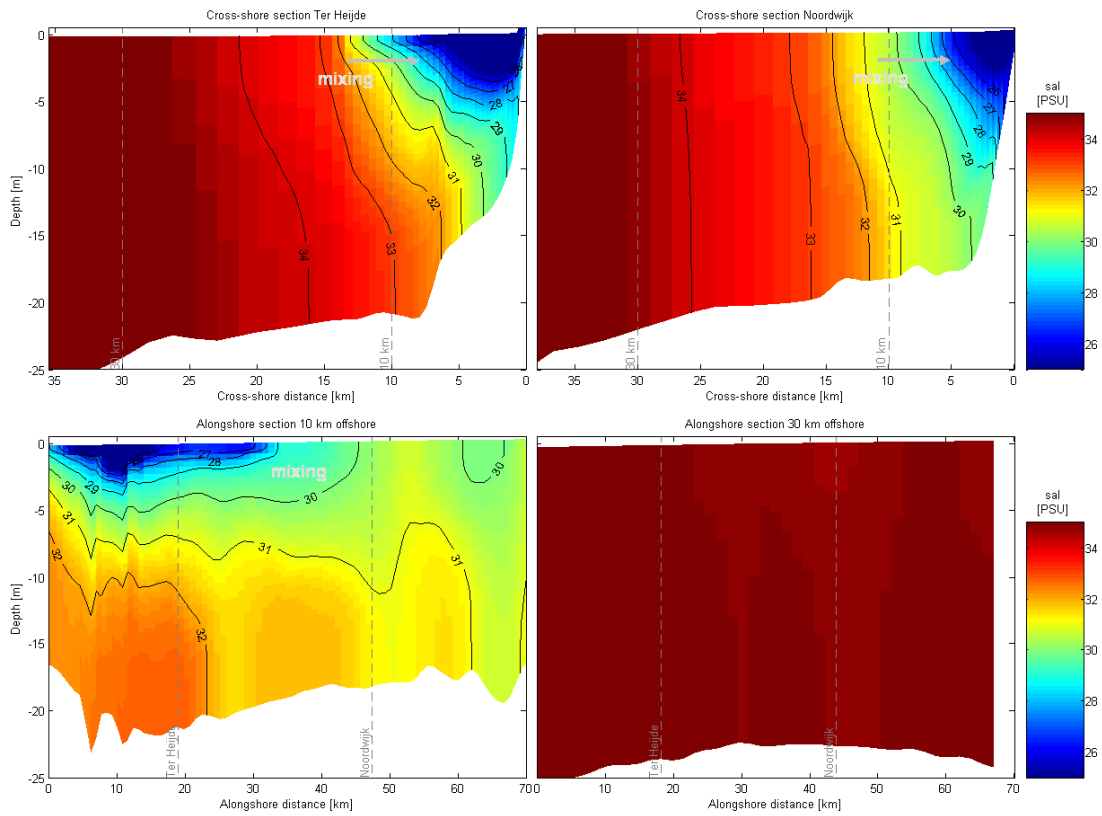


Figure 6.4: As Figure 6.3, only for the 5 ms^{-1} southerly wind forcing.

a length of 35 km a thin layer of freshwater is observed on top of the saline water column.

In Figure 6.4 the 48-hour averaged salinity profiles for the southerly wind forcing are presented. The ageostrophic response of the system is to be pushed northwards, the Ekman dynamics transport the freshwater coastwards. From the results it is likely that the southerly wind enhances mixing of the water column. In Ter Heijde some small stratification is still observed, which can be attributed to the nearby mouth of the Rotterdam Waterway.

Cross-shore winds

The offshore directed wind pushes the freshwater towards open sea by its ageostrophical response. The Ekman dynamics transport the freshwater plume northwards. It results in a stratified water column. The shape of the freshwater plume is however different from the plume created by the alongshore northerly wind. The snapshots of the salinity profile forced by the offshore directed wind are presented in the left panels of Figure 6.5. They show a more rectangular freshwater plume north of the Rotterdam Waterway, whereas the alongshore northerly wind created a more triangular plume extending south of the Rotterdam Waterway. The ageostrophic response of the freshwater plume to the wind cannot be neglected. The northward transport of the freshwater by the Ekman dynamics is good observable in the 48-hour averaged salinity structure of Noordwijk and the alongshore section 10 km offshore, see Figure A.4. Forced by the offshore directed wind the freshwater reaches the farthest north, it also results in the thinning of the freshwater plume.

In Figure A.5 the 48-hour averaged salinity profiles for the onshore directed wind are presented. Near-field stratification is found south of Ter Heijde and a vertically well-mixed water column farther north. The ageostrophic response is in onshore direction. Due to the Ekman dynamics the freshwater plume is pushed southwards. The final state of the water column can be considered as well-mixed. The snapshots of salinity in the surface layer show a well-mixed water column, see the bottom panels in Figure 6.5. Most of the freshwater is confined in front and south of the Rotterdam Waterway. Even south of the Haringvliet the freshwater plume reaches a width of over 10 km. In no other scenario a transport of that length in southward direction is observed.

In the snapshots of the salinity profiles is for both scenarios the tidal straining theorem applied to the Rhine ROFI observed. The plume structure in front of the Rotterdam Waterway is best used to observe these results. At high water (13:00) the plume has stretched maximally in offshore direction. The plume has made its maximum northward excursion at slack before ebb (17:00) and is then narrowed at low water (19:00). The plume has made its maximum southward displacement at low water (23:00).

Instabilities

It appears that baroclinic instabilities are observed in the snapshots of most of the scenarios, including those forced by a stronger wind speed (discussed hereafter). In the snapshots of the 5 ms^{-1} onshore directed wind they are most pronounced and even result in freshwater filaments. It is not possible to state what the filaments are, since they have not been analysed in this study. It is though speculated that they are baroclinic instabilities. The phenomenon is further discussed in Chapter 7.

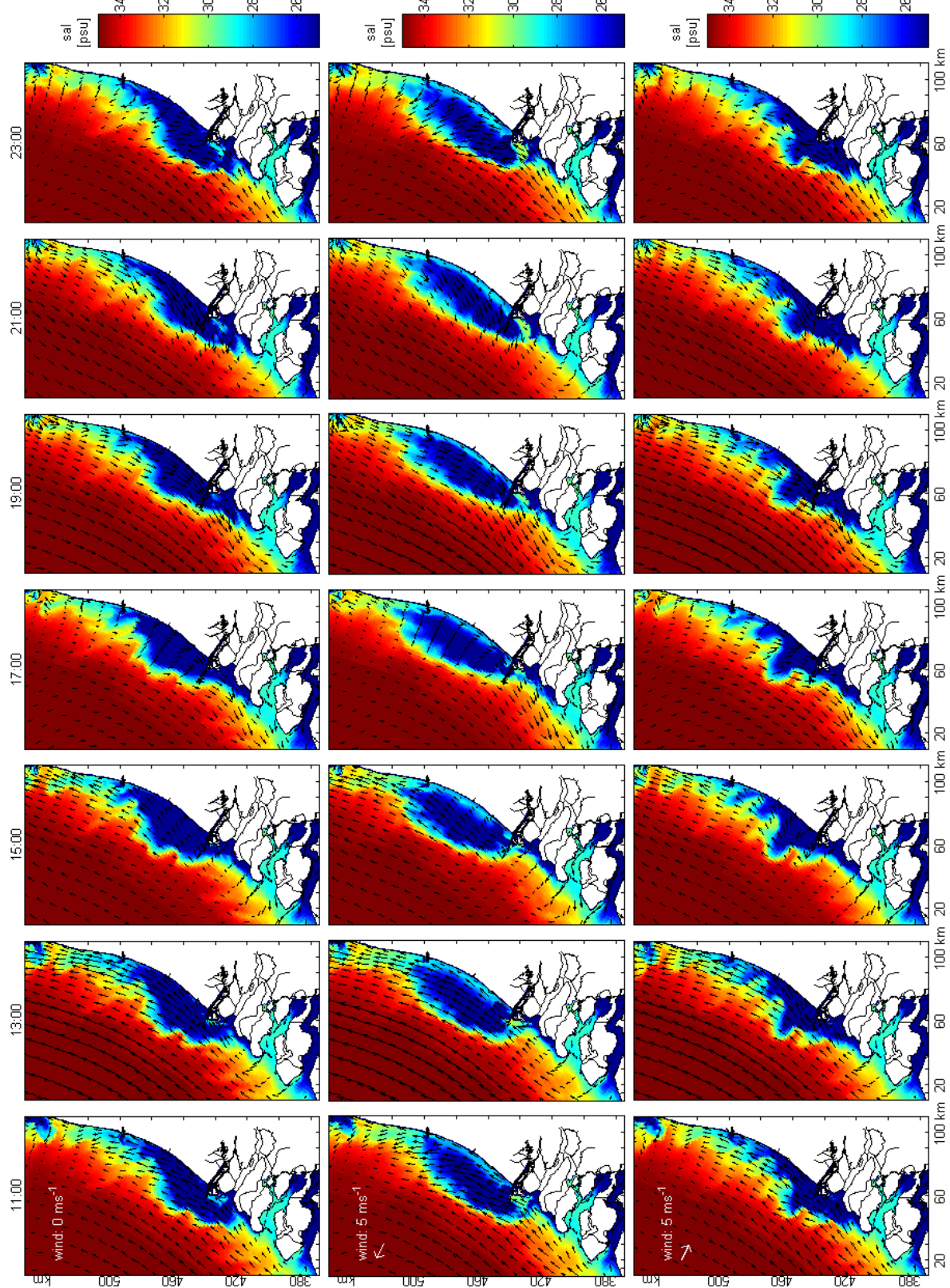


Figure 6.5: Three panels with the snapshots of the salinity profile over the last tidal cycle taken every two hours. The top panel shows the results of the reference (no wind) scenario, in the middle are the results of the 5 ms^{-1} offshore wind and in the bottom panels the results of the 5 ms^{-1} onshore wind.

6.2.2 Magnitude of the wind

Alongshore winds

The middle panels in Figure 6.6 present the snapshots of the salinity profile in the surface layer for the 10 ms^{-1} northerly wind. An increase in magnitude of the northerly wind results in a farther offshore stretching of the freshwater plume. It is accompanied by an increase of stratification. In front of the mouth of the Rotterdam Waterway the plume is at its widest, up to 60 km during high water (13:00). The plume is most narrow at low water (19:00). Also the maximum northwards and southwards displacements correspond with the tidal straining theorem in the Rhine ROFI, at slack before ebb (17:00) and at slack before flood (23:00) respectively. The shape of the plume is triangular due to the combination of an ageostrophic southward and an offshore directed Ekman response of the water column to the northerly wind.

In Figure 6.7 the 48-hour averaged salinity structures are presented for the 10 ms^{-1} alongshore northerly wind. From the cross-shore profiles it is observed that an increased northerly wind keeps the freshwater south of Noordwijk. The water column off Noordwijk can be regarded to as well-mixed. The combination of the ageostrophic and Ekman response of the system results in a wide freshwater plume in front of the mouth of the Rotterdam Waterway, see the alongshore sections 10 and 30 km offshore. Inshore off Ter Heijde the water column is stratified, the salinity of the water in the surface layer has however gone up to 30 PSU, whereas it was 25 PSU for the 5 ms^{-1} forcing.

The results of a thicker and more saline freshwater plume at the surface for increased upwelling-favourable winds follow the behaviour of the conceptual model by Fong & Geyer (2001). Due to direct shear-induced vertical wind mixing (for the increased magnitude of the wind), the salinity anomaly (the difference in salinity between the surface and bottom layer) is reduced. It is accompanied by an increase in thickness of the freshwater plume. The increased shear is generated both by the ageostrophic (frictional) response of the water column to the stronger wind and by the increasing velocities of the Ekman dynamics.

The snapshots of the salinity structure in the surface layer for the 10 ms^{-1} alongshore southerly wind are presented in the bottom panels of Figure 6.6. A close to the coast bounded freshwater column is observed. The increased magnitude of the southerly wind has resulted in a larger Ekman transport of the freshwater plume towards the coast. Due to the ageostrophic response of the system the freshwater is found north of the Rotterdam Waterway and Harinyliet. The role of tidal straining is no longer observed in all four directions. However the plume leaving the Rotterdam Waterway has swung clearly northwards at slack before ebb (17:00). If the snapshots of the 10 ms^{-1} southerly wind forcing are compared with those of the 10 ms^{-1} northerly wind forcing (middle panels), one can observe the large variability in response of the freshwater plume to the wind.

The 48-hour averaged salinity profiles for the 10 ms^{-1} southerly alongshore wind are presented in Figure 6.8. An increased magnitude of the alongshore southerly wind results in a vertically well-mixed water column. The downwelling-favourable wind has both narrowed and thickened the plume until a well-mixed state was reached.

Cross-shore winds

The snapshots of salinity for the increased (10 ms^{-1}) offshore directed wind (Figure A.13, middle panels) show that the shape and dimensions of the salinity structure do not differ a lot from the results of the 5 ms^{-1} case (see Figure 6.5). The salinity in the top layer has however gone up from 25 towards 29 PSU. The combination of the ageostrophic response of the water

column in offshore direction and the Ekman response northwards to the offshore wind results in a rectangular shape of the freshwater plume. The role of tidal straining is best observed in the part of the plume that has just entered the Rhine ROFI. At high water (13:00) it has reached its maximum width and at low water (19:00) it is most narrow. The plume has swung in maximum northward direction at slack before ebb (23:00) and in southward direction at slack before flood (23:00).

Figure A.8 presents the 48-hour averaged salinity profiles for the 10ms^{-1} offshore directed wind. The results show minimum values of salinity in the surface layer of 29 PSU. In the cross-shore sections it is observed that the plume has become thicker and more saline (a reduction of the salinity anomaly). The thickening and the reduction in the salinity anomaly are caused by direct shear-induced vertical wind mixing.

In Figure 6.6, bottom panels, the snapshots of salinity in the surface layer for the increased magnitude of the onshore directed wind are presented. A narrow plume is visible just off the coast. The ageostrophic response of the water column to the onshore directed wind has pushed all the freshwater coastward. It is also observed that the Ekman dynamics in response to the onshore directed wind have transported the freshwater south of the Rotterdam Waterway and Haringvliet. In the snapshots the theory of tidal straining is still visible. At slack before ebb (17:00) the plume has reached maximum northwards and at slack before flood (23:00) maximum southwards. For the cross-shore displacements one has to look at the 30 PSU salinity values. At high water (13:00), water with a salinity of 30 PSU has reached the farthest offshore. At low water (19:00) the freshwater plume is most narrow and bounded close to the coast.

In Figure A.9 the 48-hour averaged salinity profiles for the 10ms^{-1} onshore directed wind are presented. The results show a vertically well-mixed water column, both off the coast at Ter Heijde and at Noordwijk. If the results are compared with the results of the 5ms^{-1} onshore directed wind (Figure A.5), it is observed that the ageostrophic response of the water column to the onshore directed wind has pushed the freshwater plume even closer to the coast.

6.3 Temperature

As described in Section 3.7 stratification can be amplified by solar radiation and exchange of heat between the surface layer and the atmosphere. De Kok *et al.* (2000) describe how in late spring and summer thermal stratification can contribute up to 30% of the vertical density gradient. The scenarios in this study are based on Case 03 of the sensitivity analysis of the model. For Case 03, April 13 2007, the temperature of the air was 14 to 16 °C during the day and no clouds were present.

The scenarios that have a stratified water column experience a quick response to thermal heating and the water columns warm up during the day. In the ambient seawater such a response is not observed and the temperature of the water column remains constant. Figure 6.9 presents the snapshots of temperature in the top layer for the 5 (top panels) and 10ms^{-1} (bottom panels) northerly wind scenarios. For the 5ms^{-1} northerly wind a heating of the freshwater plume is observed during the day. The last two snapshots (21:00 and 23:00) are after sunset and the water column starts to cool down. If the temperature profiles are compared with the salinity profiles (Figure 6.2, middle panels), it is observed that most of the heating occurs in that part of the plume that has a salinity of less than 28 PSU, north of the Rotterdam Waterway. The maximum increase in temperature within the plume due to thermal heating is 0.5 °C. For the 10ms^{-1} northerly wind forcing additional mixing by the wind has occurred bringing the salinity up to 30 PSU in the top layer (Figure A.12,

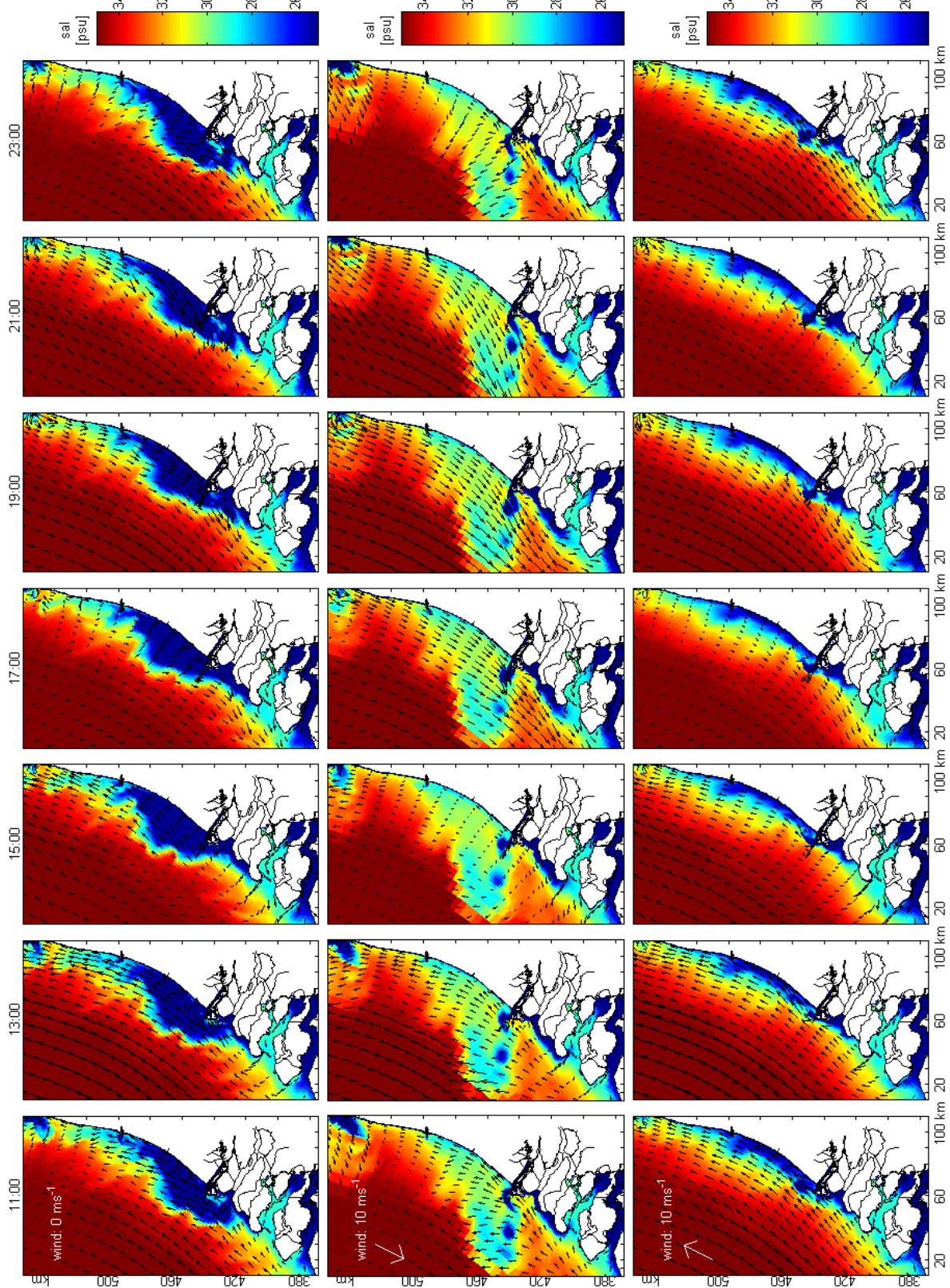


Figure 6.6: Three panels with the snapshots of the salinity profile over the last tidal cycle taken every two hours. The top panel gives the results of the no wind scenario, in the middle the results of the 10 ms^{-1} northerly wind are presented and the bottom panel gives the results for the 10 ms^{-1} southerly wind forcing.

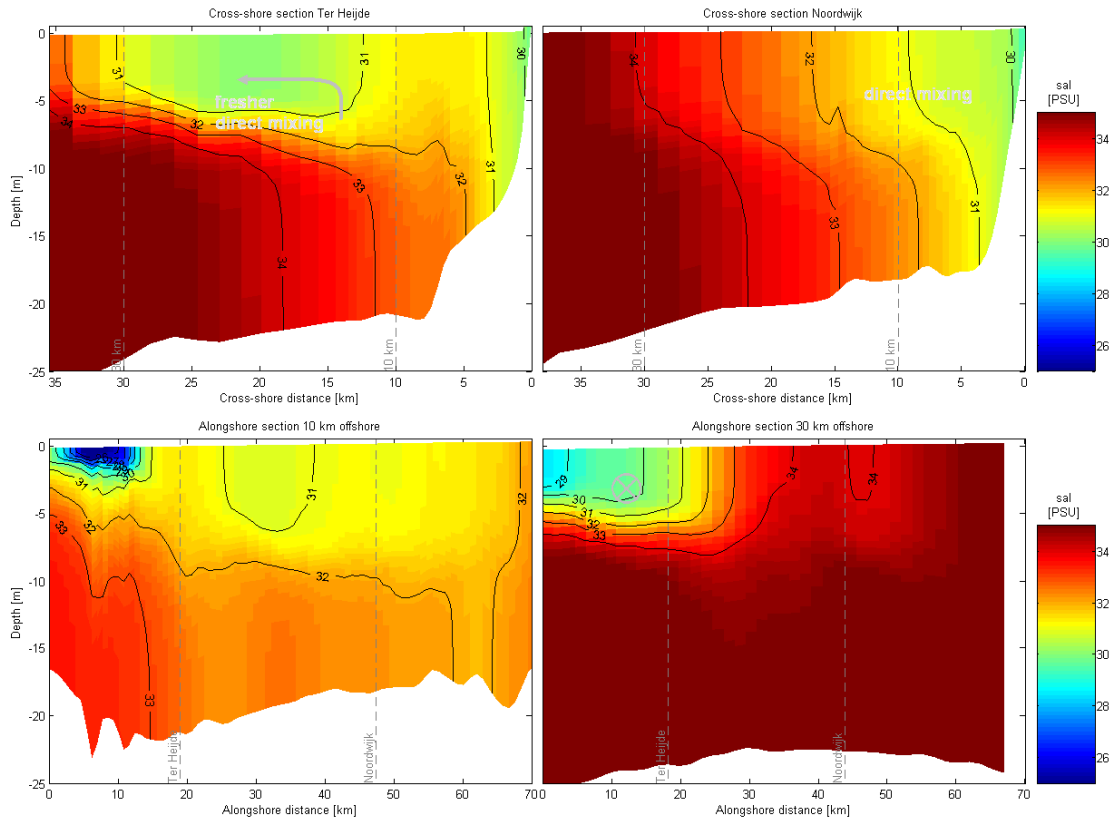


Figure 6.7: 48-hour averaged salinity profiles for the 10 ms^{-1} northerly wind forcing.

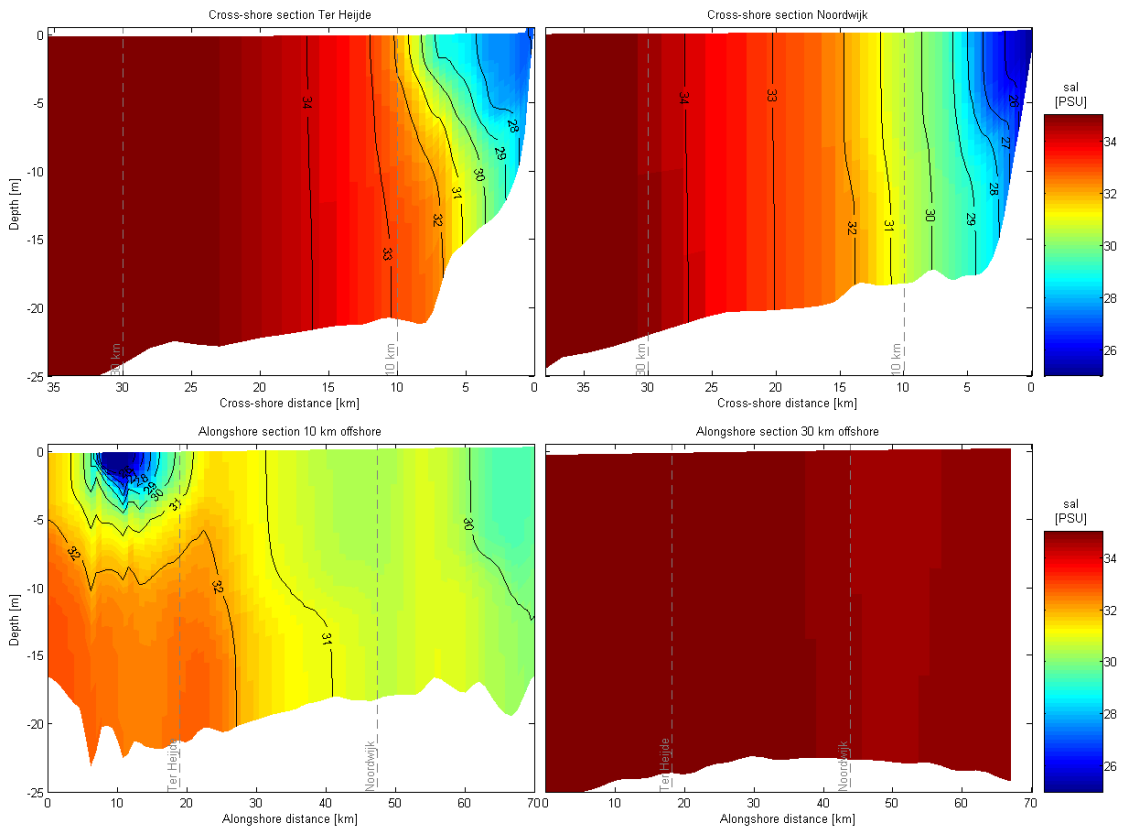


Figure 6.8: 48-hour averaged salinity profiles for the 10 ms^{-1} southerly wind forcing.

bottom panels). An increase of 0.25 °C in temperature within the plume is however still clearly observed during the day, whereas the temperature of the ambient seawater remained constant.

The scenarios that are forced by moderate downwelling-favourable winds show a small increase of temperature due to thermal heating. The water columns for the stronger downwelling-favourable winds are well-mixed and no increase in temperature of the water is observed. The snapshots of the temperature for all scenarios are found in Appendix A.

6.4 Potential Energy Anomaly analysis

Based on the potential energy anomaly (ϕ), Equation 4.1, by Simpson & Bowers (1981) a new method to analyse the competition and interaction of mixing and straining by the wind and the tide in the Rhine ROFI is introduced. The potential energy anomaly is integrated in x -, y - and z - direction over an area limited by the boundaries as given in Figure 4.5. In Figure 6.10 the results of this integrated potential energy anomaly (Equation 2.2) are plotted for all scenarios. The figure presents the amount of energy required for complete mixing of the Rhine ROFI in terajoules [TJ].

The spatial change of ϕ for all scenarios is presented in Figure 6.11. The figure shows the change of ϕ in space compared to the tidal reference scenario (no wind). The results are an instantaneous snapshot of the state of the Rhine ROFI after 50 hours of forcing by the wind (last high water in Figure 6.10, 13:00). The results of the final state of the system during high water are presented, it is the moment that the Rhine ROFI is maximally stratified due to tidal straining.

In this section the results of the integrated value of ϕ and the spatial change of ϕ are discussed together for each direction of the wind. It provides the possibility to link the results of the different methods to each other, as well as the possibility to clarify results of the one method with the other. It has to be noted that in the north of the selected area brackish water coming through the Marsdiep from the Wadden Sea in some occasions contributes to the buoyancy input.

No wind

This scenario is the reference scenario and therefore no results of the spatial change of ϕ can be presented. Only the results of the integrated value of ϕ are presented. In Figure 6.10 the thick black line is the amount of energy required for full mixing of the water column for the no wind scenario. In the absence of wind and waves and with an average river discharge, mixing and straining is in this scenario controlled by the tide. The ebb-flood tidal cycle is clearly observed, five times low water and four times high water. Following de Boer (2009), the energy required to mix the water column is maximal during high water. Due to tidal straining the water column is maximally stratified. During neap tide the ebb-flood tidal cycle can strain and mix roughly 10 TJ. At the moment of minimum stratification (low water) the energy required to fully mix the water column is 3 TJ. The fourth high water is already after neap tide, the water column is less stratified and less energy is required to bring about complete mixing.

It has to be noted that the choice of the area of integration turns out well. An almost equilibrium exists between buoyancy input from the riverine water and mixing by the tide over the period of integration. The semi-diurnal period that is observed, is in principal the internal redistribution of potential energy over the area of integration. This equilibrium must not be taken for granted, but is actually very convenient in studying the effects of wind.

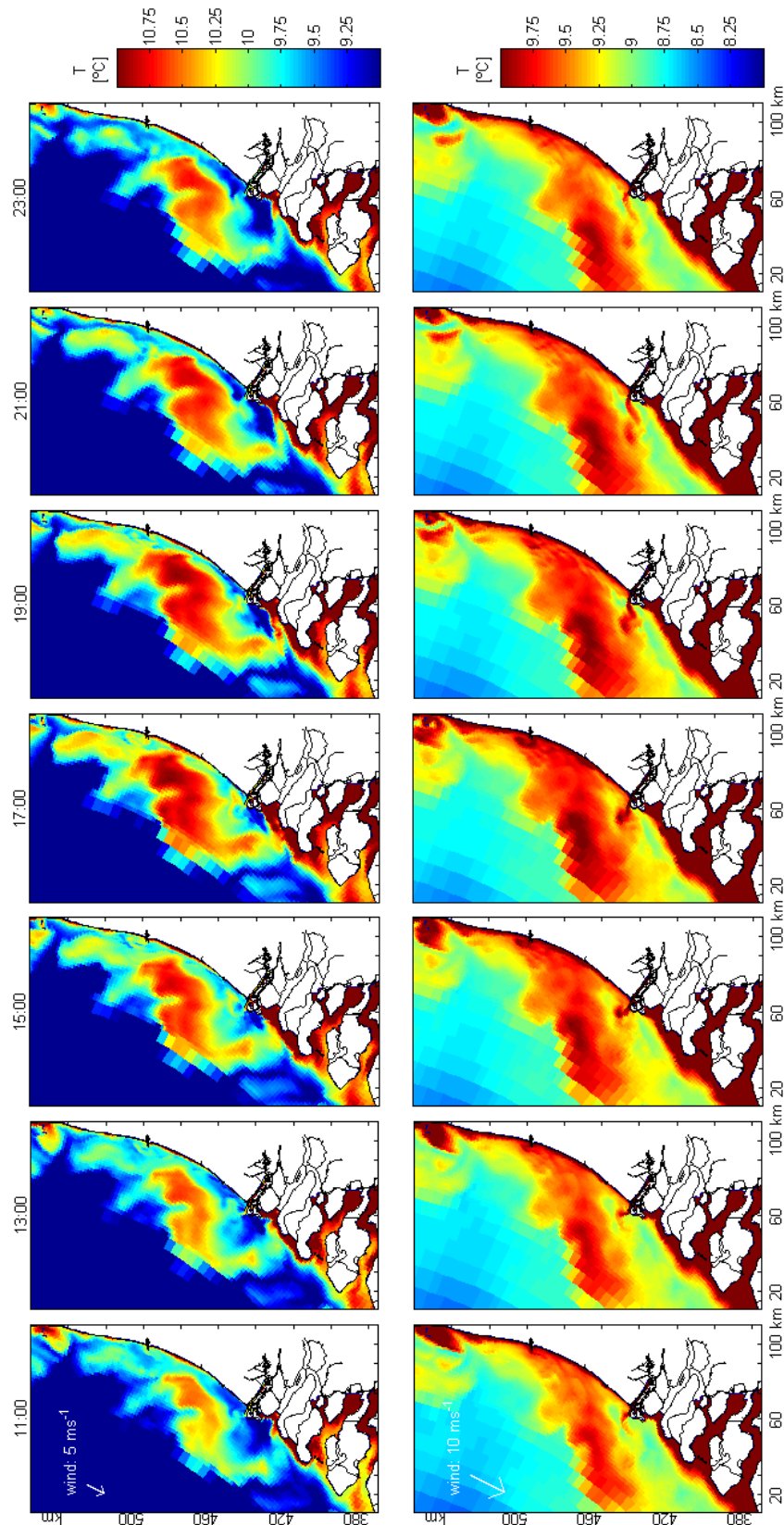


Figure 6.9: Snapshots of the temperature in the surface layer for the 5 ms^{-1} (left panels) and 10 ms^{-1} (right panels) northerly wind forcing. From both panels it can be seen that the freshwater plume heats up during the day, whereas the temperature of the ambient seawater remains constant. For the 5 ms^{-1} wind the water heats up roughly $0.5 \text{ }^{\circ}\text{C}$, for the 10 ms^{-1} wind the heating is roughly $0.25 \text{ }^{\circ}\text{C}$.

Northerly alongshore winds

In Figure 6.10 it is observed that both the results of the 5 and 10 ms^{-1} northerly wind forcing (red) have an upward trend in energy required for full mixing. Hence they result in an increase of stratification in the Rhine ROFI. Results of the 5 ms^{-1} wind follow the pattern of the reference (no wind) scenario, tidal straining and mixing is clearly observed. Over time an increase in straining is observed due to the Ekman drift which pushes the freshwater offshore. Consequently the amplitude of energy required over the ebb-flood tidal cycle also increases over time. It implies that besides the additional input of the straining-favourable wind to the straining-favourable high water, the mixing capacity of the ebb current has also increased (compared to the reference scenario). The increase in mixing by the tide is possible since the upwelling-favourable northerly wind has spread the freshwater over a larger area. A wider surface area results in an increased total amount of ebb-current induced shear to mix the same amount of freshwater.

A northerly wind of 10 ms^{-1} gives the strongest response. From low to high water the stratification increases with roughly the same rate as for the reference scenario. From high to low water the mixing by the tide is, during the first three low waters in Figure 6.10, annihilated by the straining of the wind. It is the only moment that energy input by the wind and the tide are equal to each other. In all other scenarios the ebb-flood tidal cycle is the dominant process in straining and mixing of the Rhine ROFI. The last tidal cycle the system seems to have come to a new equilibrium. The ebb-flood tidal cycle is visible again with the same amplitude in energy as the reference scenario.

The spatial change of ϕ (Figure 6.11, left panels) shows for both wind speeds an increase in far-field stratification (red area). In the near-field a decrease of ϕ is observed (blue area). For the 5 ms^{-1} wind this decrease is caused by the thinning of the freshwater plume (compare Figures 6.1 and 6.3). For the 10 ms^{-1} wind it is caused by the mixing of the plume and an accompanied decrease of the salinity anomaly (compare Figures 6.1 and 6.7). The influence of the Ekman dynamics is also observed in these results, the increase of ϕ is concentrated in front and south of the Rotterdam Waterway. In the north, especially for the 10 ms^{-1} scenario, the water from the Wadden Sea is also a contributor to ϕ .

For both winds is concluded that the upward trend in energy required for full mixing results in a more stratified water column. This conclusion is further confirmed by the results of the spatial change of ϕ . For both wind speeds the total size and magnitude of increased ϕ is larger than the size and density of decreased ϕ . The consequences of an increased wind speed are also observed in the plots of spatial change of ϕ , the total size and density of increased ϕ for the 10 ms^{-1} scenario is larger than for the 5 ms^{-1}

Offshore directed winds

For the integrated potential energy anomaly, Figure 6.10, the results of the offshore directed winds (blue) follow the results of the reference scenario. It seems that the tide is controlling the straining and mixing of the water column. The 5 ms^{-1} wind, of all results, comes closest to the results of the no wind scenario. From the results of the spatial change of ϕ (Figure 6.11, middle-left panels) is observed that the 5 ms^{-1} wind spreads the freshwater in offshore (ageostrophic response) and northerly direction (Ekman response).

Different from the results of the alongshore northerly winds, an increased magnitude of the offshore directed wind (10 ms^{-1}) does not result in an increase of the integrated value of ϕ . Compared to the 5 ms^{-1} offshore wind, 2 to 3 TJ less energy is required to fully mix the

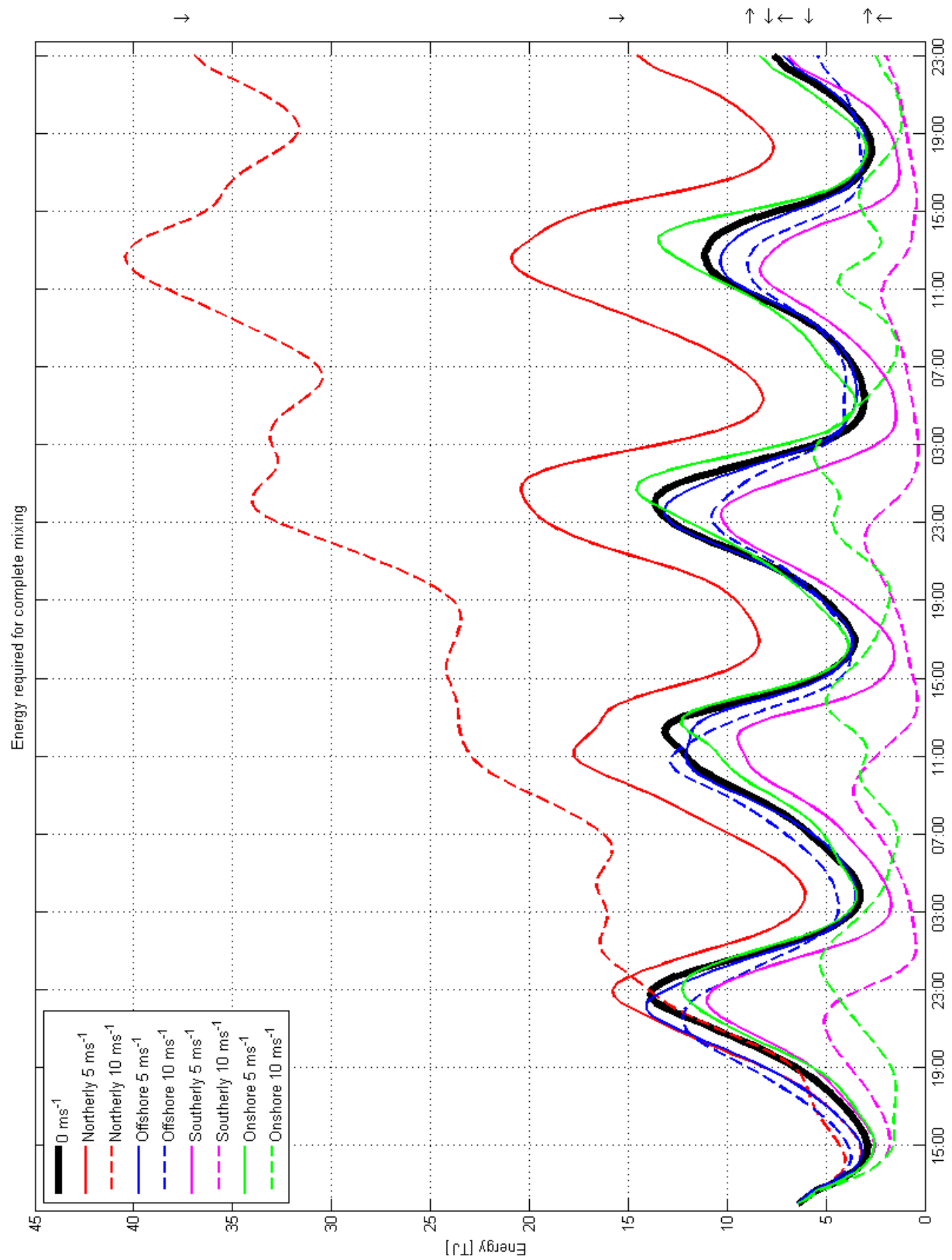


Figure 6.10: The integrated values of ϕ over time. The values represent the total amount of energy required over time for a completely mixed water column. In all results the tide is the dominant process in mixing and straining of the water column.

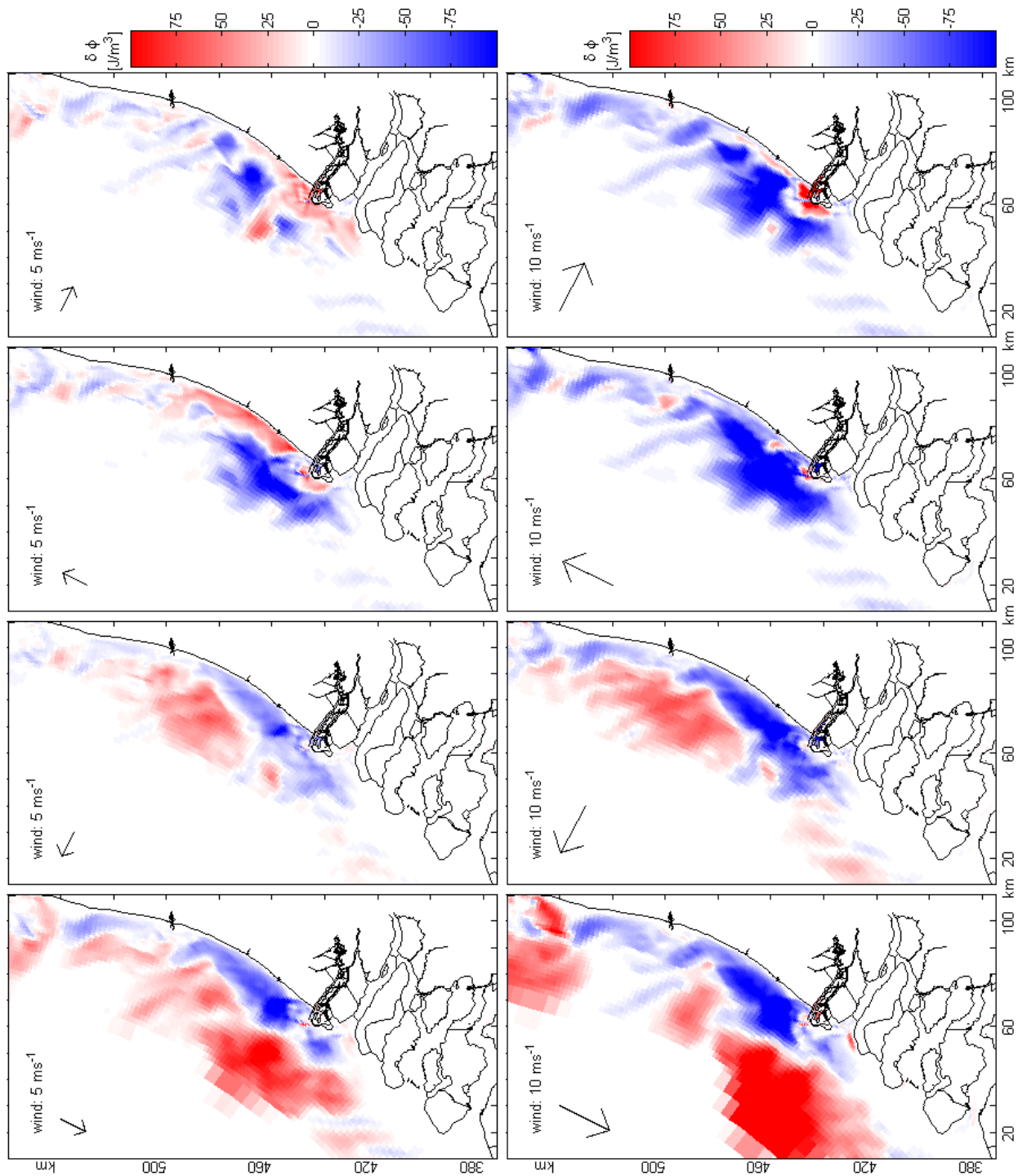


Figure 6.11: Plots of the spatial change of ϕ for all scenarios. The plots are made by subtracting the values of ϕ for the no wind scenario at high water from the values of ϕ for the relevant scenario at high water.

water column at high water. At low water no large differences between the results of the two wind speeds exist for the amount of integrated ϕ .

The plots of the spatial change of ϕ can be used to clarify the reduction in the integrated value of ϕ for the 10 ms^{-1} wind. Compared to the 5 ms^{-1} scenario, a clear increase of ϕ occurs in the far-field, indicating increased stratification in the far-field. This increase is however accompanied by an even stronger decrease of ϕ in the near-field. It can be concluded that although the total amount of stratification has decreased, a further spreading of the freshwater plume over the Rhine ROFI can be achieved by an increased offshore directed wind.

From the plots of the spatial change of ϕ it is further concluded that an offshore directed wind results in a northwards transport of the freshwater plume. The increase in stratification (red area) is situated north of the Rotterdam Waterway. The influence of the water coming from the Wadden Sea is not observed in the results, most presumably it is transported northwards by the Ekman dynamics, out of our area of interest.

Southerly alongshore winds

In the results of Section 6.2.1 is observed that southerly alongshore winds work mixing-favourable. In Figure 6.10 the integrated value of ϕ for the southerly wind scenarios is plotted in magenta. It is observed that the amount of energy required to fully mix the Rhine ROFI is for both wind speeds always smaller than for the scenarios forced by alongshore northerly winds, offshore directed winds (only not in the last 2 hours of the 10 ms^{-1} results) and no wind (reference).

Compared to the reference scenario a 5 ms^{-1} southerly wind decreases the integrated value of ϕ , both during low and high water, with roughly 2 TJ. Most presumably the decrease is caused by the Ekman dynamics that force the freshwater plume in onshore direction. From the results of the spatial change of ϕ for the 5 ms^{-1} wind scenario (Figure 6.11, middle-right panels) is observed that, compared to the reference scenario, a large decrease of ϕ occurs in the far-field of the Rhine ROFI between the mouth of the Rotterdam Waterway and Noordwijk. It is accompanied by an increase of ϕ in the near-field up to as far north as IJmuiden. From the results of the integrated potential energy anomaly it is known that for the spatial change of ϕ , the total decrease (blue area) has to be larger than the total increase (red area). In the north a small decrease in ϕ is observed due to the brackish water of the Wadden Sea.

It is known from Figure 6.8 that for an increased southerly wind the freshwater plume is further narrowed and becomes thicker until a vertically well-mixed water column is established. The results of the integrated value of ϕ present that around high water the southerly wind adds 10 TJ of mixing into the system. Around low water the difference in total amount of ϕ with the no wind scenario is 3 TJ. It is also around low water that the Rhine ROFI comes closest, of all scenarios, to a completely well-mixed state where only 0.5 TJ of additional mixing is required. The plot of the spatial change of ϕ supports the results as found from the integrated value of ϕ . A clear reduction of ϕ is observed in both the near- and far-field of the Rhine ROFI. In the north a small contribution in reduction of ϕ is made by water coming from the Wadden Sea.

In the results of the integrated value of ϕ is observed that for the 10 ms^{-1} southerly wind the periods of straining last longer than the periods of mixing. This deformation can be attributed to the combined interaction and competition of the tide and the wind. From low to high water the tidal current is directed northwards and in favour of straining. The ageostrophic response of the freshwater plume to the southerly alongshore wind is also in northern direction. It

is this response that elongates the straining-favourable period from low to high water. Vice versa is the mixing-favourable period from high to low water shortened by the ageostrophic response of the water column to the wind.

Onshore directed winds

Onshore winds work mixing-favourable. In Figure 6.10 the integrated values of ϕ for the scenarios forced by an onshore directed wind are plotted in green. For the 10 ms^{-1} wind it is observed that indeed less energy is required to fully mix the water column. For the 5 ms^{-1} onshore wind the amount of energy required to mix the water column during high water increases however over time. At the begin of the calculations the integrated values of ϕ are smaller than for the reference scenario, during the last high water the value lies 3 TJ above. In Section 6.2.1 it was observed that for a 5 ms^{-1} onshore directed wind so-called filaments of fresh water came to existence over time. The presence of these filaments have to cause that more energy is required to fully mix the water column. In the snapshots of local ϕ , Figure A.19 bottom panels, the filaments are clearly present during high water.

In the results of the spatial change of ϕ for the onshore directed winds (Figure 6.11, right panels) is observed that most of the area in the far-field of the Rhine ROFI is blue, indicating a decrease of ϕ . This decrease is caused by the mixing of the onshore directed wind. In the near-field, concentrated around the mouth of the Rotterdam Waterway, the value of ϕ has increased. In the ageostrophic response to the wind the freshwater is pushed landwards. The Ekman response transports the freshwater southwards, clarifying the concentration of increased ϕ around the mouth of the Rotterdam Waterway. In the far-field also some isolated areas of increased ϕ (red areas) are present, they are most probably caused by the freshwater filaments as discussed above. In the north the small area of increased ϕ (red) is most probably due to brackish water of the Wadden Sea that is transported by the Ekman dynamics into our field of interest.

The 10 ms^{-1} onshore directed wind works definitively in favour of mixing. From the results of the integrated value of ϕ is observed that it is maximal 5 TJ around high water that has to be put into the system to bring about complete mixing. Also during low water less energy is required to completely mix the system (compared to the reference scenario). The striking phenomenon in the results is however the double peak around high water. The snapshots of local ϕ , Figure A.21 bottom panels, suggest a temporal increase in near-field stratification, most presumably caused by the pulsed release of freshwater from the Rotterdam Waterway around high water. Also in the results of the other scenarios sometimes small deviations around high water in the value of integrated ϕ are observed.

The results of the spatial change of ϕ show almost everywhere in the near- and far-field a decrease of ϕ . The ageostrophic response of the system to the wind and the direct vertical wind-induced mixing favour mixing of the water column over the entire Rhine ROFI. The assumption that the pulsed release of freshwater by the Rotterdam Waterway around high water clarifies the double peak in the integrated value of ϕ , is supported by the results of the spatial change of ϕ . A clear near-field increase of ϕ is observed near the mouth of the Rotterdam Waterway. The hypothesis is further supported by the timing of the plot of change of ϕ , which is around high water.

Tide versus wind

In all results of the integrated potential energy anomaly (Figure 6.10) the ebb-flood tidal cycle is visible in straining and mixing of the water column. Results of the 10 ms^{-1} northerly and southerly alongshore wind show the largest deviation from the reference scenario. But

also for these scenarios the ebb-flood tidal cycle is observed in the variation in amount of energy over time.

In the spatial change of ϕ (Figure 6.11) a trend of a couple of days is observed for northerly and southerly alongshore winds before the system has reached a new equilibrium. It follows especially from the 10 ms^{-1} wind scenarios. In the results of the offshore and onshore directed winds a trend is not so much observed, but a shift in amplitude is clearly present.

6.5 Upwelling and downwelling

The results of the vertical velocity ω are presented to investigate upwelling and downwelling in the Rhine ROFI. For each scenario the vertical velocity is plotted twice: at slack before flood and at slack before ebb. It was decided to present the values of ω in the middle layer of the model. From analysis it followed that the vertical velocities were at its maximum in the middle of the water column. From this analysis also followed that the same pattern as found in the middle layer of the water column was also found in the other layers of the model.

First the results of upwelling and downwelling for the tidal reference scenario will be presented. Thereafter the results of the influence of wind on upwelling and downwelling are presented. The order is to first present the combination of wind with downwelling-favourable conditions by the tide and thereafter wind in combination with tidally upwelling-favourable conditions.

No wind

In Figure 6.12 the results of up- and downwelling for the no wind scenario are presented. The vertical velocities ω are presented at slack before ebb (left panel) and at slack before flood (right panel). It has to be noted that the vertical velocities are very small. Although the results show a patchy distribution of positive and negative vertical velocities, in front of the coast a 5 km wide band of negative (left panel) and positive (right panel) vertical velocities ω is observed. The results follow the theory of tidal upwelling and downwelling by de Boer *et al.* (2009), see Figure 2.1. Slack before ebb results in downwelling and slack before flood in upwelling. The results of upwelling are especially well represented.

Tidal downwelling, varying winds

In Figure 6.13 the results of all wind scenarios under downwelling-favourable tidal conditions (slack tide before ebb begins) are presented. The results seem to show no consistency. If for example the upper four panels are compared, not a clear increase in downwelling is observed once the wind switches from an upwelling-favourable (left and middle-left panel) to a downwelling-favourable (middle-right and right panel) direction. The possibilities for the existence of such a patchy distribution of positive and negative vertical velocities are further discussed in Chapters 7 and 8.

If the results of the northerly alongshore wind (left panels) are compared with the results of the reference scenario (Figure 6.12, left panel) it is observed that a small band of positive vertical velocities has come to existence just off the coast. For an increased magnitude of the wind this band is somewhat widened. From the results where the tide and wind work both in favour of downwelling (discussed hereafter), it is however not possible to state whether these results are of physical nature. In the results of the offshore directed wind (middle-left panels) the same behaviour in upwelling and downwelling as for the northerly alongshore wind is observed. A small band with a positive vertical velocity exists that is further widened under an increased magnitude of the wind.

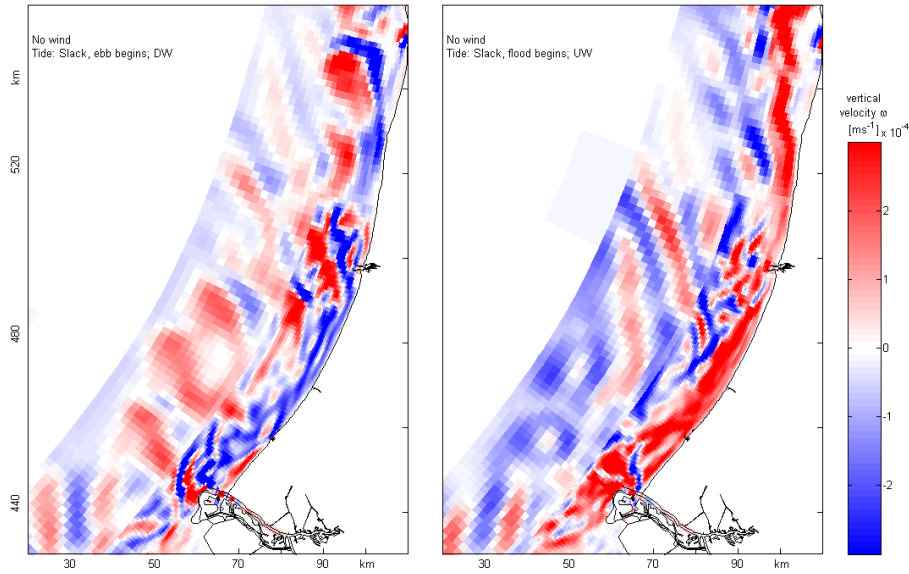


Figure 6.12: Tidal upwelling and downwelling, represented by the vertical velocity ω , for the no wind scenario. The snapshots are taken in the middle layer of the water column, the same pattern is found over the entire depth of the water column. The left picture is taken at slack before ebb begins, which is in favour of downwelling. The right picture is at slack before flood begins and thereby in favour of upwelling.

The patterns of the vertical velocities in the results of the moderate alongshore southerly (top middle-right panel) and the moderate onshore directed (top right panel) wind seem to be consistent with the results of the tidal reference scenario in the far-field. Between the mouth of the Rotterdam Waterway and IJmuiden a band of upwelling is observed. This band is not expected since both the direction of the wind and the tide are in favour of downwelling. Compared to downwelling by the tide only, an increase in downwelling is expected once a downwelling-favourable wind is added to the system. For an increased magnitude of the downwelling-favourable wind (lower left panels) the results deviate even further from what is expected. An increase in upwelling in the near-field is observed, whereas the combination of the tide and the wind should result in increased downwelling.

Tidal upwelling, varying winds

In Figure 6.14 the results of upwelling and downwelling under upwelling-favourable tidal conditions are presented. These results show more consistency with the physics than the results of the downwelling-favourable tidal conditions (Figure 6.13).

The scenarios that are forced by an upwelling-favourable wind show a clear band of upwelling water in front of the coast. The band has a width of 7 km for the northerly (top left panel) and 5 km for the offshore directed wind (top middle-left panel). Compared to the reference scenario (Figure 6.12, right panel) the additional upwelling by the northerly alongshore wind has resulted in a wider band of upwelling, especially between Noordwijk and IJmuiden. Additional upwelling by the offshore directed wind is not observed in the results.

An increased upwelling-favourable northerly alongshore wind results in a wider band of upwelling, roughly 10 km wide (bottom left panel). Off the coast of IJmuiden an area without upwelling or downwelling is observed. It seems to be linked to the shape of the freshwater plume for this scenario (Figure 6.6, bottom panels). Also for the offshore directed wind an

increased wind speed results in a wider band of 7 km of upwelling (bottom middle-left panel). Here an area without upwelling or downwelling is not observed.

From the scenarios that are forced by a moderate downwelling-favourable wind it can be concluded that upwelling by the tide is the dominant process. Both for the 5 ms^{-1} southerly alongshore wind (top middle-right panel) and the 5 ms^{-1} onshore directed wind (top left panel) a 5 km wide band of upwelling is observed in front of the coast that does not differ much from the results of the reference scenario. An increased magnitude of the downwelling-favourable winds results in a patchy, inconsistent distribution of up- and downwelling over the Rhine ROFI. The total amount of upwelling does however decrease.

6.6 Presentation of the results

This chapter showed among other things the challenge of presenting the results of the physical analysis. The processes act in x -, y - and z - direction and also have changing profiles over time. To be able to present the results of each scenario in a single image, and thereby facilitating an easy comparison between the scenarios, a new method of presenting the results was derived, see Figure 6.15. It was decided not to present the variation of the physical processes over the ebb-flood tidal cycle. Most interest is in the stratification of the Rhine ROFI and therefore the results as found during high water are presented. From tidal perspective it is the moment in time that the Rhine ROFI is maximally stratified.

First the 28, 30 and 32 PSU isohalines in the surface layer are plotted. The isohalines show where the freshwater is situated. If, at the seaward side of the plume, the isohalines lie close to each other a freshwater front is present. If the isohalines lie farther away from each other the water column is presumably well-mixed over the vertical. In the upper-left corner the amount of energy required to fully mix the water column over the area limited by the boundaries of the same figure is presented. The values follow from Figure 6.10. By knowing the values of all eight scenarios a good mutual comparison is possible. Finally the local values of ϕ are plotted. It presents the size and location of stratification in the Rhine ROFI. For the plot a lower limit of 50 Jm^{-3} as value for ϕ is.

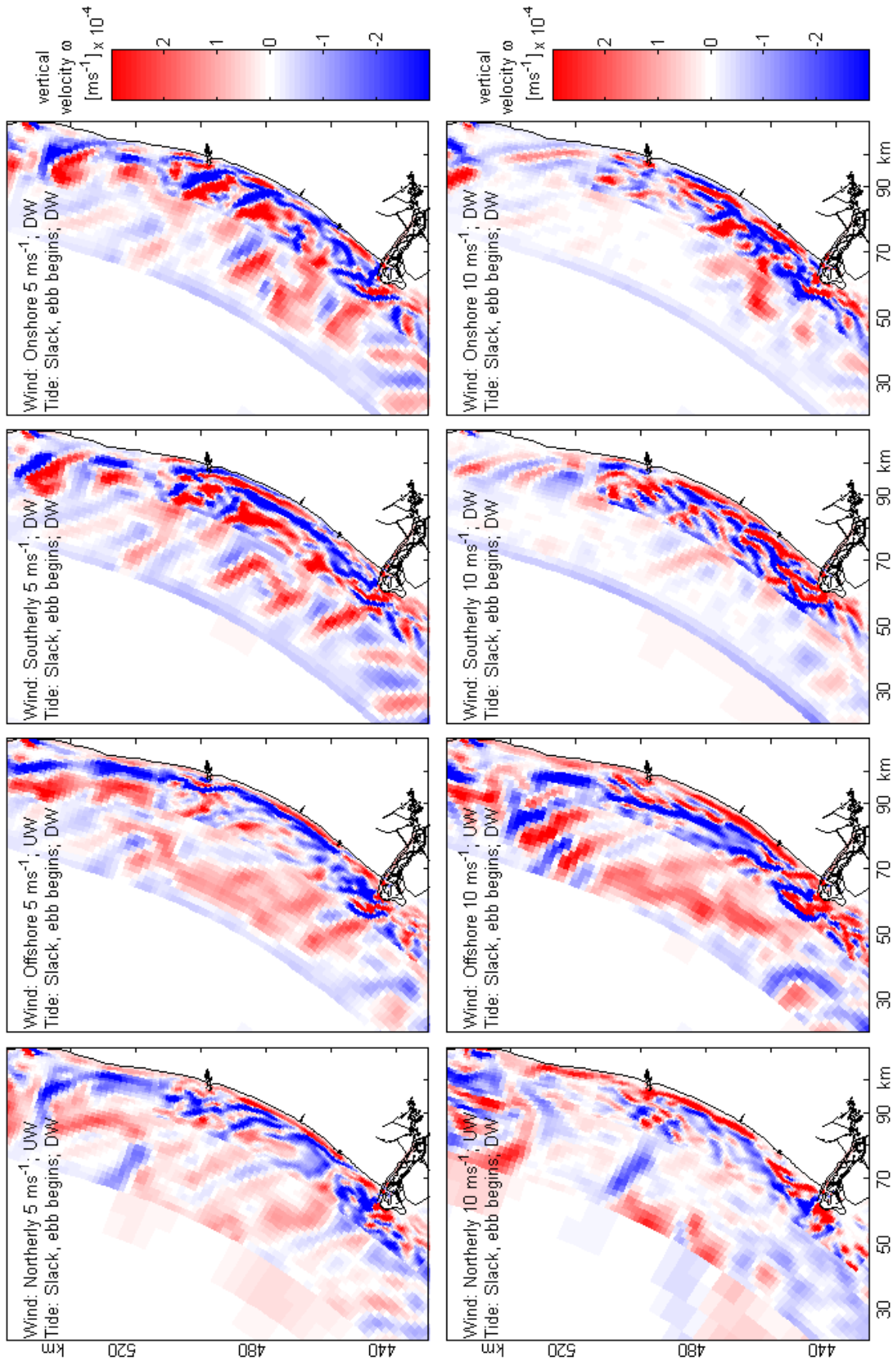


Figure 6.13: Upwelling and downwelling in the middle layer of the water column for all scenarios. The figures are taken at slack tide when ebb begins, the tide works downwelling-favourable. The same velocity profile is seen over the entire depth of the water column.

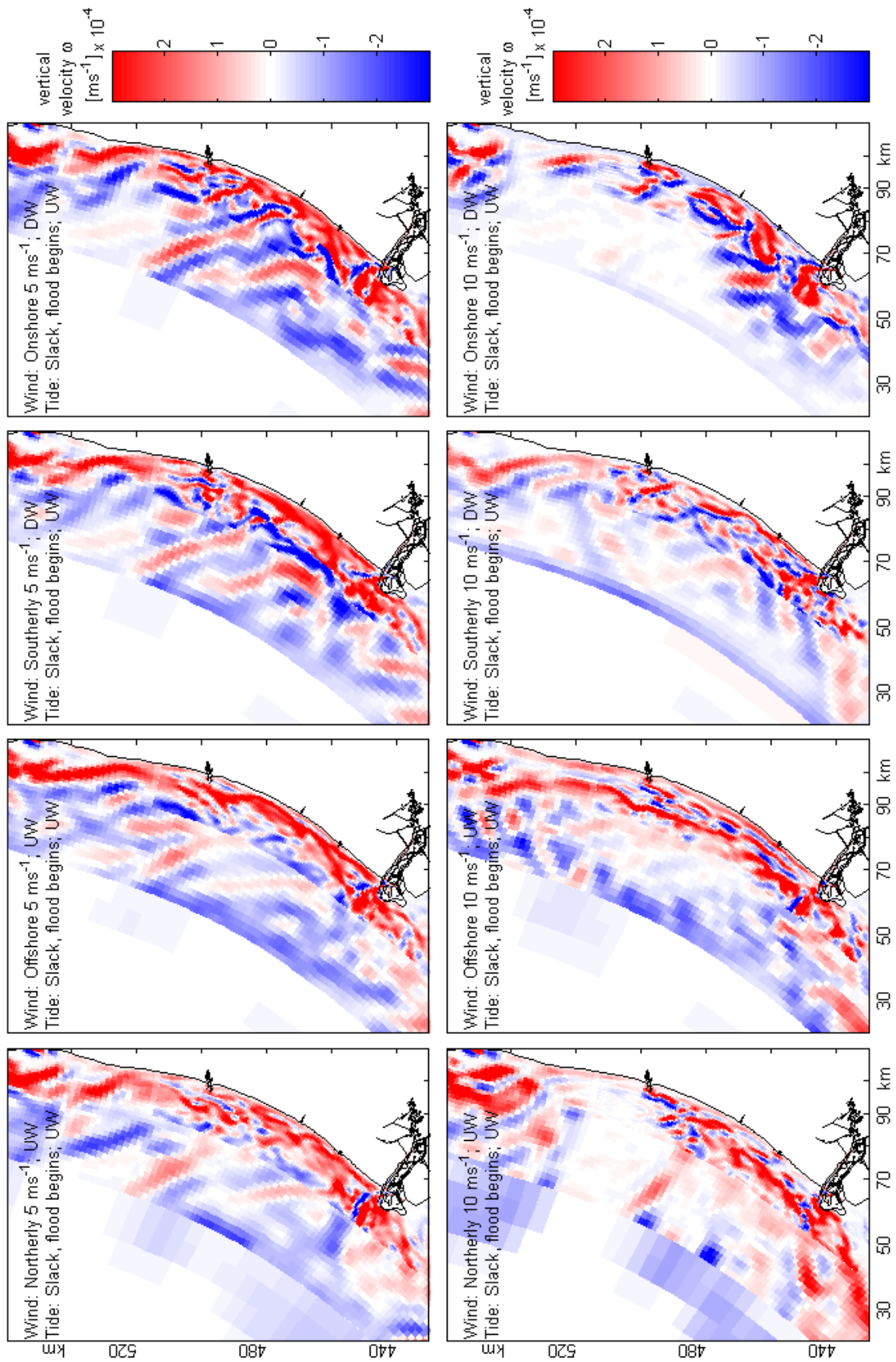


Figure 6.14: As Figure 6.13, only here the figures are taken at slack tide when flood begins, the tide works therefore upwelling-favourable.

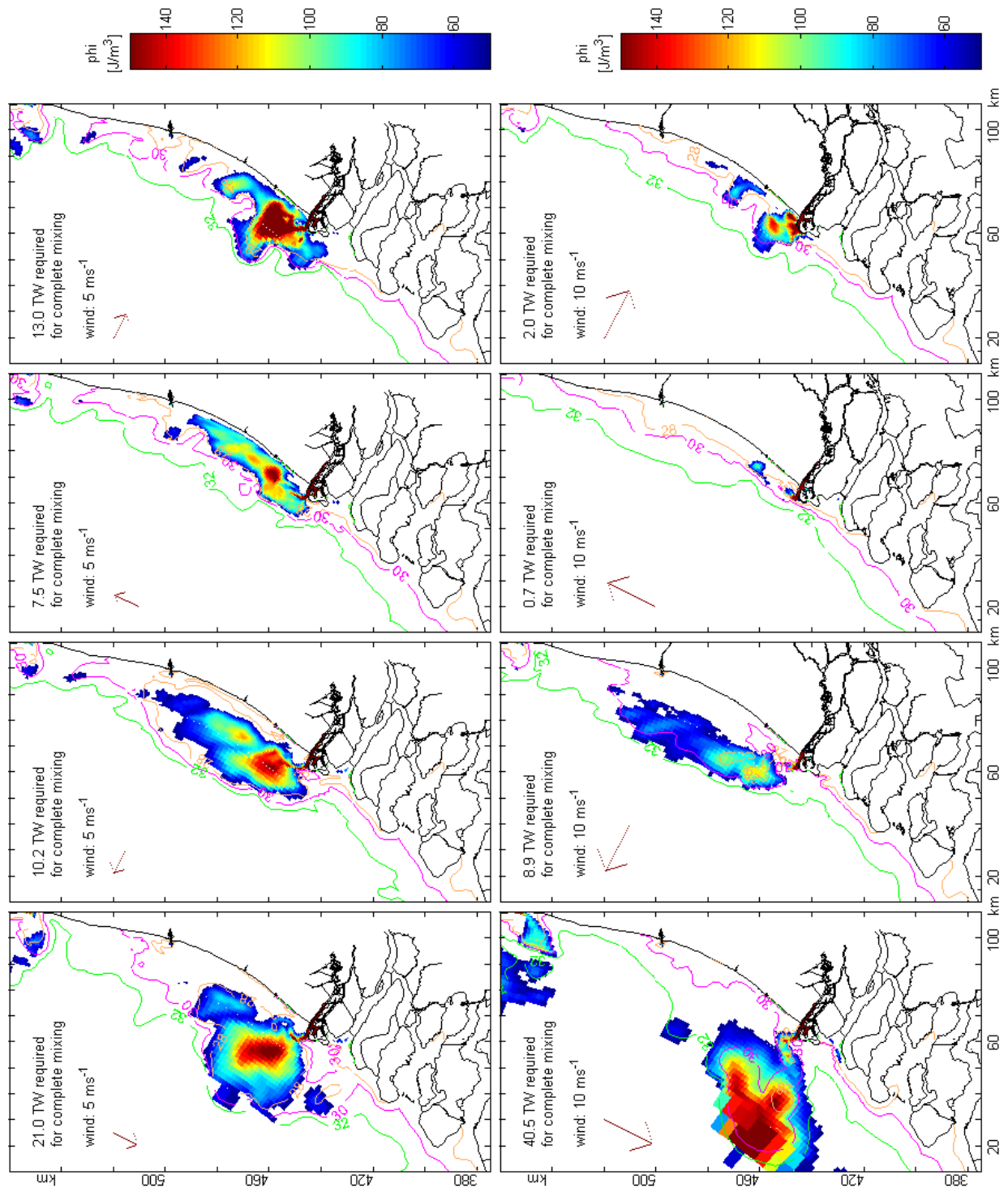


Figure 6.15: Overview of the results for all scenarios. In all figures we see, during high water, (a) the salinity structure in the top layer by the 28, 30 and 32 PSU isohalines, (b) the size and location of the stratification by ϕ and (c) the total amount of energy required to fully mix the water column.

Chapter 7

Discussion

A series of numerical experiments was used to study the interaction and competition between the wind and the tide in mixing and stratifying of the water column. The response of the Rhine ROFI to winds varying in direction and magnitude (including a no wind scenario as reference) has been investigated under typical neap tide conditions and an average river discharge. The model used incorporates the actual bathymetry and coastline of The Netherlands; it was run with a vertical resolution of 48 sigma-layers.

The model results show highly variable results for the size and shape of the Rhine ROFI when forced by winds varying in direction and magnitude. The results of the tidal reference scenario (no wind) are consistent with the theory of tidal straining in the Rhine ROFI as found by Simpson & Souza (1995) and extended by de Boer *et al.* (2007). The freshwater plume as found in this study (see Figure 6.2, top panels) differs however in size and shape from the plume as found in the idealised model of de Boer *et al.* (2007). It is likely that the actual bathymetry and coastline of The Netherlands (see Figure 4.4) influence the results. This thought is further supported by results of a modelling study by Chao (1988), where the presence of a seaward bottom slope enhanced a downstream coastal jet. In remote sensing SST observations, reported by Arentz (2005) and de Boer *et al.* (2009), the shape of the Rhine ROFI in the northward direction is markedly different from the results of the idealised model.

From the results of this study it is not possible to determine in which parts of the plume cross-shore straining and alongshore straining (advection) occurs. However, following the results of the full potential energy anomaly equation by de Boer *et al.* (2007), it is most likely that alongshore straining (and advection) occurs in the southern and northern edges of the bulge of the freshwater plume (the wider part of the plume around the head of the Rotterdam Waterway), whereas cross-shore straining is most likely to occur in the downstream coastal current.

The results of the influence of wind varying in direction and magnitude on the Rhine ROFI are summarised in Figure 7.1. The figure presents the contribution of the different components to the response of the freshwater plume as a function of direction and magnitude of the wind. In general the response of a plume to a wind stress consists of a geostrophic (Ekman) transport, directed to the right with respect to the wind stress, and an ageostrophic transport component in the direction of the wind stress. The relative importance of both depends primarily on the degree of vertical mixing. Moreover, the direction of the geostrophic flow also depends on the presence of the coastline. An increased magnitude of the wind typically results in both a stronger geostrophic and ageostrophic response of the freshwater plume, in addition it gives rise to direct vertical wind-induced mixing.

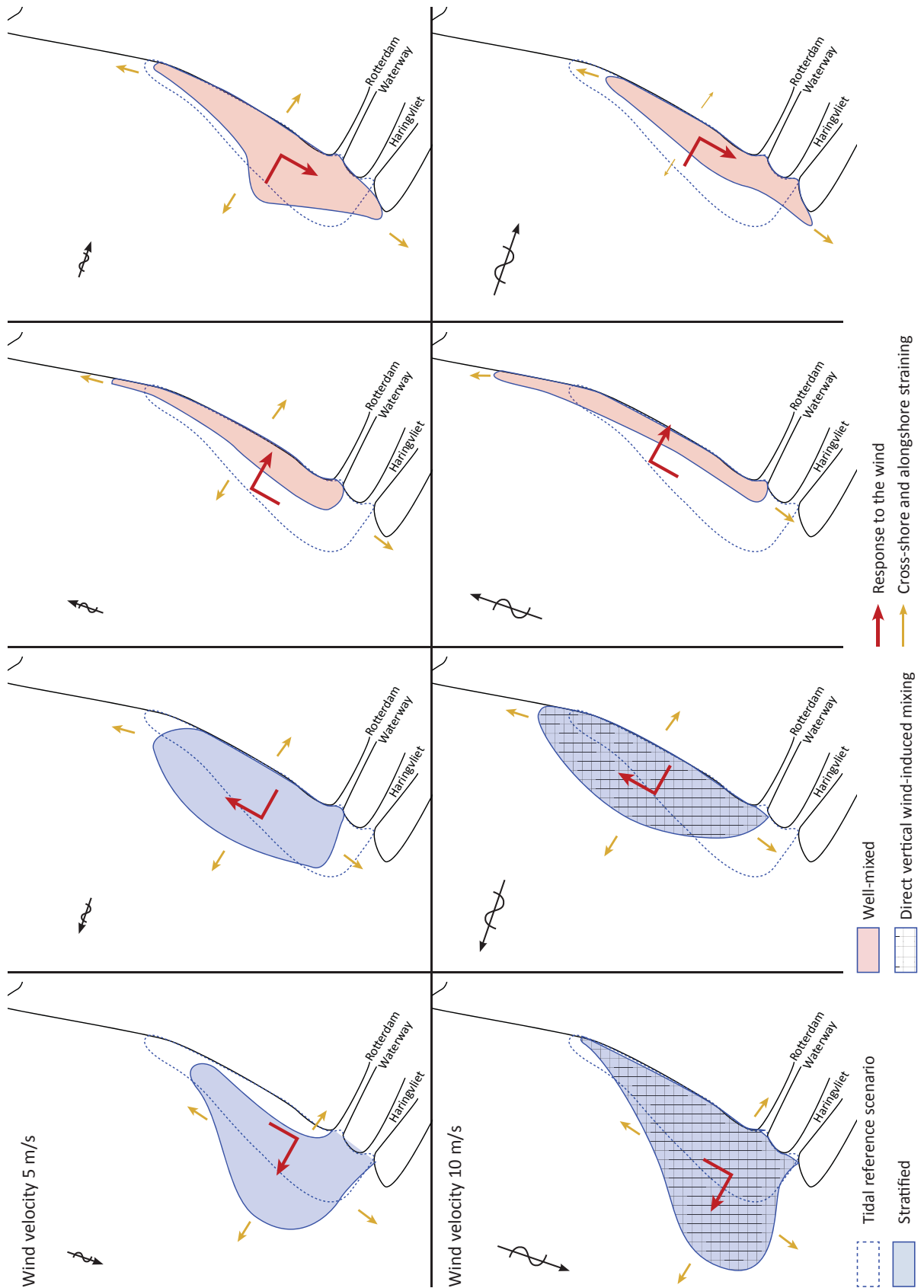


Figure 7.1: A sketch that summarises the wind-driven motions in the Rhine ROFI. The top panels present the 5 m s^{-1} wind scenarios, the bottom panels the 10 m s^{-1} scenarios. In horizontal direction the response of the Rhine ROFI to the different directions of the wind are discussed.

Alongshore northerly and offshore directed winds cause a response of the water column that widens the freshwater plume in the offshore direction. It results in an increase of stratification. For the 5 ms^{-1} northerly wind scenario a separation of the freshwater plume from the coast is observed in the snapshots of salinity (Figure 6.2, middle panels). The phenomenon is supported by modelling studies of Fong & Geyer (2001) where a separation of the plume for a moderate upwelling-favourable wind was observed. The results of the alongshore northerly wind in particular, demonstrate the importance of Ekman dynamics. The plume forced by the offshore directed wind has however also been pushed northwards, a tendency which is in line with observations in the Rhine ROFI by de Boer *et al.* (2009). The results as found are supported by studies on upwelling-favourable winds in the United States (e.g. Chao & Boicourt (1986); Fong *et al.* (1997) and Kourafalou *et al.* (1996a)). An increased magnitude of the wind further confirms the important role by Ekman dynamics, the plume forced by the alongshore northerly wind has stretched even farther offshore. A 10 ms^{-1} wind also favours direct shear-induced vertical wind mixing. Direct vertical mixing results in a reduced salinity anomaly (difference in salinity between the surface and bottom layer), accompanied by an increase in the thickness of the freshwater plume. The same phenomenon is described in the plume studies at the east coast of the United States by Chao (1988) and Fong & Geyer (2001). For all four scenarios tidal straining is observed in the cross-shore and alongshore direction, in line with the theory for the Rhine ROFI by de Boer *et al.* (2007). However, as stated above, it was not possible within the scope of this study to identify the exact locations of the different components.

The combined Ekman and ageostrophic response of the water column to alongshore southerly and onshore directed winds favours mixing and pushes the freshwater shoreward. It is in line with Chao & Boicourt (1986), who observed narrowing of a river plume for downwelling-favourable winds. Forced by the alongshore southerly wind the water column is in a more well-mixed state than if forced by the onshore directed wind. The plume has also been pushed ageostrophically northwards, whereas the Ekman component of the wind for the onshore wind scenario has pushed the water column southwards. In the results tidal straining is still observed in both cross-shore and alongshore direction. Forcing by an increased alongshore southerly and onshore directed wind results in an even further vertically well-mixed Rhine ROFI. In the alongshore direction tidal straining is observed. For the onshore directed wind, cross-shore tidal straining hardly happens and is only observed to a small extent around the mouth of the Rotterdam Waterway. For the alongshore southerly wind it can not be observed anymore.

In most of the model results a meandering freshwater plume is observed in the alongshore direction. The meandering is most pronounced for a 5 ms^{-1} onshore directed wind forcing, in that scenario it even resulted in the creation of freshwater filaments. Forced by a wind in the same direction, filaments of freshwater were also observed in remote sensing SST images of the Rhine ROFI, reported in de Boer *et al.* (2009). From the analysis as performed it is not possible to identify which specific factor causes the growth of the meanders, but we observed that a combination of the ebb-flood tidal cycle, the wind and the pulsed release of freshwater by the Rotterdam Waterway caused the creation. Kourafalou *et al.* (1996a) observed meandering of river plumes during periods of low mixing energy, which was caused by baroclinic instabilities and which grew for an increased input of buoyancy. Increased mixing reduced or even eliminated the meanders.

Stratification can be amplified by solar radiation and exchange of heat between the surface layer and the atmosphere. The results in this study are based on an April case with an average air temperature during the day of $15 \text{ }^\circ\text{C}$, a seawater temperature of $9 \text{ }^\circ\text{C}$ and an initial riverine water temperature of $10 \text{ }^\circ\text{C}$. The results of the temperature in the plume showed a limited

effect of heat exchange with the atmosphere. Both the small difference in temperature of the riverine water and the seawater and the limited effect of heat exchange with the atmosphere show a relatively limited impact on the buoyancy. It provides the possibility to use salinity as a proxy of the density to describe the dynamical processes in the Rhine ROFI. In the analysis of the potential energy anomaly (ϕ), discussed hereafter, both the effect of salinity and temperature are incorporated.

The integrated potential energy anomaly is introduced as a new application of the potential energy anomaly (ϕ). By integrating ϕ over depth and over an area enclosing the Rhine ROFI, the total amount of energy required to fully mix the freshwater plume has been found. It results in one single value, which can be plotted over time. A comparison between the different scenarios is easily made, see Figure 6.10. This application of the ϕ concept has been found a powerful tool in analysing the competition and interaction of mixing and straining by the wind and the tide. In all results straining and mixing are visible over the ebb-flood tidal cycle. In combination with the integrated potential energy anomaly the spatial change of ϕ is presented for the Rhine ROFI, see Figure 6.11.

The results of the tidal reference scenario show that the Rhine ROFI is maximally stratified at high water and closest to a well-mixed state at low water. The absence of wind and waves and the implementation of an average river discharge cause straining and mixing by the tide to dominate the state of the water column. The process of tidal straining found in the Rhine ROFI by Simpson & Souza (1995) and de Boer *et al.* (2007) is observed in the results.

Compared to the tidal reference scenario, northerly alongshore winds favour stratification. The 10 ms^{-1} scenario gives the most stratified conditions with respect to this study. The results show that the mixing capacity of the tide can be met by a stratifying capacity of the wind. It is observed that wind-straining and tidal straining do not strongly augment each other during the flood stages: the rate of change in ϕ does not increase much in a relative sense, however straining winds mostly add to the longer-timescale increase of ϕ . Over time the Rhine ROFI seems to come to a new equilibrium. The long-term trend in the change of ϕ becomes less and the variations are again dominated by the periods of straining and mixing related to the ebb-flood tidal cycle. This behaviour is in correspondence with the conceptual model of Fong & Geyer (2001). They state that if an upwelling-favourable wind is sustained long enough, the final response of the freshwater plume will be to stop widening and approach a steady state uniform thickness.

For moderate offshore directed winds the integrated value of the potential energy anomaly does not change much compared to the tidal reference scenario. However, both the size and location of the freshwater plume have clearly altered, see the spatial redistribution of ϕ (Figure 6.11). For an increased offshore directed wind the same redistribution of ϕ is observed. The integrated potential energy anomaly presents a decrease in the amount of energy required for a fully mixed water column. This scenario is very interesting, it seems that the different physical factors and processes are all interacting with each other and have similar magnitudes. Tidal mixing, tidal straining, depth mean advection and direct vertical wind-induced mixing occur. With the integrated potential energy anomaly analysis tool as presented here it is not possible to individually identify those and other subtle processes. These detailed processes are however important in analysing wind-mixing and wind-straining. It is only with a full potential energy anomaly analysis, such as the one by de Boer *et al.* (2007), that these processes can be identified individually.

Onshore directed winds are expected to work in favour of mixing. From the integrated value of ϕ it is however observed that for the 5 ms^{-1} scenario, more energy is required than for the tidal reference scenario. A local increase of ϕ due to an accumulation of river water, just

north of the mouth of the Rotterdam Waterway, seems to dominate the decrease elsewhere. For the increased magnitude of the onshore directed wind a double peak in the integrated value of ϕ is observed around high water. Snapshots of ϕ (Figure A.21) suggest a temporal increase in the near-field stratification around high water, most presumably caused by the release of freshwater from the Rotterdam Waterway.

The results of the integrated value of ϕ show that southerly alongshore winds work in favour of mixing. From the plots of the spatial change of ϕ it is observed that a decrease of ϕ in the far-field is accompanied by an increase in the near-field. An increased magnitude of the wind results in a decrease of ϕ over the entire Rhine ROFI. For this scenario the Rhine ROFI comes closest to a completely well-mixed state.

The influence of the wind on upwelling and downwelling by the tide is investigated. The tidal reference scenario is consistent with de Boer *et al.* (2009). Off the coast the results show downwelling at slack before ebb and upwelling at slack before flood. By adding moderate downwelling winds to upwelling-favourable tidal conditions, it is concluded that the tidal influence is dominant. If wind is added to a tidally induced downwelling system, it results in a patchy distribution of positive and negative vertical velocities over the Rhine ROFI and the surrounding area. These patchy results differ from what would be expected in idealised conditions. It is presumed that both bathymetric variations and alongshore gradients in current and density play a role. An increased wind speed does not lead to a notable increase in upwelling or downwelling. Here it must be realised that the wind driven component is relatively small with respect to the tidal component of upwelling and downwelling and that the locally patched distributions of the vertical velocities dominate the signal.

Chapter 8

Conclusions & recommendations

The research presented in this thesis has improved our understanding of the hydrodynamics acting in the Rhine ROFI when it is stratified. Since stratification is the key to the distribution of SPM (suspended particle matter), a further understanding of the hydrodynamics in the Rhine ROFI is indispensable. To that end the study has been valuable for predicting the situation concerning (temporary increased concentrations of) SPM and turbidity in the Rhine ROFI during and after the construction of Maasvlakte 2. Here some of the numerical aspects of the MoS² ZUNO-DD model are discussed, accompanied with recommendations for an improvement of the model in the future. The numerical aspects follow from both the sensitivity analysis in Chapter 5 and from the physical interpretation of the numerical results in Chapter 6. Thereafter the implications of the physical results for the Port of Rotterdam Authority are discussed, together with recommendations for future research.

A sensitivity analysis of the numerical model provided an indication of the effect of the number and distribution of σ -layers over the vertical on the reproduction of stratification in the Rhine ROFI in the model. The original implementation of 12 non-equidistant distributed σ -layers reproduces the state of the Rhine ROFI reasonably well; see also Cronin *et al.* (2010). The lack of field data for proper validation restricts us to qualitative conclusions. It is however concluded that the solution is sensitive to changes in the vertical resolution if 24 instead of 12 layers are used, particularly under stratified conditions. The differences in solution between 24 and 48 layers are relatively small. Future validation of the hydrodynamic model on the basis of field data (salinity, temperature, velocities) is extremely valuable for the further development of an accurate three-dimensional model of the North Sea.

The analysis of stratification in the Rhine ROFI is also affected by the resolution of the horizontal grid. In a coarser grid less resolution of the gradients (a form of numerical diffusion) in salinity, temperature and potential energy is available. Processes of mixing and straining affecting the stratification that are calculated on the finest numerical grid should in principal give the most accurate solutions. It was observed that under certain stratified conditions the freshwater plume reached into the intermediate grid. A reduced resolution of the grid does not have to be of concern if the processes of interest act on a larger scale. However horizontal numerical diffusion reduces vertical gradients as well. Numerical accuracy of the solutions may decrease as the freshwater plume first leaves and then re-enters the fine grid. For future studies it is recommended to enlarge the fine grid of the model in the seaward direction, roughly between the Haringvliet and Noordwijk.

In this study the main focus was on the freshwater plume in the area within the highest resolution grid and close to the river mouths. Additionally, the most important analyses are of a relative nature (all conducted within the same model setup). The 48-hour averaging of the salinity profiles also introduces diffusion. Therefore, the effects of the horizontal resolution

are not deemed to affect the conclusions of this study.

In the analysis of the vertical velocities associated with upwelling and downwelling (Section 6.5) patchy distributions of positive and negative velocities were observed. When interpreting these patchy distributions it must be noted that the model solves the equations of motion under the hydrostatic assumption, the irregular bathymetry should be taken into account and the fact that bathymetric gradients are relatively large in the near-coastal zone. Hence it is an open question to what extent the numerical artefacts play a role in the patchy distribution of positive and negative vertical velocities.

The physical interpretation of the modelling studies has shown that the wind-driven motions of the freshwater plume under stratified conditions are largely influenced by the Coriolis force. Thereby they play an important role in the hydrodynamics of the Rhine ROFI. Under neap tide conditions the size and shape of the freshwater plume and the accompanying stratification have been found to be highly variable. At the start of the research it was thought that the behaviour of stratification in the Rhine ROFI would be largely dominated by tidally-induced bottom friction due to the shallowness of the system. Stratification is the key to understanding the distribution of SPM in the Rhine ROFI; consequently a better understanding of the role of tides and wind in the Rhine ROFI is indispensable. It is recommended to extend the study on the various factors and physical processes acting in the Rhine ROFI. In addition a more quantifiable study of the different processes is preferred. Such studies will contribute to the ability to predict the situation concerning SPM in the Rhine ROFI.

By having increased the number of layers in the present MoS²ZUNO-DD model and with the recommendation for a seaward extension of the fine grid, this study has contributed to the ability to model the Rhine ROFI. An improved numerical model enhances the possibility to predict the impact of the construction of Maasvlakte 2 on the Southern North Sea, both on the long and short term. The improved knowledge of the hydrodynamics in the Rhine ROFI will also contribute to the interpretation of the measurements that are being carried out by the Port of Rotterdam Authority. Additionally the main findings of the model can be used for an improvement of the DELWAQ model by Deltares for the calculation of SPM concentrations in the Southern North Sea.

Appendix A

Supporting figures

48-hour averaged salinity profiles:

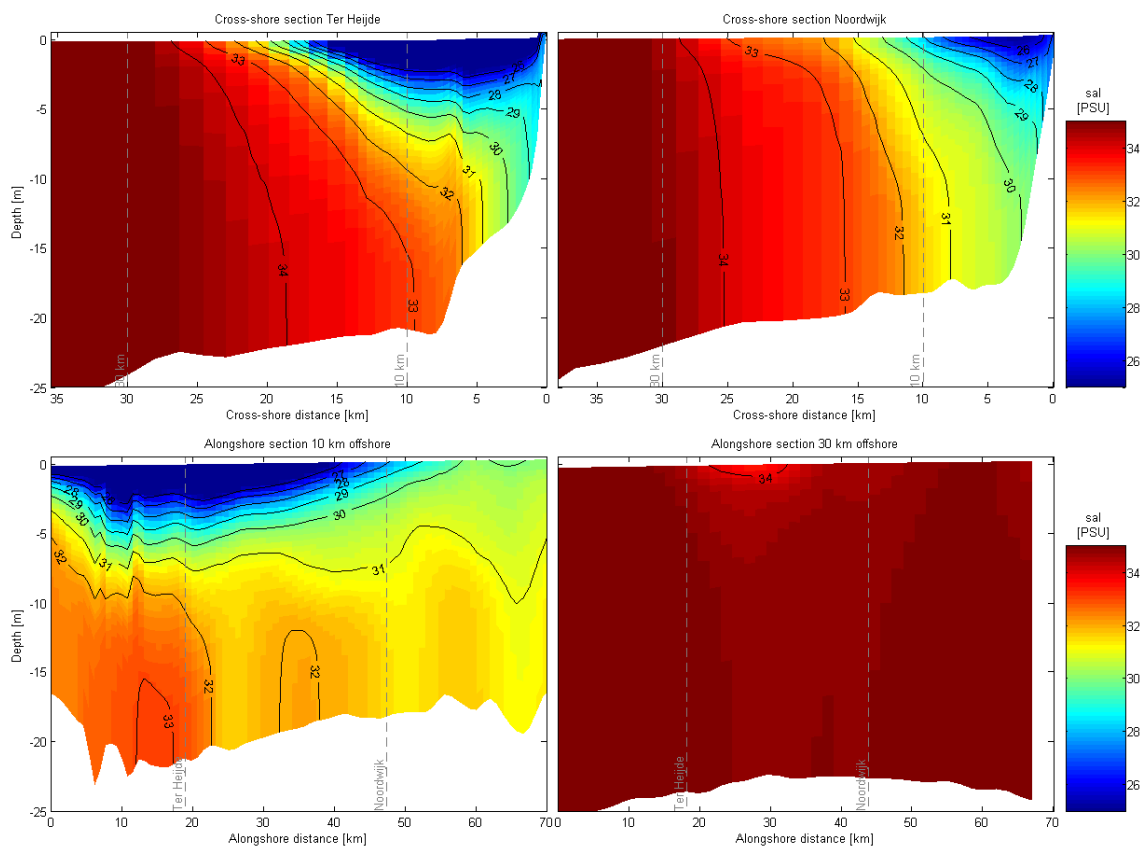


Figure A.1: 48-hour averaged salinity profiles of the no wind scenario.

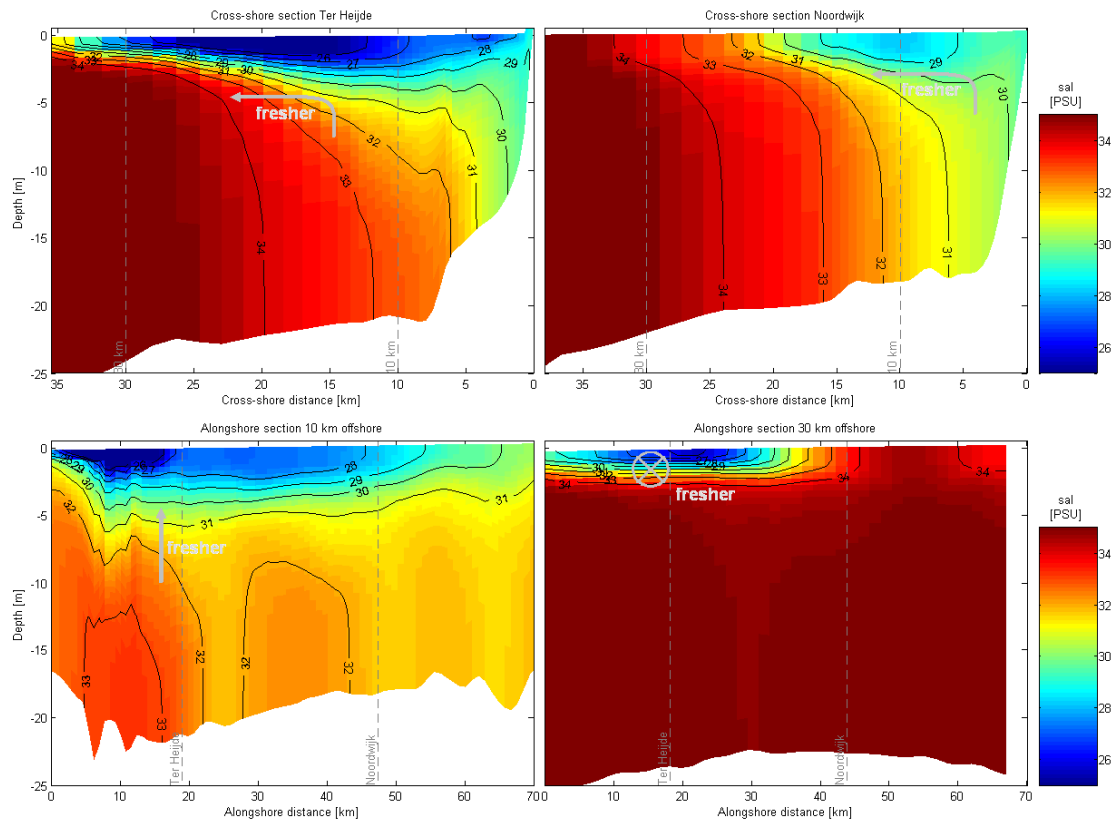


Figure A.2: 48-hour averaged salinity profiles for the 5 ms^{-1} northerly wind scenario.

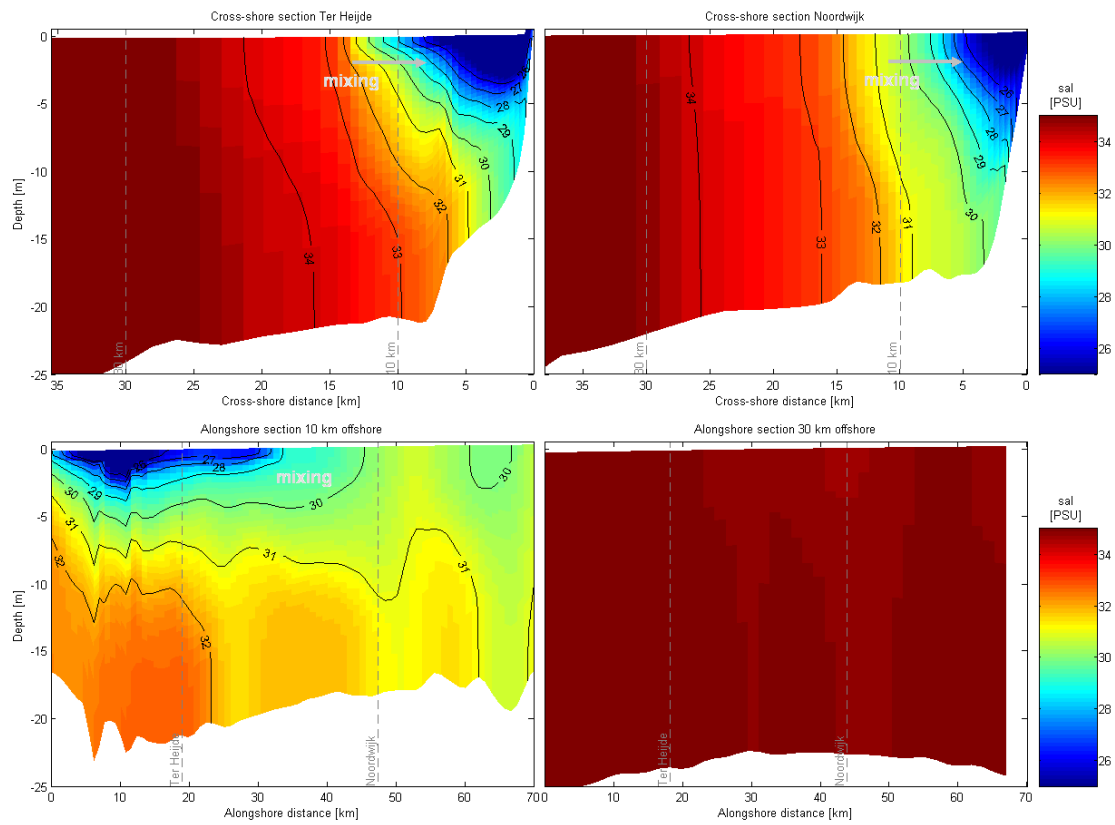


Figure A.3: 48-hour averaged salinity profiles for the 5 ms^{-1} southerly wind scenario.

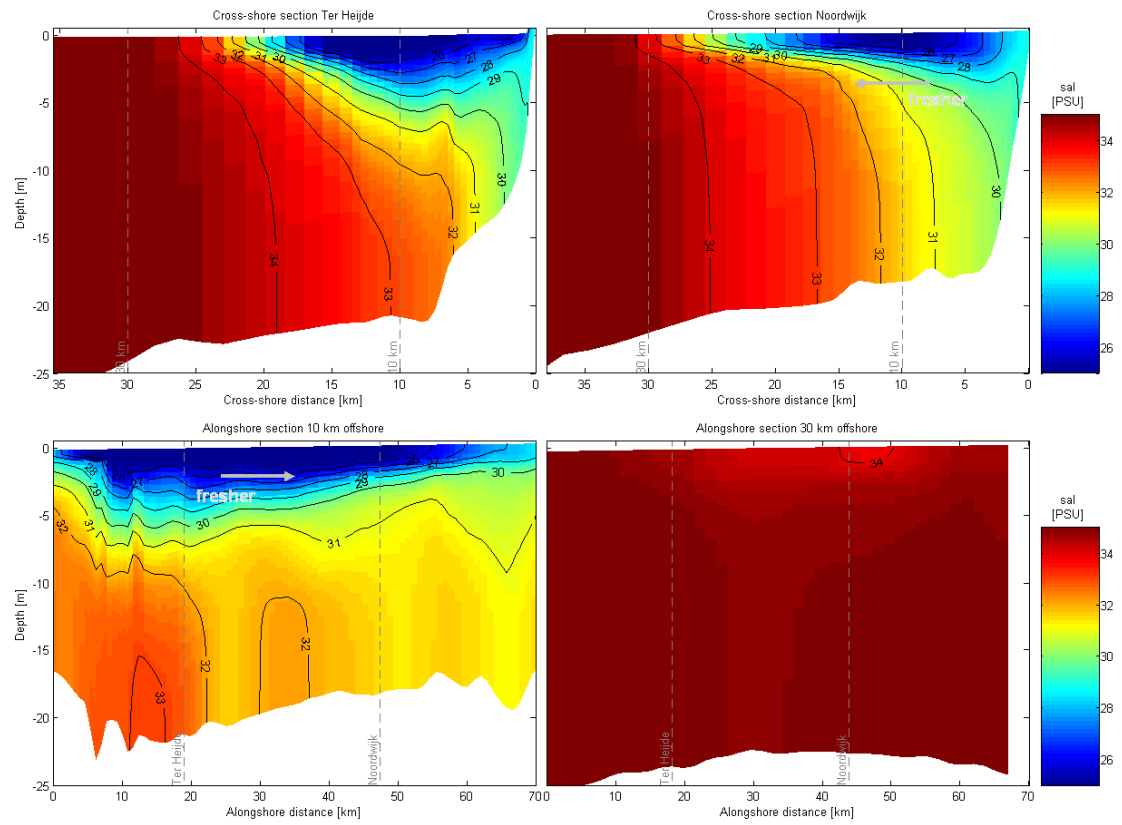


Figure A.4: 48-hour averaged salinity profiles for the 5 ms^{-1} offshore wind scenario.

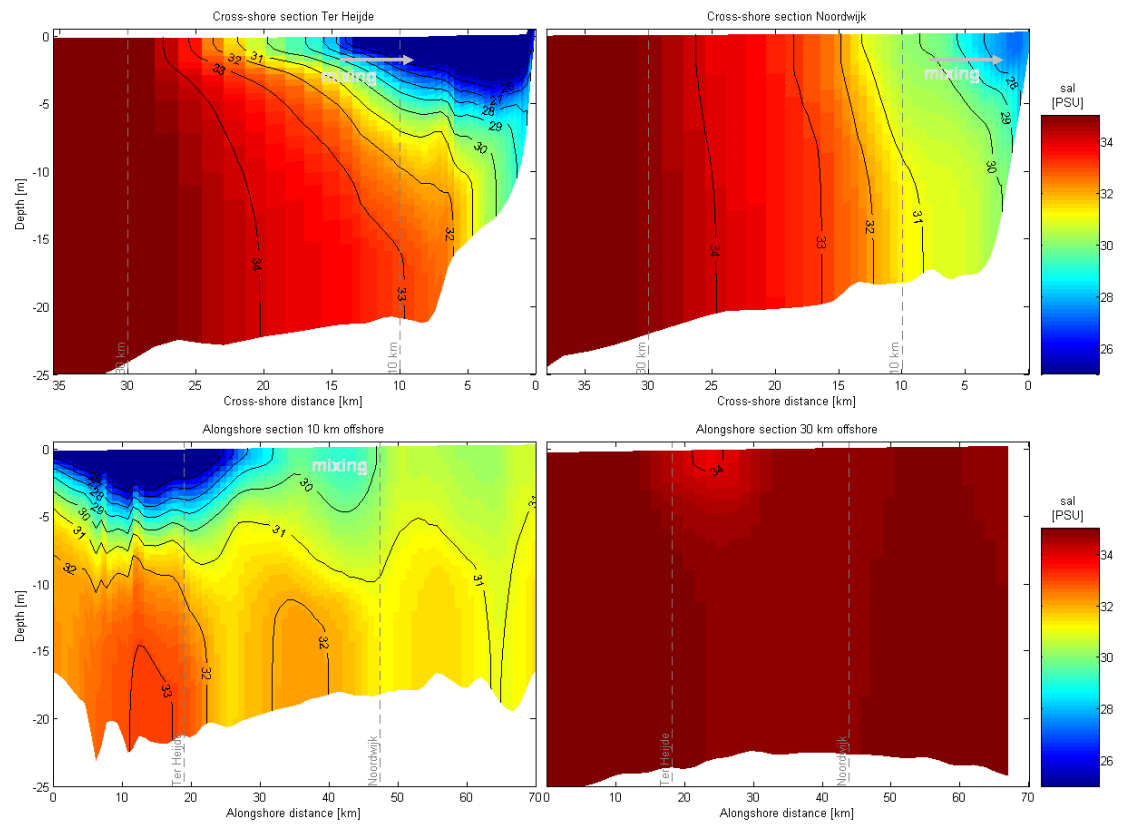


Figure A.5: 48-hour averaged salinity profiles for the 5 ms^{-1} onshore wind scenario.

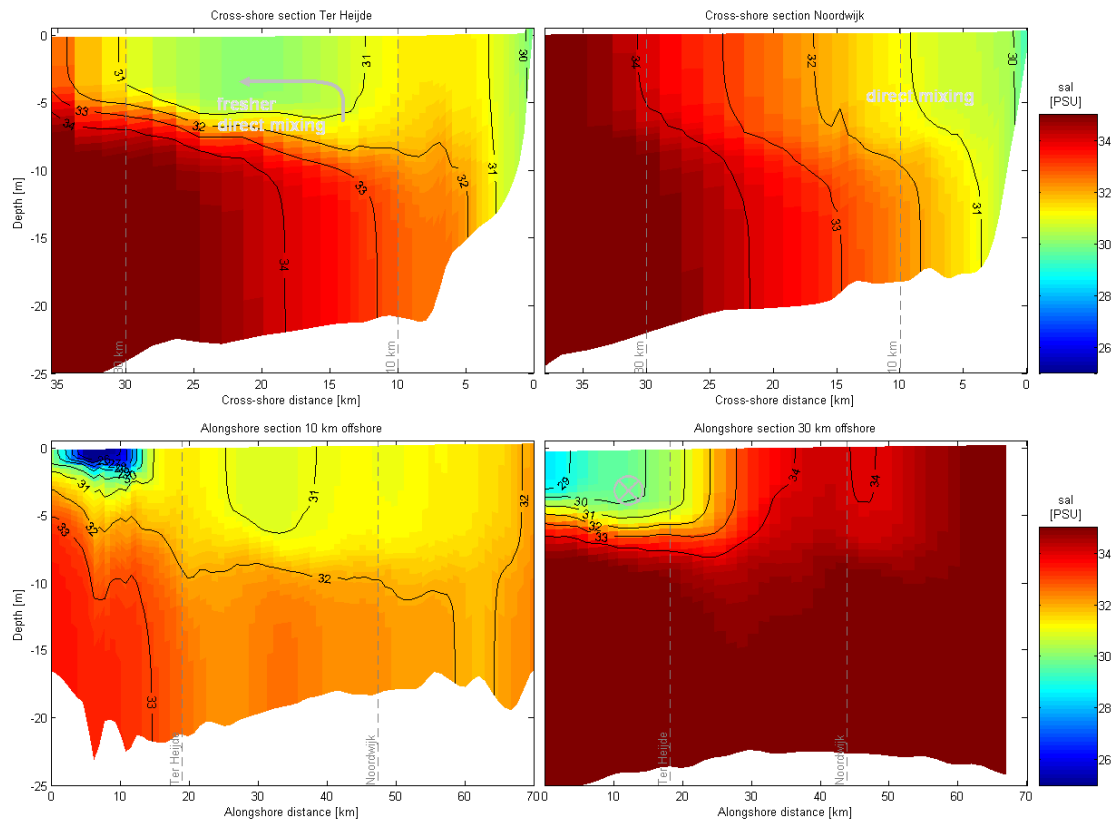


Figure A.6: 48-hour averaged salinity profiles for the 10 ms^{-1} northerly wind scenario.

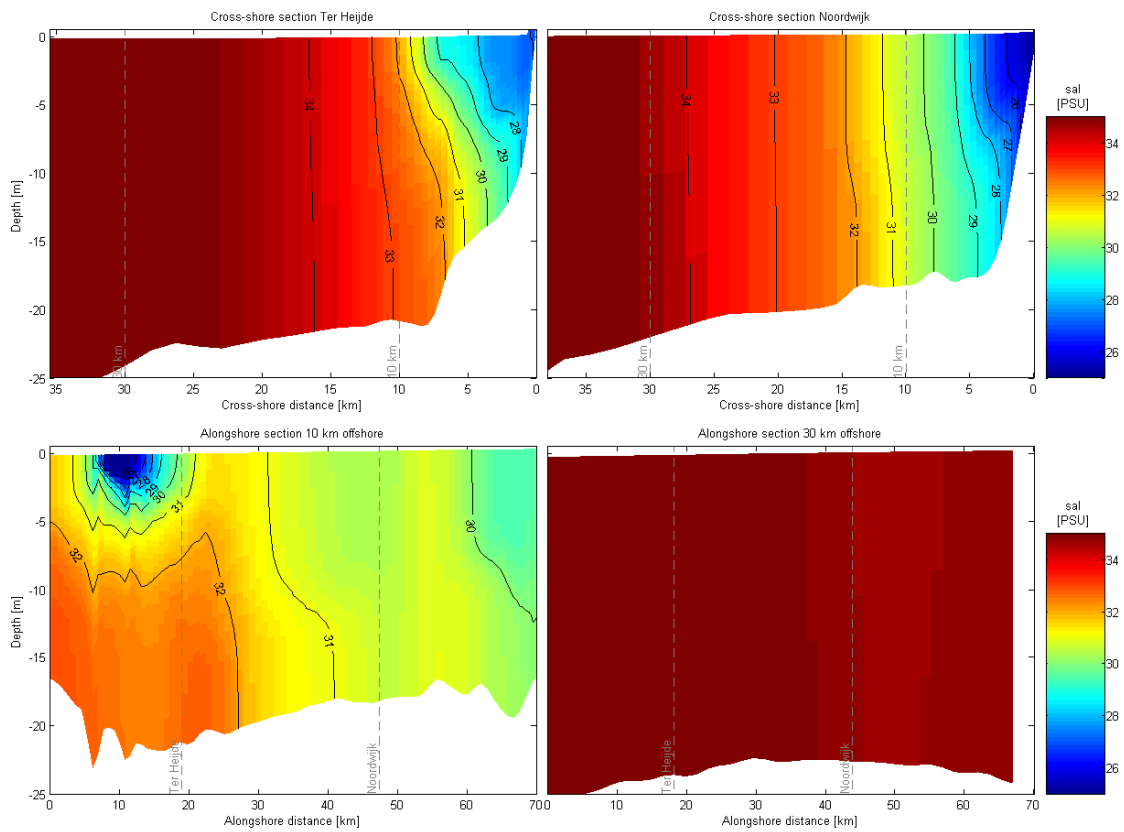


Figure A.7: 48-hour averaged salinity profiles for the 10 ms^{-1} southerly wind scenario.

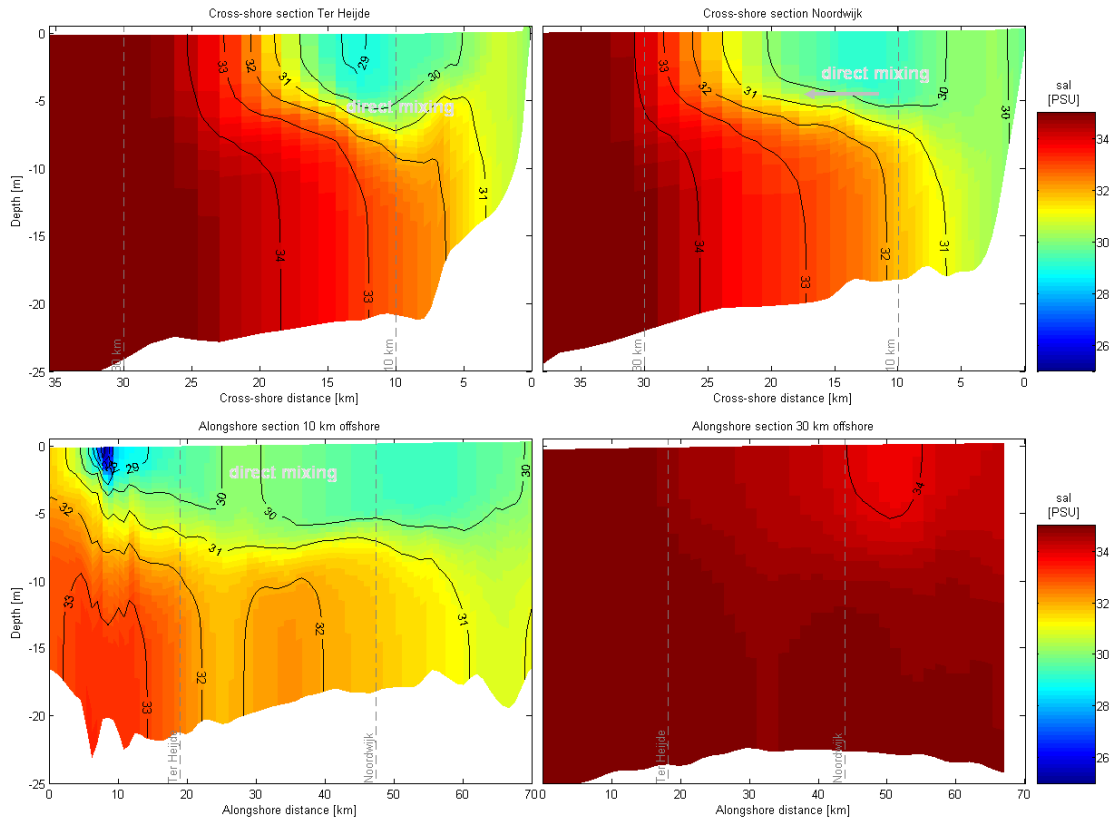


Figure A.8: 48-hour averaged salinity profiles for the 10 ms^{-1} offshore wind scenario.

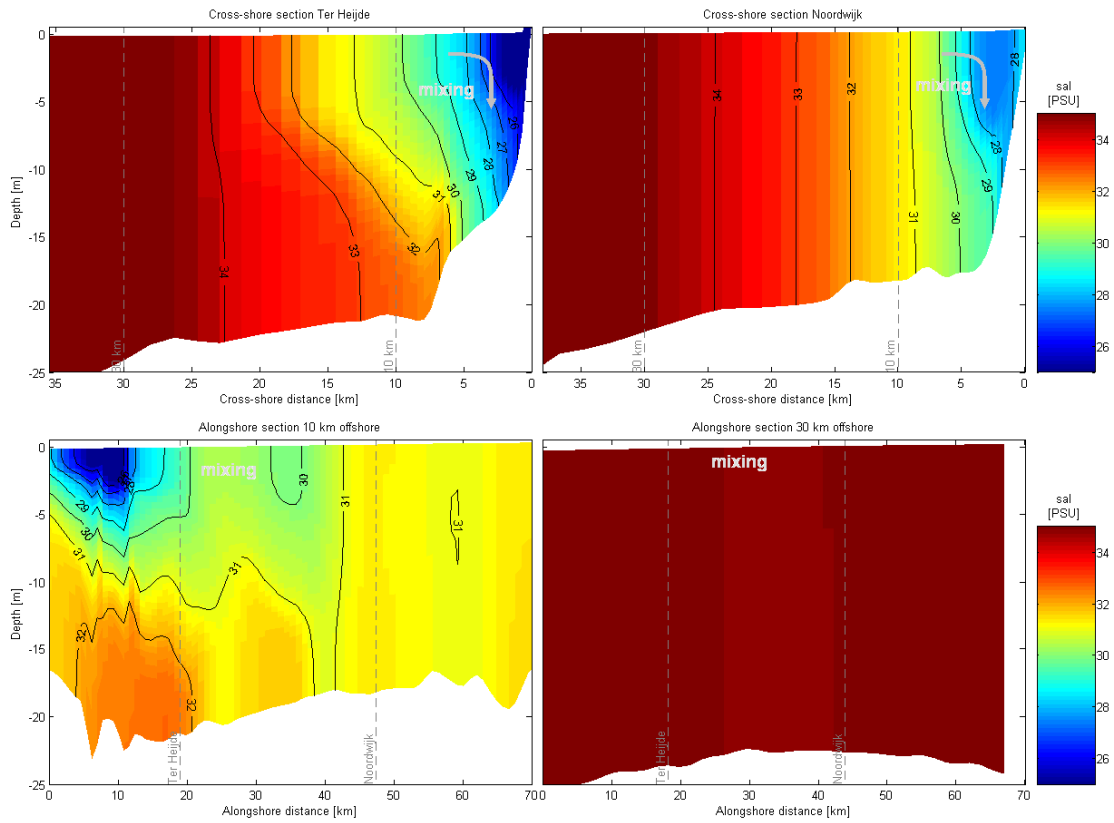


Figure A.9: 48-hour averaged salinity profiles for the 10 ms^{-1} onshore wind scenario.

Salinity snapshots:

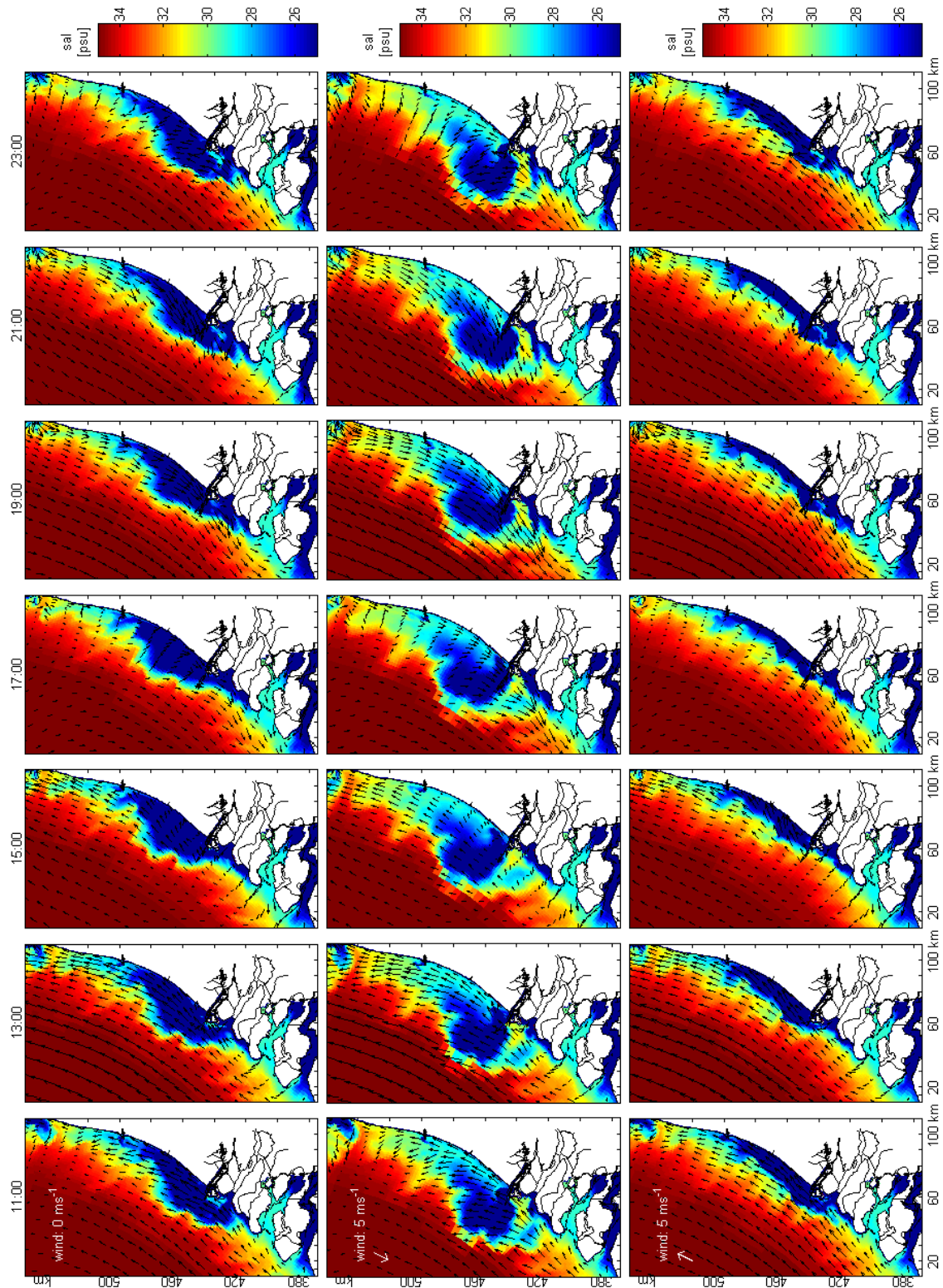


Figure A.10: Snapshots of the salinity profiles over the last tidal cycle taken every two hours. The top panel gives the results of the no wind scenario, in the middle the results of the 5 ms⁻¹ northerly wind and in the bottom the results for the 5 ms⁻¹ southerly wind forcing.

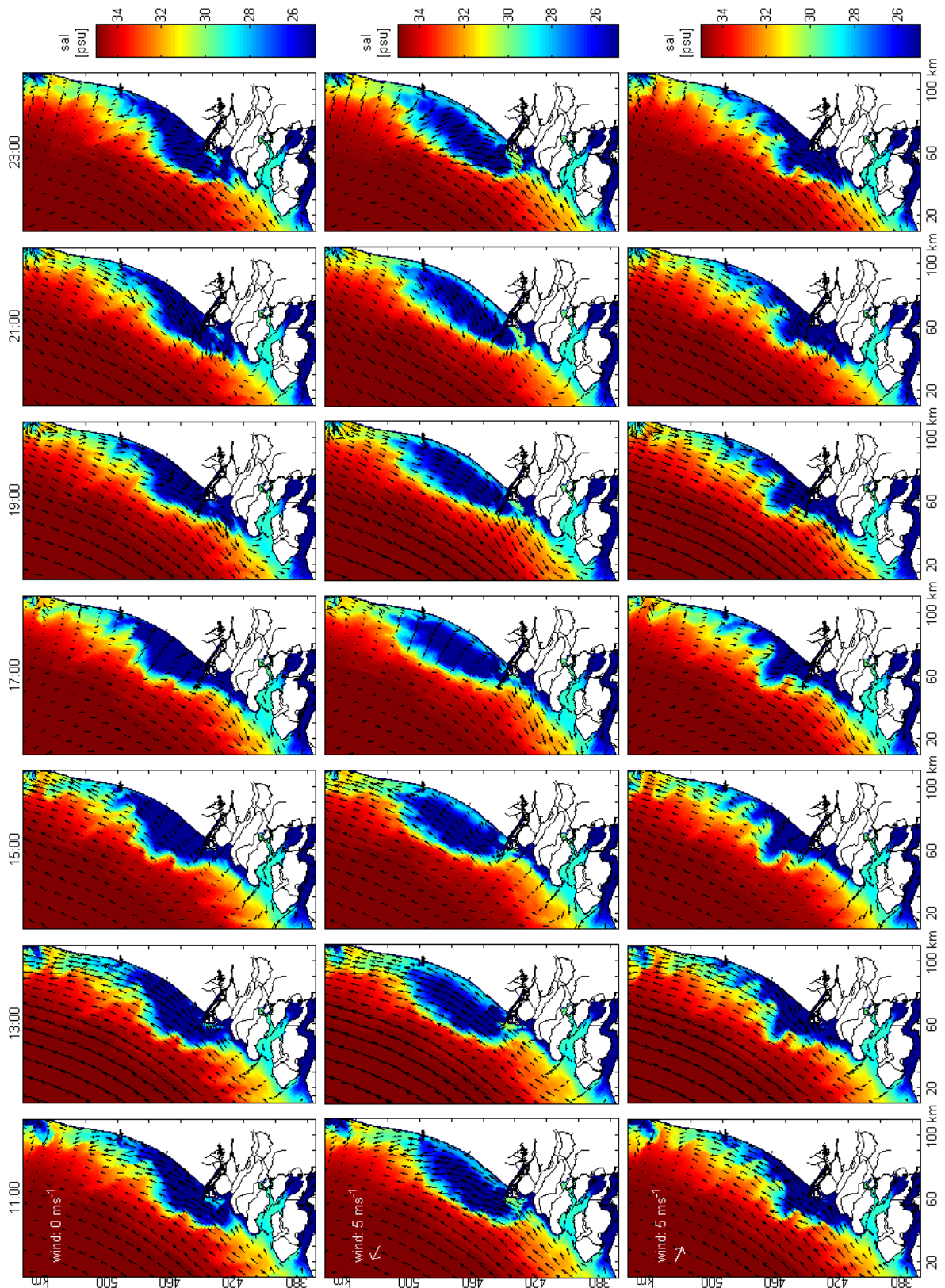


Figure A.11: Snapshots of the salinity profiles over the last tidal cycle taken every two hours. The top panel gives the results of the no wind scenario, in the middle the results of the 5 ms⁻¹ offshore wind and in the bottom the results for the 5 ms⁻¹ onshore wind forcing.

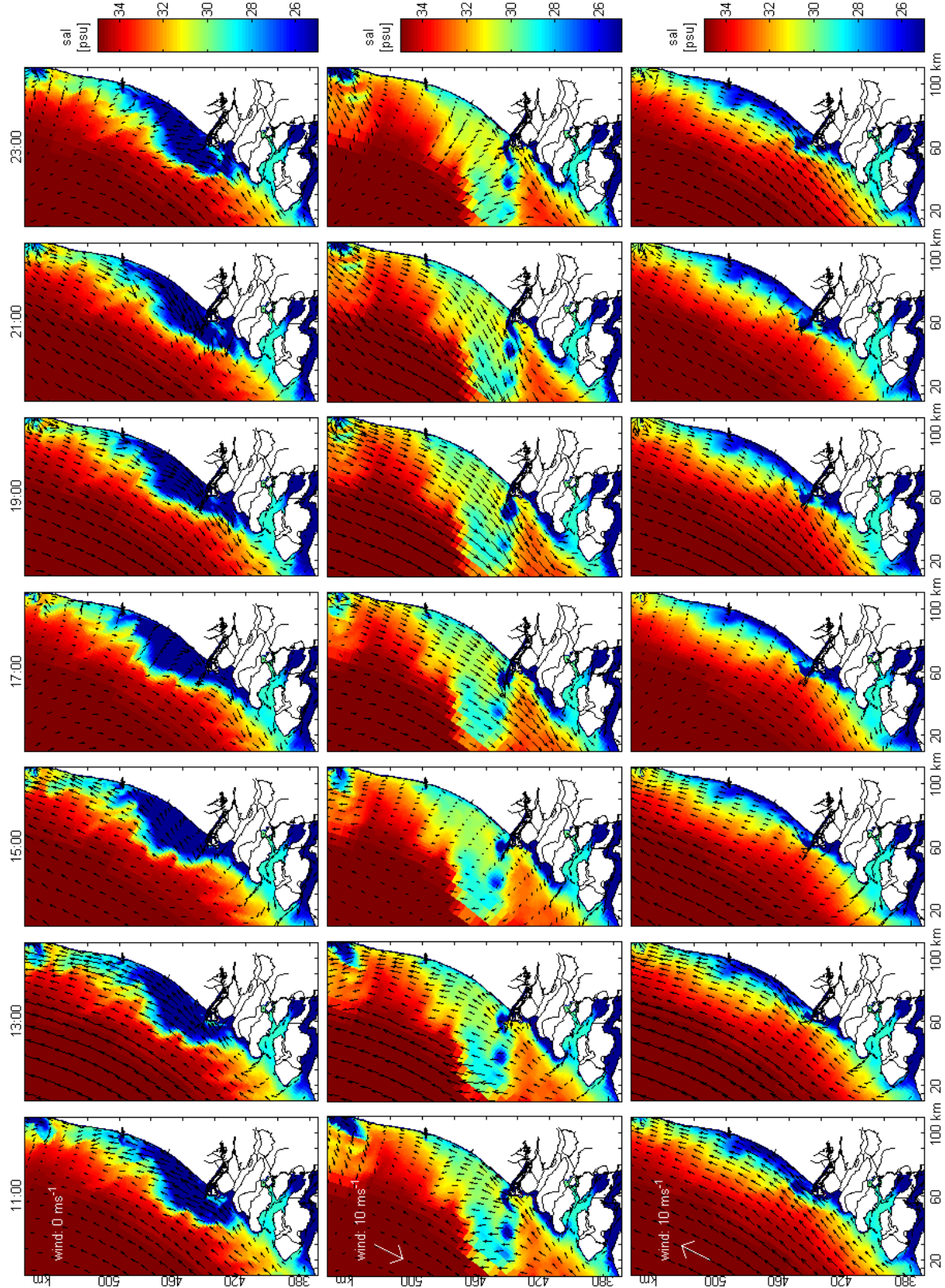


Figure A.12: Snapshots of the salinity profiles over the last tidal cycle taken every two hours. The top panel gives the results of the no wind scenario, in the middle the results of the 10 ms^{-1} northerly wind and in the bottom the results for the 10 ms^{-1} southerly wind forcing.

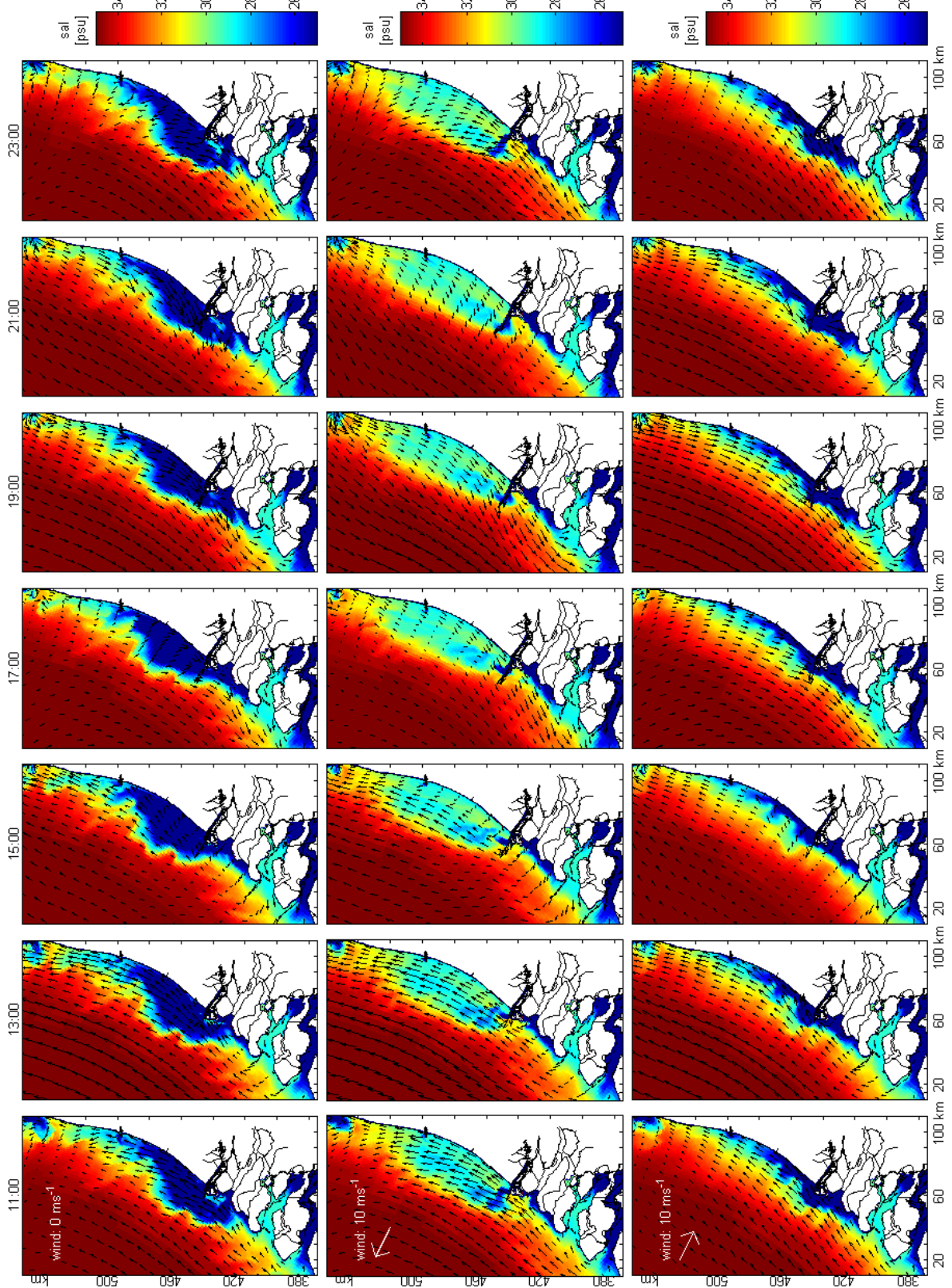


Figure A.13: Snapshots of the salinity profiles over the last tidal cycle taken every two hours. The top panel gives the results of the no wind scenario, in the middle the results of the 10 ms⁻¹ offshore wind and in the bottom the results for the 10 ms⁻¹ onshore wind forcing.

Temperature snapshots

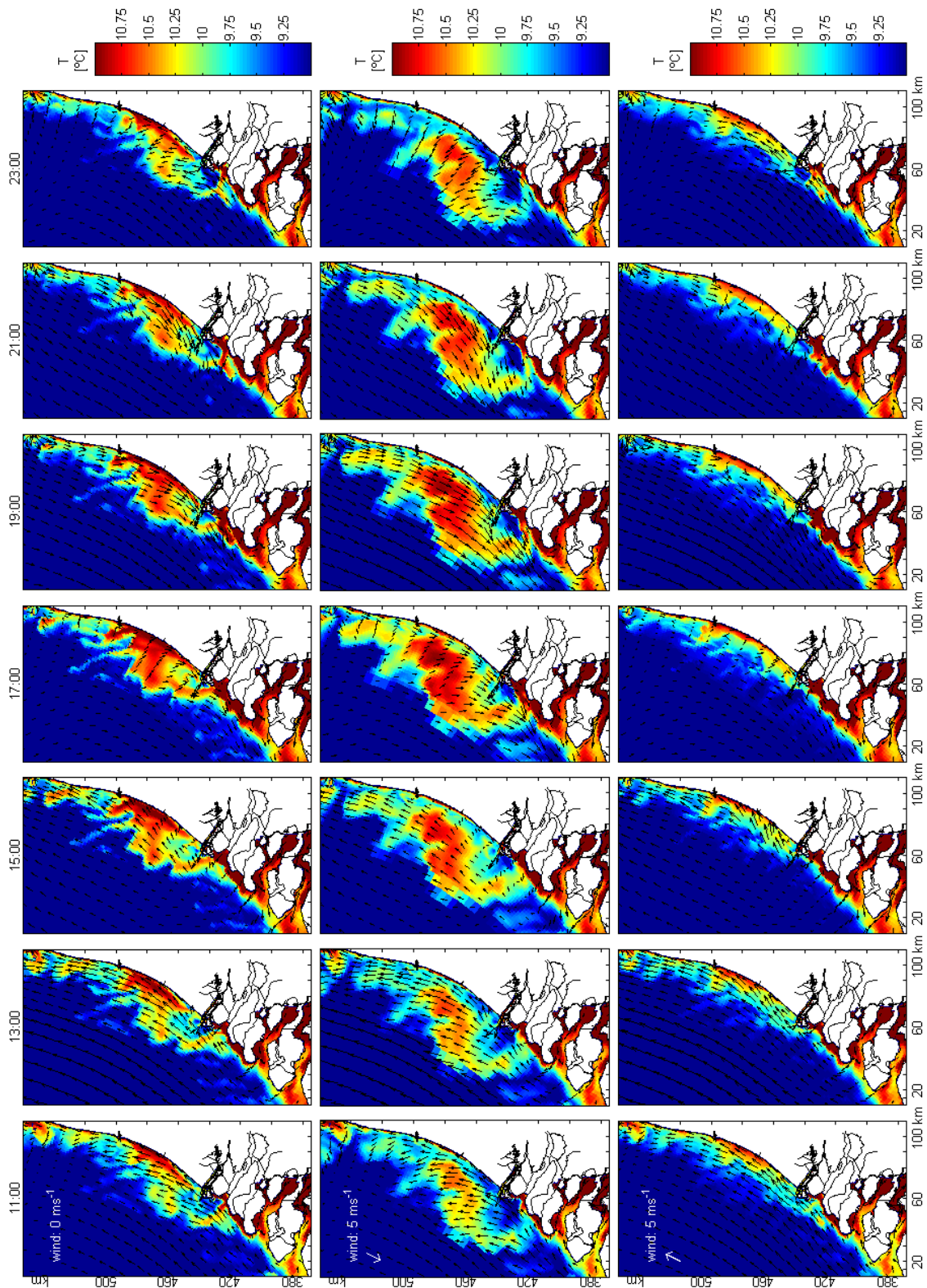


Figure A.14: Snapshots of the temperature profiles over the last tidal cycle taken every two hours. The top panel gives the results of the no wind scenario, in the middle the results of the 5 ms⁻¹ northerly wind and in the bottom the results for the 5 ms⁻¹ southerly wind forcing.

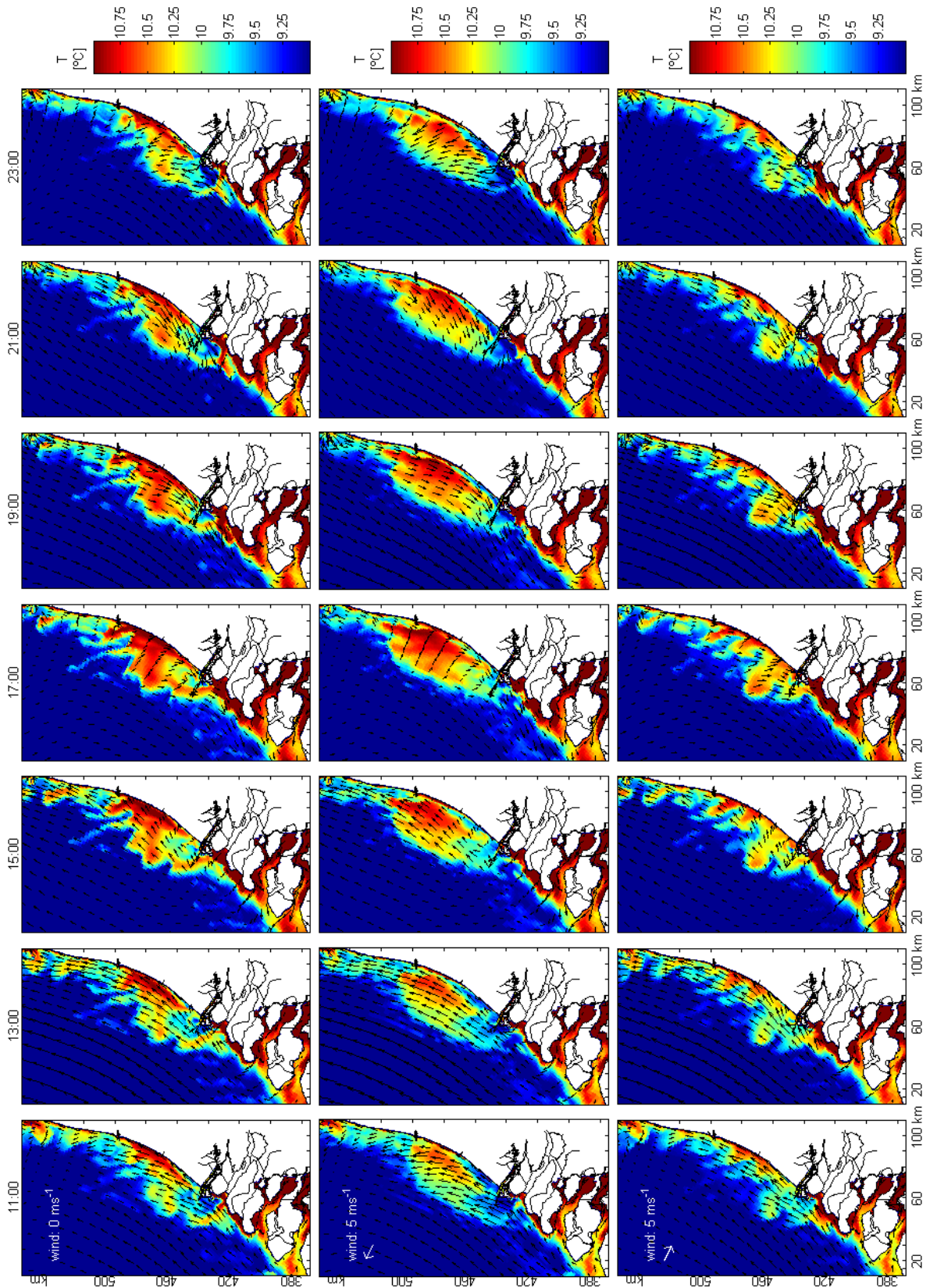


Figure A.15: Snapshots of the temperature profiles over the last tidal cycle taken every two hours. The top panel gives the results of the no wind scenario, in the middle the results of the 5 ms⁻¹ offshore wind and in the bottom the results for the 5 ms⁻¹ onshore wind forcing.

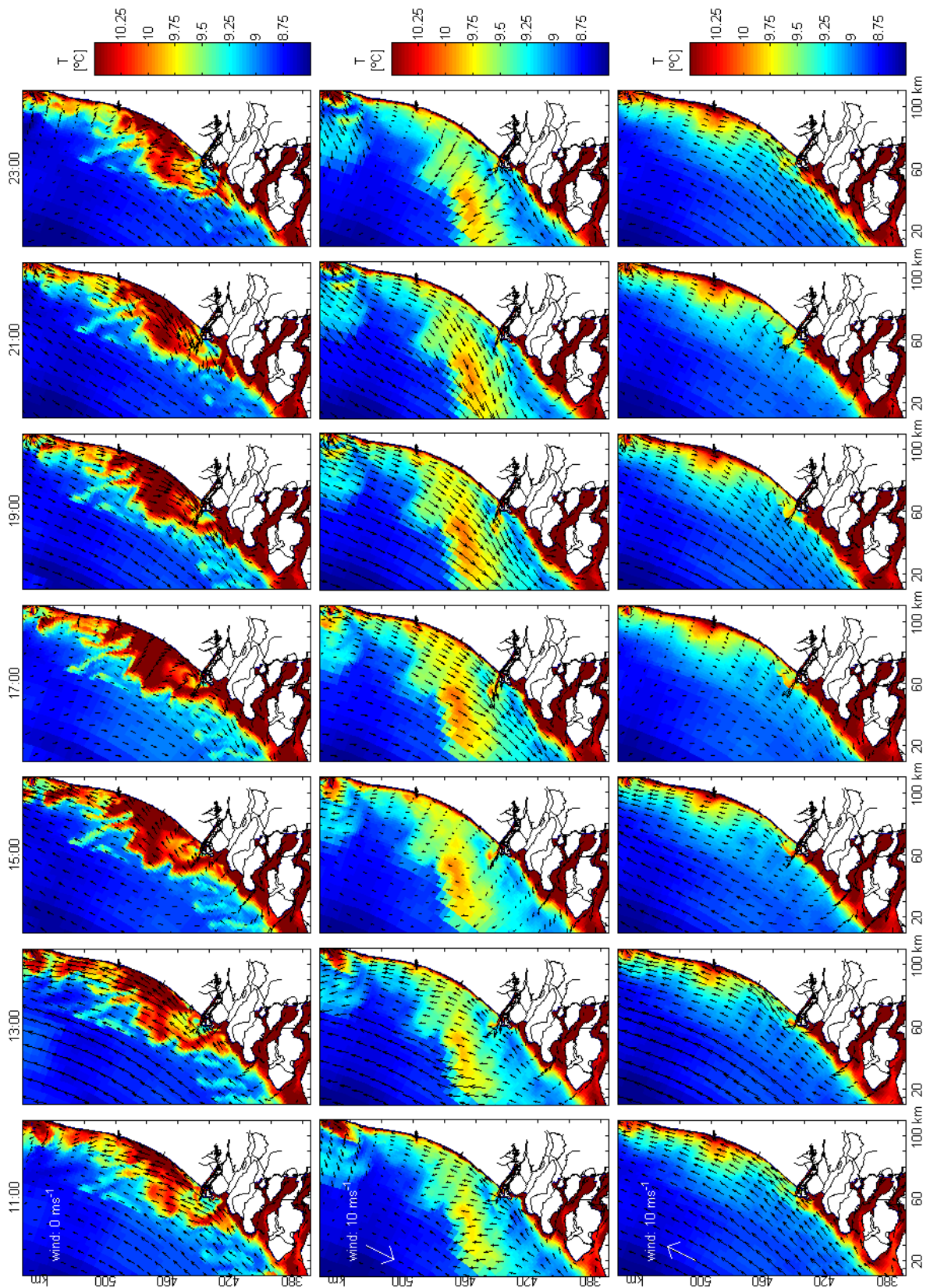


Figure A.16: Snapshots of the temperature profiles over the last tidal cycle taken every two hours. The top panel gives the results of the no wind scenario, in the middle the results of the 10 ms^{-1} northerly wind and in the bottom the results for the 10 ms^{-1} southerly wind forcing.

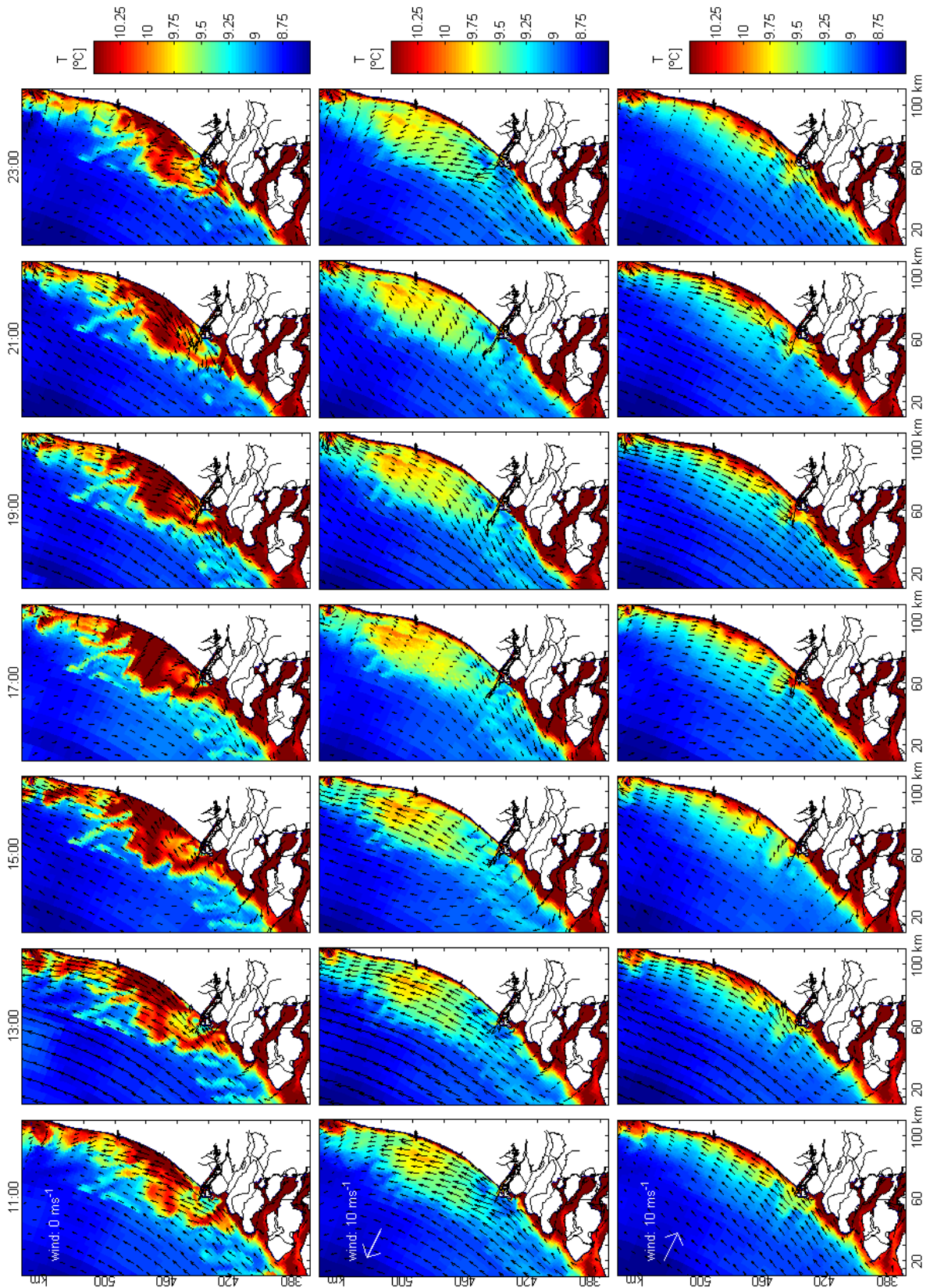


Figure A.17: Snapshots of the temperature profiles over the last tidal cycle taken every two hours. The top panel gives the results of the no wind scenario, in the middle the results of the 10 ms⁻¹ offshore wind and in the bottom the results for the 10 ms⁻¹ onshore wind forcing.

Potential energy anomaly snapshots

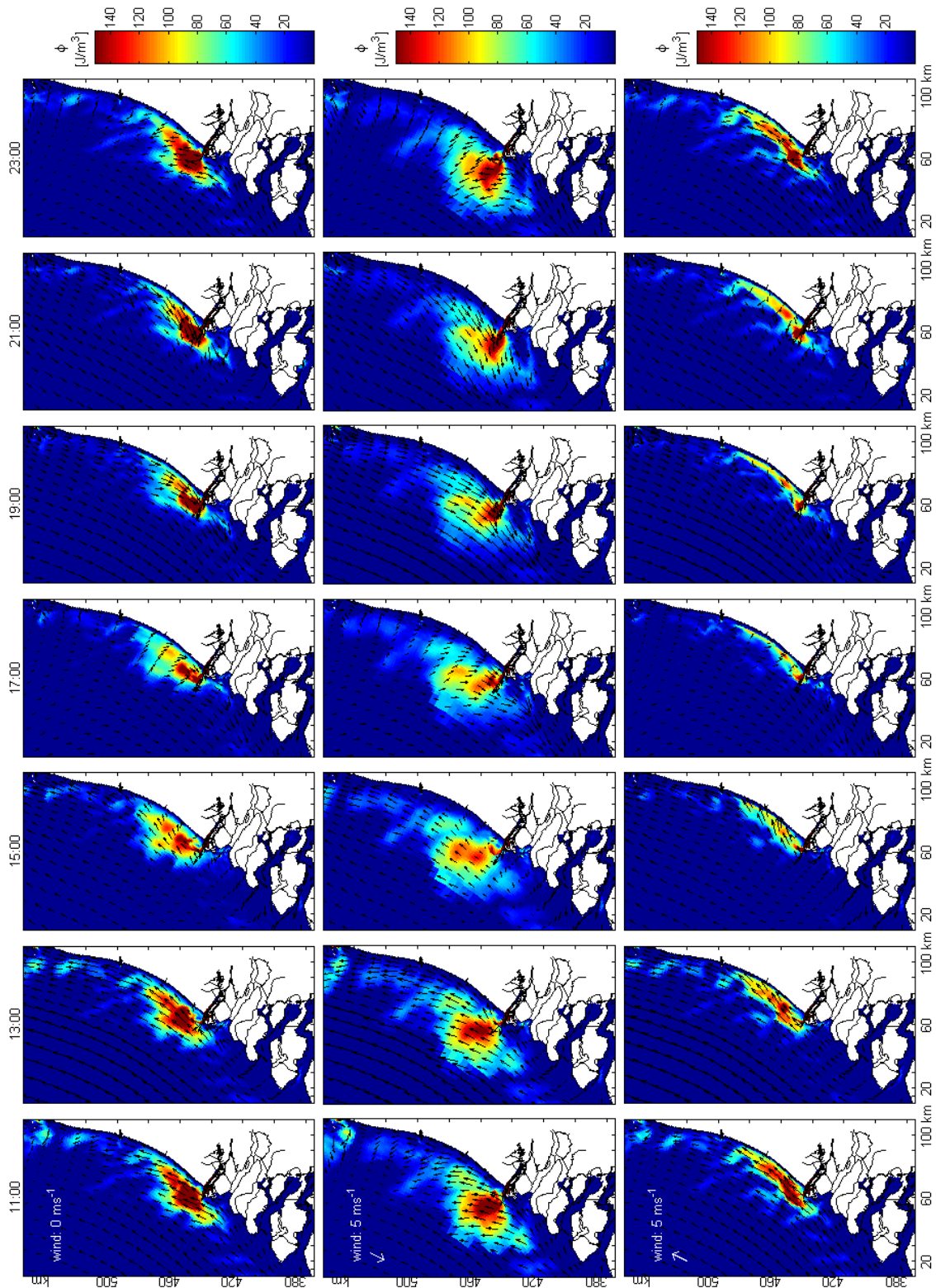


Figure A.18: Snapshots of the potential energy anomaly profiles over the last tidal cycle taken every two hours. The top panel gives the results of the no wind scenario, in the middle the results of the 5 ms⁻¹ northerly wind and in the bottom the results for the 5 ms⁻¹ southerly wind forcing.

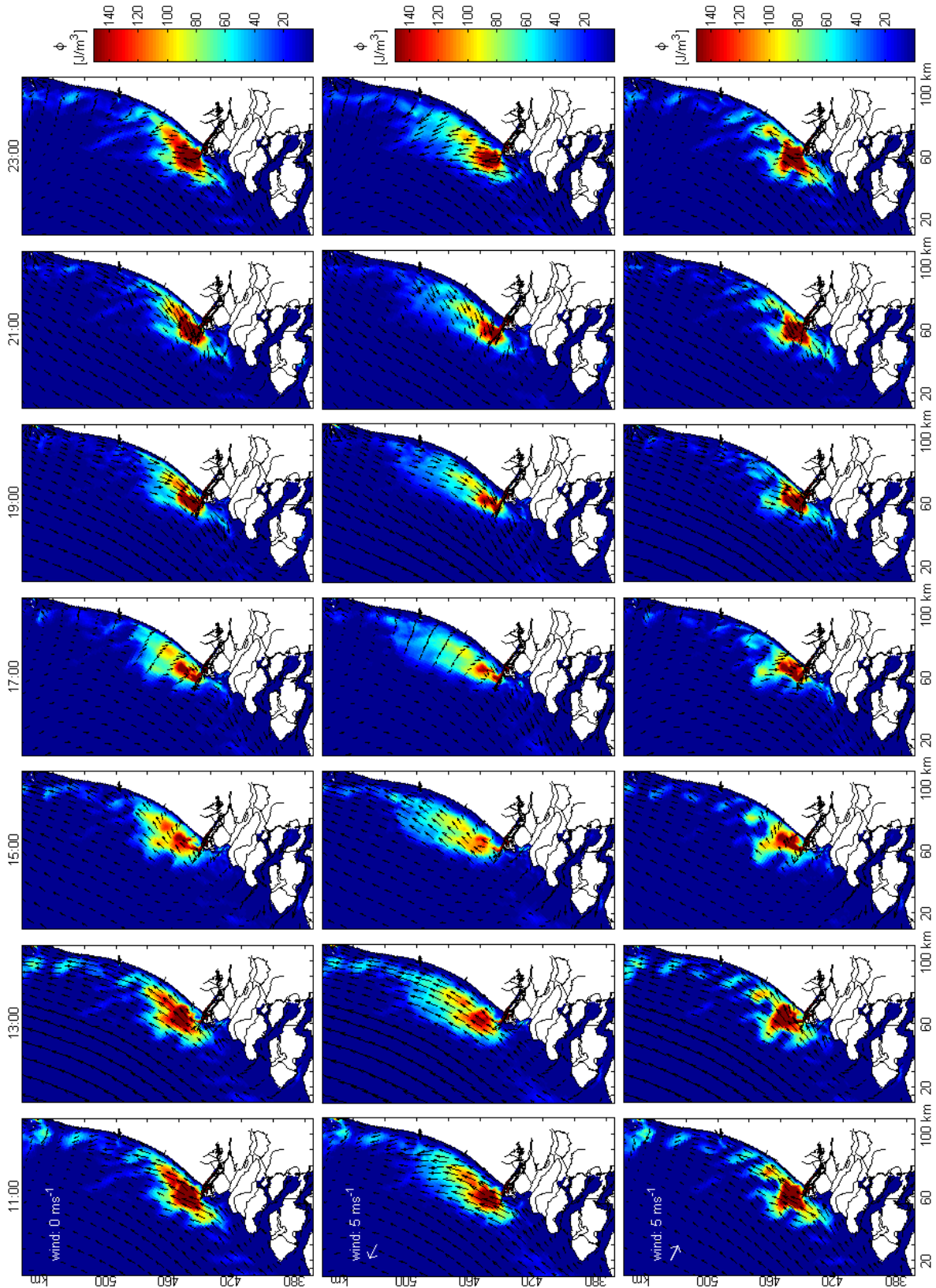


Figure A.19: Snapshots of the potential energy anomaly profiles over the last tidal cycle taken every two hours. The top panel gives the results of the no wind scenario, in the middle the results of the 5 ms^{-1} offshore wind and in the bottom the results for the 5 ms^{-1} onshore wind forcing.

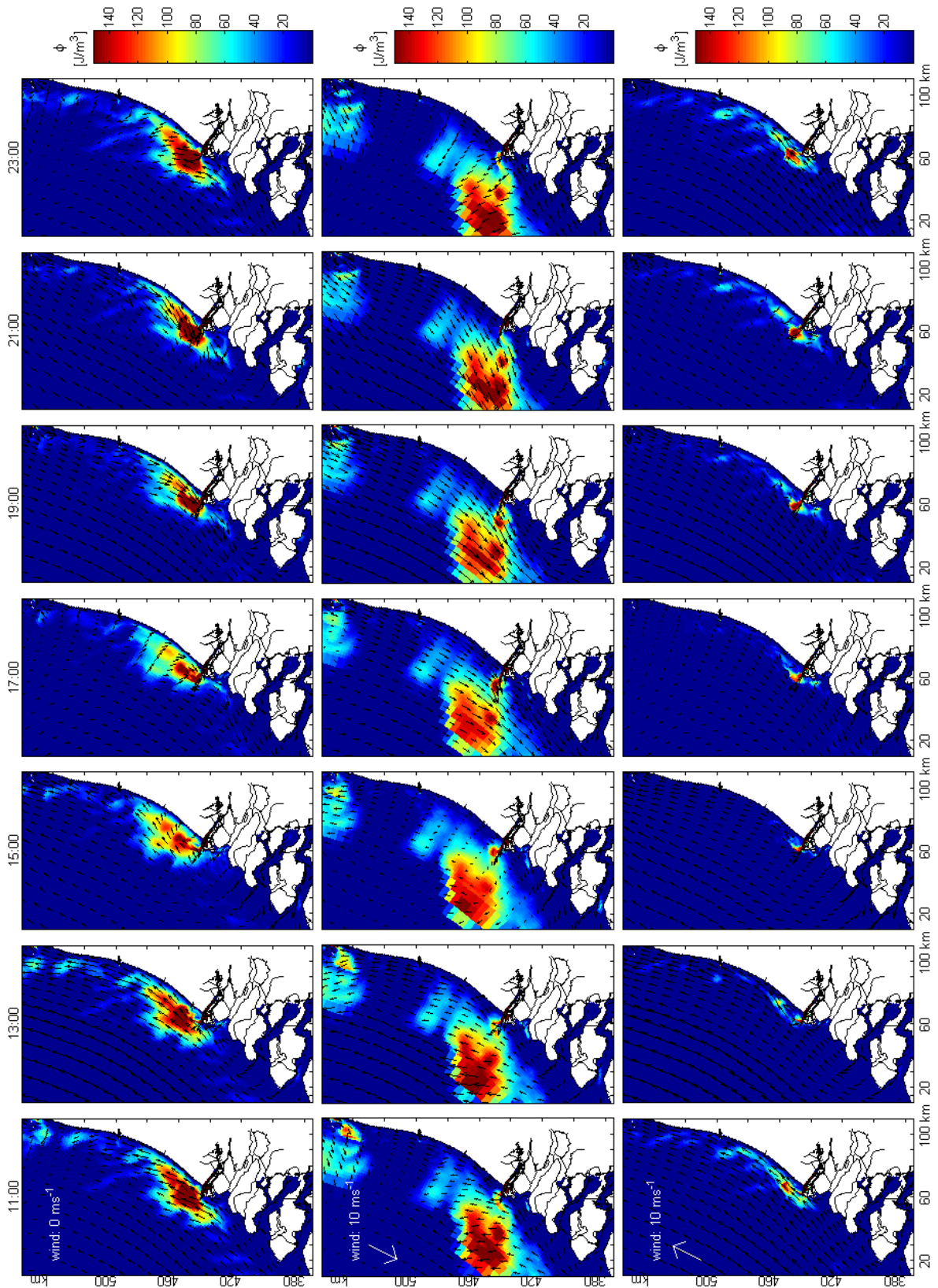


Figure A.20: Snapshots of the potential energy anomaly profiles over the last tidal cycle taken every two hours. The top panel gives the results of the no wind scenario, in the middle the results of the 10 ms⁻¹ northerly wind and in the bottom the results for the 10 ms⁻¹ southerly wind forcing.

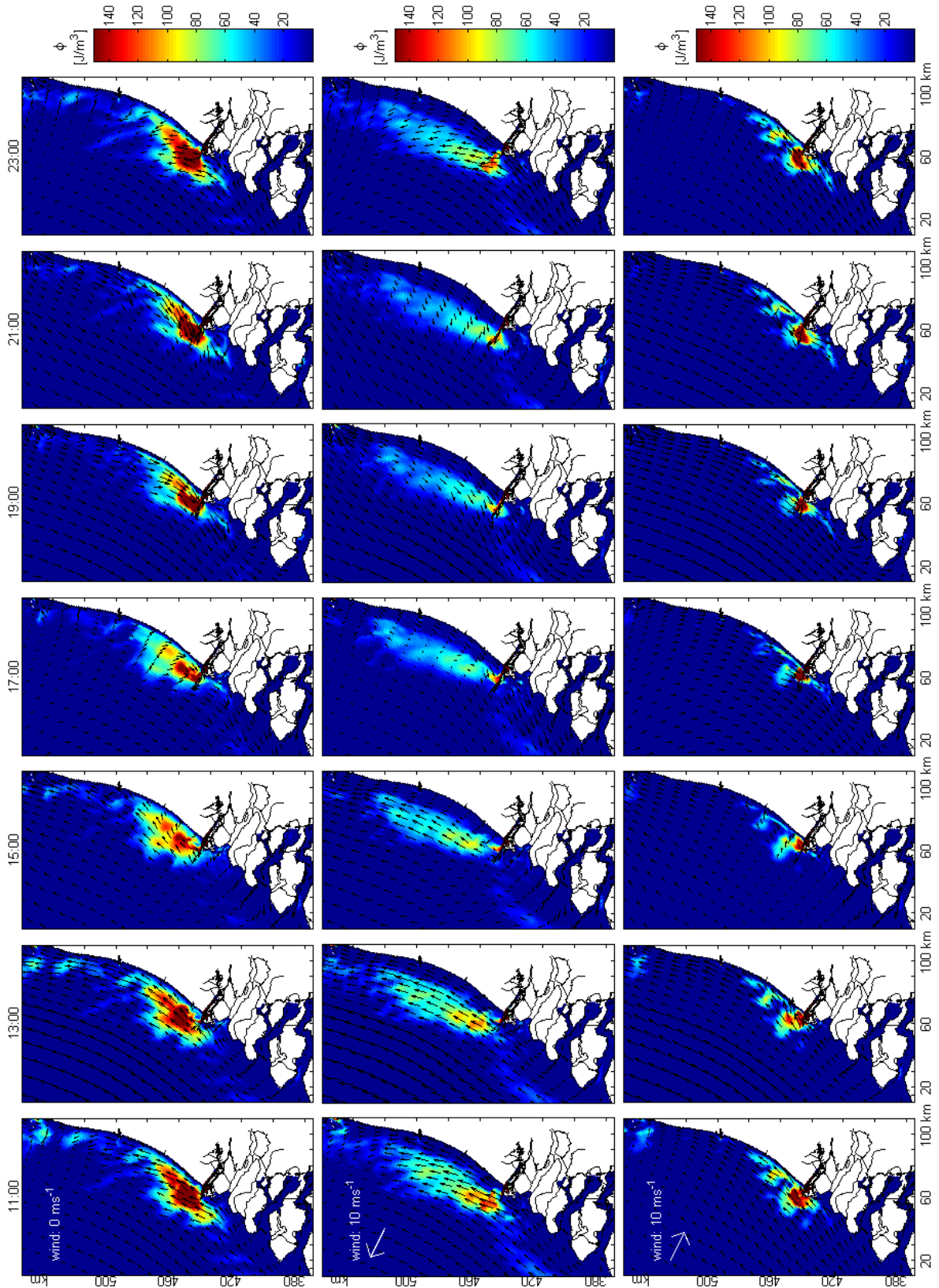


Figure A.21: Snapshots of the potential energy anomaly profiles over the last tidal cycle taken every two hours. The top panel gives the results of the no wind scenario, in the middle the results of the 10 ms^{-1} offshore wind and in the bottom the results for the 10 ms^{-1} onshore wind forcing.

Appendix B

Mathematical support

Heaps:

Heaps (1972) uses the equations of continuity and motion for his theorem. The equation of continuity for an incompressible fluid is given by:

$$\frac{\partial u}{\partial x} + \frac{\partial v}{\partial y} + \frac{\partial w}{\partial z} = 0. \quad (\text{B.1})$$

The three-dimensional equations of motion under the f -plane approximation, that is to assume a constant Coriolis force, and where the Coriolis terms are neglected in z -direction, are given by:

$$\frac{\partial u}{\partial t} + u \frac{\partial u}{\partial x} + v \frac{\partial u}{\partial y} + w \frac{\partial u}{\partial z} = -\frac{1}{\rho} \frac{\partial p}{\partial x} + fv + \text{other forces} \quad (\text{B.2})$$

$$\frac{\partial v}{\partial t} + u \frac{\partial v}{\partial x} + v \frac{\partial v}{\partial y} + w \frac{\partial v}{\partial z} = -\frac{1}{\rho} \frac{\partial p}{\partial y} - fu + \text{other forces} \quad (\text{B.3})$$

$$\frac{\partial w}{\partial t} + u \frac{\partial w}{\partial x} + v \frac{\partial w}{\partial y} + w \frac{\partial w}{\partial z} = -\frac{1}{\rho} \frac{\partial p}{\partial z} - g + \text{other forces} \quad (\text{B.4})$$

From here, Heaps (1972) considered the motion of water bounded by a straight infinitely long coast with cross-shore sections of the same geometry. It provides the possibility to eliminate the dependency in alongshore direction from the equations of motion and continuity:

$$\frac{\partial}{\partial x} \int u dz + \frac{\partial}{\partial y} \int v dz = 0 \quad (\text{B.5})$$

$$-\frac{1}{\rho} \frac{\partial p}{\partial x} + N \frac{\partial^2 u}{\partial z^2} = -fv \quad (\text{B.6})$$

$$-\frac{1}{\rho} \frac{\partial p}{\partial y} + N \frac{\partial^2 v}{\partial z^2} = fu \quad (\text{B.7})$$

$$-\frac{1}{\rho} \frac{\partial p}{\partial z} + g = 0. \quad (\text{B.8})$$

x and y are the Cartesian co-ordinates in cross-shore and alongshore direction respectively, z is the depth below the surface. u and v are the components of the current at depth z . ρ is the density of the water and p the pressure at any position in the sea. N is a coefficient of eddy viscosity (assumed to be a known function of x). f is the geostrophic coefficient, $2\omega \sin$

ϕ , where ω is the angular speed of Earth's rotation and ϕ the latitude. g is the acceleration of Earth's gravity.

Under the assumption of hydrostatic pressure,

$$p = p_a + g\rho(z + \zeta), \quad (\text{B.9})$$

and the elimination of dependency in y -direction, the steady-state equations of continuity and motion become:

$$\frac{\partial}{\partial x} \int_{-\zeta}^h u dz = 0, \quad (\text{B.10})$$

$$N \frac{\partial^2 u}{\partial z^2} = -fv + g(z + \zeta) \frac{1}{\rho} \frac{\partial \rho}{\partial x} + g \frac{\partial \zeta}{\partial x}, \quad (\text{B.11})$$

$$N \frac{\partial^2 v}{\partial z^2} = fu. \quad (\text{B.12})$$

In the frictionless limit case of (B.11), only the generated Coriolis force is present to balance the cross-shore pressure gradient. This will result in an alongshore geostrophic flow in northward direction, the 'thermal wind balance'. Conversely, with friction being important, the pressure gradient is balanced by the non-uniform velocity shear generated by the cross-shore exchange current, 'estuarine circulation'. Heaps formulas combine the alongshore thermal wind balance and the cross-shore estuarine circulation in a joint residual current structure.

Prandle:

Prandle (1982a) derived analytical solutions to the linearised flow equations. The flow equations follow from Bowden *et al.* (1959) and are expressed on a Cartesian grid. A homogeneous water column with a vertically uniform eddy viscosity is presumed. The vertical components of the velocity and acceleration terms, the convective terms and the density effects are disregarded:

$$\frac{\partial u}{\partial t} - fv = -g \frac{\partial \zeta}{\partial x} + \frac{\partial}{\partial z} N \frac{\partial u}{\partial z}, \quad (\text{B.13})$$

$$\frac{\partial v}{\partial t} + fu = -g \frac{\partial \zeta}{\partial y} + \frac{\partial}{\partial z} N \frac{\partial v}{\partial z}, \quad (\text{B.14})$$

where z is the vertical axis positive up from the sea bed, u and v are the velocities in x and y direction, f is the Coriolis parameter, g the gravitational acceleration, ζ the surface elevation and N the vertical eddy viscosity. De Boer (2009) gives the boundary conditions:

$$z = 0 : \frac{\partial u}{\partial z} = 0, \frac{\partial v}{\partial z} = 0 \quad (\text{B.15})$$

$$z = -D : \frac{\partial u}{\partial z} = su, \frac{\partial v}{\partial z} = sv \quad (\text{B.16})$$

The linearised bottom friction s is given by $s = 8kU/3\pi E$, where U is the depth averaged velocity and k a friction parameter introduced by Prandle (1982b). With the introduction of complex vector notation, the velocity vector R and the pressure gradient G are:

$$R = R_1^+ + R_2^- = u + iv \quad (\text{B.17})$$

$$G = G_1^+ + G_2^- = \frac{\partial \eta}{\partial x} + i \frac{\partial \eta}{\partial y} \quad (\text{B.18})$$

Here R (and analogously G) are defined in the complex plane as:

$$R^\pm = |R^\pm| \exp(i\phi_\pm) \exp(\pm i\omega t) \quad (\text{B.19})$$

where ω is the angular frequency and ϕ the phase in the complex plane. Substituting R into B.13 and B.14, the anti-clockwise and clockwise motions are respectively:

$$i(f + \omega)R_1^+ = G_1^+ + \frac{\partial}{\partial z} \left(N \frac{\partial R_1^+}{\partial z} \right), \quad (\text{B.20})$$

$$i(f - \omega)R_2^- = G_2^- + \frac{\partial}{\partial z} \left(N \frac{\partial R_2^-}{\partial z} \right). \quad (\text{B.21})$$

As can be seen this decoupling into phasors makes it possible to solve the momentum equations separately. On a Cartesian grid this is impossible since the u and v momentum equations are coupled together through the Coriolis parameter f . By assuming a solution of the form $R^\pm = [a \exp(-\alpha z) + b \exp(\alpha z) + c] \cdot \exp(\pm i\omega t)$, and dividing by the expression for the depth-averaged current $\langle u \rangle = \int_{-D}^0 u(z) dz$ (neglecting the integral over $D \pm \eta$) the following solution is obtained:

$$\frac{R^\pm}{\langle R^\pm \rangle} = \frac{\cosh(\alpha^\pm [z - D]) - [\cosh(\alpha + D)] - \frac{\alpha^\pm}{s} \cdot [\sinh(\alpha \pm D)]}{-[\cosh(\alpha^\pm D)] + \left(\frac{1}{a^\pm D} - \frac{\alpha^\pm}{s} \right) \cdot [\sinh(\alpha^\pm D)]} \quad (\text{B.22})$$

where $\alpha^\pm = (1 - i)\sqrt{(f + \omega)/2E} \equiv 1/\delta^\pm$ is the inverse of the boundary layer height. From the solutions for R the ellipse properties can be evaluated:

$$\begin{aligned} A_{\text{major}} &= |R^+| + |R^-| && \text{Major axis} \\ A_{\text{minor}} &= |R^+| - |R^-| && \text{Minor axis, positive in } \exp(+i\omega t) \text{ direction} \\ \psi &= \frac{1}{2}(\phi_- + \phi_+) && \text{Inclination} \\ \phi &= \frac{1}{2}(\phi_- - \phi_+) && \text{Phase} \\ E &= \frac{A_{\text{major}}}{A_{\text{minor}}} = \frac{|R^+| + |R^-|}{|R^+| - |R^-|} && \text{Ellipticity, positive in } \exp(+i\omega t) \text{ direction} \end{aligned}$$

For the sake of numerical results u and v can also be written as tidal propagation constituents:

$$u = A \cos(\omega t) + B \sin(\omega t), \quad (\text{B.23})$$

$$v = C \cos(\omega t) + D \sin(\omega t). \quad (\text{B.24})$$

The ellipse properties become:

$$A_{\text{major}} = \frac{1}{2} |(A + D) + i(C - B)| + \frac{1}{2} |(A - D) + i(C + B)| \quad (\text{B.25})$$

$$A_{\text{minor}} = \frac{1}{2} |(A + D) + i(C - B)| - \frac{1}{2} |(A - D) + i(C + B)| \quad (\text{B.26})$$

$$\psi = \frac{1}{2} \arg \left(\frac{1}{2} [(A + D) + i(C - B)] \right) + \frac{1}{2} \arg \left(\frac{1}{2} [(A - D) + i(C + B)] \right) \quad (\text{B.27})$$

$$\phi = \frac{1}{2} \arg \left(\frac{1}{2} [(A + D) + i(C - B)] \right) - \frac{1}{2} \arg \left(\frac{1}{2} [(A - D) + i(C + B)] \right). \quad (\text{B.28})$$

Bibliography

- L. Arentz (2005). Remote sensing of the river Rhine plume. *MSc. thesis Delft University of Technology, Department of Civil Engineering and Geosciences.*
- G. Barenblatt, M. Bertsch, R. Passo, V. Prostokishin & M. Ughi (1993). A mathematical model of turbulent heat and mass transfer in stably stratified shear flow. *Journal of Fluid Mechanics*, 253:341–358. ISSN 0022-1120.
- I. Berdeal, B. Hickey & M. Kawase (2002). Influence of wind stress and ambient flow on a high discharge river plume. *J. Geophys. Res.*, 107:3130.
- R. Berkenbosch (2007). Milieueffectrapport Aanleg Maasvlakte 2 Samenvatting. *Havenbedrijf Rotterdam NV–Projectorganisatie Maasvlakte 2, report 9R7008 A1/R012/MVZ/Rott1.*
- K. Bowden, L. Fairbairn & P. Hughes (1959). The distribution of shearing stresses in a tidal current. *Geophysical Journal of the Royal Astronomical Society*, 2(4):288–305. ISSN 1365-246X.
- H. Burchard & R. Hofmeister (2008). A dynamic equation for the potential energy anomaly for analysing mixing and stratification in estuaries and coastal seas. *Estuarine, Coastal and Shelf Science*, 77(4):679–687. ISSN 0272-7714.
- S. Chao (1988). Wind-driven motion of estuarine plumes. *Journal of Physical Oceanography*, 18(8):1144–1166. ISSN 0022-3670.
- S. Chao & W. Boicourt (1986). Onset of estuarine plumes. *Journal of Physical Oceanography*, 16(12):2137–2149. ISSN 0022-3670.
- K. Cronin, G. Keetels, Y. Friocourt & M. Blaas (2010). mos2: WP3: Model setup and calibration. *Deltares.*
- G. Csanady (1982). *Circulation in the coastal ocean.* Springer. ISBN 9027714002.
- G. de Boer (2009). *On the interaction between tides and stratification in the Rhine Region of Freshwater Influence.* Ph.D. thesis, Delft University of Technology.
- G. De Boer & J. Pietrzak (in prep.). Tidal straining induced upwelling and the distribution of suspended particulate matter. ? ISSN ?
- G. de Boer, J. Pietrzak & J. Winterwerp (2007). Using the potential energy anomaly equation to investigate tidal straining and advection of stratification in a region of freshwater influence. *Ocean Modelling*, 22(1-2):1–11.
- G. de Boer, J. Pietrzak & J. Winterwerp (2009). SST observations of upwelling induced by tidal straining in the Rhine ROFI. *Continental Shelf Research*, 29(1):263–277. ISSN 0278-4343.

- J. De Kok (1996). A two-layer model of the Rhine plume. *Journal of marine systems*, 8(3-4):269–284.
- J. De Kok, C. De Valk, J. Van Kester, E. De Goede & R. Uittenbogaard (2000). Salinity and temperature stratification in the Rhine plume. *Estuarine, Coastal and Shelf Science*, 53(4):467–475.
- M. de Nijs & J. Pietrzak (2011). An explanation for salinity-and SPM-induced vertical countergradient buoyancy fluxes. *Ocean Dynamics*, pp. 1–28. ISSN 1616-7341.
- M. de Nijs, J. Pietrzak & J. Winterwerp (2010a). Advection of the salt wedge and evolution of the internal flow structure in the Rotterdam Waterway. *Journal of Physical Oceanography*. ISSN 1520-0485.
- M. De Nijs, J. Winterwerp & J. Pietrzak (2009). On harbour siltation in the fresh-salt water mixing region. *Continental Shelf Research*, 29(1):175–193. ISSN 0278-4343.
- M. de Nijs, J. Winterwerp & J. Pietrzak (2010b). The effects of the internal flow structure on SPM entrapment in the Rotterdam Waterway. *Journal of Physical Oceanography*. ISSN 1520-0485.
- W. De Ruijter, A. Van der Giessen & F. Groenendijk (1993). Current and density structure in the Netherlands coastal zone. *Coastal and estuarine studies*, pp. 529–529. ISSN 0938-0949.
- W. de Ruijter, A. Visser & W. Bos (1997). The Rhine outflow: a prototypical pulsed discharge plume in a high energy shallow sea. *Journal of Marine Systems*, 12(1-4):263–276.
- Deltares (2009). Delft3D-flow, version 3.14, user manual.
- D. Fong & W. Geyer (2001). Response of a river plume during an upwelling favorable wind event. *Journal of geophysical research*, 106(C1):1067–1084. ISSN 0148-0227.
- D. Fong, W. Geyer & R. Signell (1997). The wind-forced response on a buoyant coastal current: Observations of the western Gulf of Maine plume. *Journal of Marine Systems*, 12(1-4):69–81. ISSN 0924-7963.
- D. A. Fong & W. R. Geyer (2002). The alongshore transport of freshwater in a surface-trapped river plume*. *Journal of Physical Oceanography*, 32(3):957–972.
- N. Heaps (1972). Estimation of density currents in the Liverpool Bay area of the Irish Sea. *Geophysical Journal of the Royal Astronomical Society*, 30(4):415–432.
- B. Hickey, S. Geier, N. Kachel & A. MacFadyen (2005). A bi-directional river plume: The Columbia in summer. *Continental Shelf Research*, 25(14):1631–1656. ISSN 0278-4343.
- B. Hickey, L. Pietrafesa, D. Jay & W. Boicourt (1998). The Columbia River plume study: Subtidal variability in the velocity and salinity fields. *Journal of Geophysical Research*, 103(C5):10339. ISSN 0148-0227.
- V. Kourafalou, T. Lee, L. Oey & J. Wang (1996b). The fate of river discharge on the continental shelf 2. Transport of coastal low-salinity waters under realistic wind and tidal forcing. *Journal of Geophysical Research*, 101(C2):3435–3455. ISSN 0148-0227.
- V. Kourafalou, L. Oey, J. Wang & T. Lee (1996a). The fate of river discharge on the continental shelf 1. Modeling the river plume and the inner shelf coastal current. *Journal of geophysical research*, 101(C2):3415–3434. ISSN 0148-0227.

- G. Lacroix, K. Ruddick, J. Ozer & C. Lancelot (2004). Modelling the impact of the Scheldt and Rhine/Meuse plumes on the salinity distribution in Belgian waters (southern North Sea). *Journal of Sea Research*, 52(3):149–163.
- A. Lee (1980). North Sea: physical oceanography. *The North-west European shelf seas: The sea bed and the sea in motion*, 2:467–493.
- O. Phillips (1972). Turbulence in a strongly stratified fluid—is it unstable? In *Deep Sea Research and Oceanographic Abstracts*, volume 19, pp. 79–81. Elsevier. ISSN 0011-7471.
- J. Pietrzak & G. De Boer (in prep.). On the roles of wind driven and tidal straining induced upwelling in a Region of Freshwater Influence. ? ISSN ?
- J. Pietrzak, G. de Boer & M. Eleveld (2011). Mechanisms controlling the intra-annual mesoscale variability of SST and SPM in the southern North Sea. *Continental Shelf Research*.
- D. Prandle (1982a). The vertical structure of tidal currents and other oscillatory flows. *Continental Shelf Research*, 1(2):191–207.
- D. Prandle (1982b). The vertical structure of tidal currents and other oscillatory flows. *Continental Shelf Research*, 1(2):191–207. ISSN 0278-4343.
- W. Rodi (1984). Turbulence models and their application in Hydraulics, State-of-the-art paper sur l'état de connaissance. In *Paper presented by the IAHR-Section on Fundamentals of Division II: Experimental and Mathematical Fluid Dynamics, The Netherlands*.
- J. Simpson (1996). Physical processes in the ROFI regime. *Journal of marine systems*, 12(1-4):3–15.
- J. Simpson, W. Bos, F. Schirmer, A. Souza, T. Rippeth, S. Jones & D. Hydes (1993). Periodic stratification in the Rhine ROFI in the North Sea. *Oceanologica acta*, 16(1):23–32.
- J. Simpson & D. Bowers (1981). Models of stratification and frontal movement in shelf seas. *Deep Sea Research Part A. Oceanographic Research Papers*, 28(7):727–738. ISSN 0198-0149.
- J. Simpson, J. Brown, J. Matthews & G. Allen (1990). Tidal straining, density currents, and stirring in the control of estuarine stratification. *Estuaries and Coasts*, 13(2):125–132.
- J. Simpson & A. Souza (1995). Semidiurnal switching of stratification in the region of freshwater influence of the Rhine. *Journal of Geophysical Research*, 100(C4):7037–7044. ISSN 0148-0227.
- T. Smolders (2010). Stratification in the Rhine ROFI. *MSc. thesis Delft University of Technology, Department of Civil Engineering and Geosciences*.
- A. Souza & J. Simpson (1996). Controls on stratification in the Rhine ROFI system. *Journal of Marine Systems*, 12(1-4):311–323.
- G. Stelling (1984). On the construction of computational methods for shallow water problems. *Rijkswaterstaat communications*, (35).
- G. Stelling & J. Van Kester (1994). On the approximation of horizontal gradients in sigma co-ordinates for bathymetry with steep bottom slopes. *International journal for numerical methods in fluids*, 18(10):915–935. ISSN 1097-0363.

- J. Suijlen & R. Duin (2002). Atlas of near-surface Total Suspended Matter concentrations in the Dutch coastal zone of the North Sea. *Report RIKZ/2002.059*.
- J. Van Alphen, W. De Ruijter & J. Borst (1988). Outflow and three-dimensional spreading of Rhine River water in the Netherlands coastal zone. *Physical processes in estuaries*, pp. 70–92.
- A. Visser, A. Souza, K. Hessner & J. Simpson (1994). The effect of stratification on tidal current profiles in a region of freshwater influence. *Oceanologica acta*, 17(4):369–381.
- M. Visser & R. te Utrecht (1993). *On the transport of fine marine sediment in the Netherlands coastal zone*. Universiteit Utrecht. ISBN 9039301298.

List of Figures

2.1	Rhine ROFI stratified	4
3.1	3D residual current structure Rhine ROFI	8
3.2	Tidal straining	12
3.3	Rhine ROFI wind influence	17
4.1	Coarse, intermediate and fine hydrodynamical grid	21
4.2	Intermediate and fine hydrodynamical grid	21
4.3	Fine hydrodynamical grid	21
4.4	Bathymetry of the coast of The Netherlands	22
4.5	Observation stations and transects	24
5.1	Salinity and eddy viscosity profiles vertical grid analysis	31
5.2	Salinity profiles Case 03, Noordwijk 30	32
5.3	Distribution of ϕ	33
5.4	Schematic staircase	33
5.5	Topview salinity and potential energy, Scenario 06; 15h00	34
6.1	No wind scenario, 48-hour averaged salinity profiles	37
6.2	Snapshots salinity profiles no wind, 5 ms ⁻¹ northerly and southerly	38
6.3	5 ms ⁻¹ northerly wind, 48-hour averaged salinity profiles	39
6.4	5 ms ⁻¹ southerly wind, 48-hour averaged salinity profiles	39
6.5	Snapshots salinity profiles no wind, 5 ms ⁻¹ offshore and onshore	41
6.6	Snapshots salinity profiles no wind, 10 ms ⁻¹ northerly and southerly	44
6.7	10 ms ⁻¹ northerly wind, 48-hour averaged salinity profiles	45
6.8	10 ms ⁻¹ southerly wind, 48-hour averaged salinity profiles	45
6.9	Snapshots of temperature, 5 and 10 ms ⁻¹ northerly wind	47
6.10	Integrated values of ϕ over time	49
6.11	Spatial change of ϕ	50
6.12	Tidal upwelling and downwelling, slack before ebb and flood	54
6.13	Upwelling and downwelling by the tide and wind, slack before ebb	56
6.14	Upwelling and downwelling by the tide and wind, slack before flood	57
6.15	Overview of the results for the different forcings by the wind	58
7.1	Sketch of the wind-driven motions in the Rhine ROFI	60
A.1	48-hour averaged salinity profiles, no wind scenario	67
A.2	48-hour averaged salinity profiles, 5 ms ⁻¹ northerly wind	68
A.3	48-hour averaged salinity profiles, 5 ms ⁻¹ southerly wind	68
A.4	48-hour averaged salinity profiles, 5 ms ⁻¹ offshore wind	69
A.5	48-hour averaged salinity profiles, 5 ms ⁻¹ onshore wind	69
A.6	48-hour averaged salinity profiles, 10 ms ⁻¹ northerly wind	70

A.7	48-hour averaged salinity profiles, 10 ms^{-1} southerly wind	70
A.8	48-hour averaged salinity profiles, 10 ms^{-1} offshore wind	71
A.9	48-hour averaged salinity profiles, 10 ms^{-1} onshore wind	71
A.10	Snapshots salinity profiles, part 1	72
A.11	Snapshots salinity profiles, part 2	73
A.12	Snapshots salinity profiles, part 3	74
A.13	Snapshots salinity profiles, part 4	75
A.14	Snapshots temperature profiles, part 1	76
A.15	Snapshots temperature profiles, part 2	77
A.16	Snapshots temperature profiles, part 3	78
A.17	Snapshots temperature profiles, part 4	79
A.18	Snapshots potential energy anomaly profiles, part 1	80
A.19	Snapshots potential energy anomaly profiles, part 2	81
A.20	Snapshots potential energy anomaly profiles, part 3	82
A.21	Snapshots potential energy anomaly profiles, part 4	83